Selfconsistent calculations of mesonic properties at nonzero temperature

Dissertation
zur Erlangung des Doktorgrades
der Naturwissenschaften

vorgelegt beim Fachbereich Physik
der Johann Wolfgang Goethe–Universität
in Frankfurt am Main

von
Dirk Röder
aus Frankfurt am Main

Frankfurt 2005
(D 30)

vom Fachbereich Physik der
Johann Wolfgang Goethe–Universität als Dissertation angenommen

Dekan: Prof. Dr. W. Aßmus

Gutachter: Prof. Dr. Dirk H. Rischke
JProf. Dr. Adrian Dumitru

Datum der Disputation: 13.12.2005

Für meine Frau Julia
und meine Söhne Justus und Philipp.

Table of Contents

List of Figures

–I–

Introduction

1.1 Four fundamental forces

Modern physics believes that matter is held together through four fundamental forces, gravity, the weak interaction, the electromagnetic force, and the strong interaction (cf. Tab. 1.1). In this section, I briefly discuss some aspects and differences of these forces.

The force with the smallest relative strength is gravity, which couples two particles together via their mass, and which acts on all known particles. It is the most "common" force in our everyday life, and describes how the apple falls down from the tree. Newton's theory of gravity (17th century) describes this force as a long-range interaction between two bodies. In modern physics interactions are described as an exchange of virtual particles, which "carry" the force from one particle to another. Such a modern theory of gravity is Einstein's theory of general relativity (20th century). The exchange particle for the gravity is the graviton with vanishing mass. The range R of the force can be estimated by the mass m of the exchange particles [HKS95]

$$R \approx \frac{h}{2\pi mc} \quad , \tag{1.1}$$

where $h = 6.626\,0693 \times 10^{-34}\,Js$ is Planck's constant, and $c = 299\,792\,458\,ms^{-1}$ the velocity of light. The mass of the graviton is zero and therefore the range of gravity is infinity, as one expects. As mentioned above, gravity is very weak compared to the other three forces, thus it does not play an important role in microscopic processes. Indeed, gravity is the only one of the four forces where the interaction between two particles with equal charge is attractive, and not re-

force	relative strength	range $[m]$	exchange particle	interaction between two particles with equal charge
gravity	10^{-38}	∞	graviton	attractive
weak interaction	10^{-5}	10^{-18}	$W^{\pm}$, Z^0	repulsive
EM interaction	10^{-2}	∞	photon	repulsive
strong interaction	1	10^{-15}	gluon	repulsive

Table 1.1: The four fundamental forces of nature by comparison.

pulsive. This fact, together with the infinite range of gravity, leads to its extreme importance in all astrophysical phenomena.

Another fundamental force is the so called weak interaction, which acts on all fermions (particles with spin 1/2). The exchange particles of the weak interaction are the very massive Z^0 and $W^{\pm}$ bosons, their masses are ~ 80 times larger than the mass of the proton [EHO+04]. Therefore this interaction is of short range $R \approx 10^{-18}$ m, which is ~ 1000 times smaller than an atomic nucleus. It is very important for all decay processes (involving fermions), e.g., the beta decay of the neutron

$$n \rightarrow p + e^- + \bar{\nu_e}, \tag{1.2}$$

where n is a neutron, p a proton, e^- an electron, and $\bar{\nu_e}$ an anti-neutrino.

The electromagnetic (EM) force acts on all particles with electric charge. Maxwell was the first (19th century) who could unify the electric and the magnetic interactions in one theory. A modern description of this interaction is quantum electrodynamics (QED) (20th century). The mass of the exchange particles, the photons, is zero, and therefore the range of the electromagnetic interaction is infinity. It is, in addition to gravity, very common in our everyday life, and is used to light our rooms and to power our hi-fi systems. In the 20th century, Glashow, Weinberg, and Salam worked out that the electromagnetic and the weak interaction can be unified in one theory, the electroweak theory.

Last but not least, the strongest of the fundamental forces is the strong interaction, all particles which experience this force are called hadrons. The modern theory of strong interaction is quantum chromodynamics (QCD) (this name can be traced back to the name of the QCD charge: colour). The exchange particles are 8 different massless gluons, thus one would expect, from Eq. (1.1), that the

range of this force is infinity. However, this is not the case, the range of the strong interaction is $R \approx 10^{-15}$ m (of the order of an atomic nucleus). The reason for this is that the gluons can interact with *themselfs*, which leads to the finite range of the force and many other complications. QCD is the theory that this thesis is based on, and I will focus on it in the next sections.

1.2 Quantum Chromodynamics

In this section I discuss some aspects of QCD which are important for my thesis, especially the chiral and the $Z(N_c)$ symmetry. Certainly, this introduction is far from complete, for more details see e.g. [Wei95a, PS95, Wei95b, Kug97, CL84, GSS01, HM84].

As mentioned above, modern physics believes that QCD is the best theory we have to describe the strong interaction between the bosonic gluons and the fermionic quarks. Like all fundamental forces (apart from gravity) it is based on a local gauge symmetry, the $SU(3)_c$ colour symmetry. As shown in [tHV72] it is a renormalizable theory, which means that divergences can be regularised via the introduction of a finite number of counter terms to the Lagrangian of the theory. Another important fact is that QCD is an asymptotically free theory [GW73, Pol73], i.e., the interaction between gluons and quarks becomes weaker with increasing energy. One expects that this leads to a so-called quark-gluon plasma (QGP) at large temperatures and/or chemical potentials [CP75], which means that the quarks and the gluons are no longer confined together but can behave as free particles in a plasma. The phase transition between hadronic matter, which is the state of matter under "normal" conditions in our universe today, and the QGP is extensively discussed in this thesis.

The QCD Lagrangian is given by

$$\mathcal{L} = \bar{\psi}(i\gamma^\mu D_\mu - m)\psi - \frac{1}{4}F_a^{\mu\nu}F^a_{\mu\nu}, \tag{1.3a}$$

where

$$D_\mu \equiv \partial_\mu - igA^a_\mu T_a, \tag{1.3b}$$

is the covariant derivative, and

$$F_a^{\mu\nu} = \partial^\mu A_a^\nu - \partial^\nu A_a^\mu + g f_{abc} A_b^\mu A_c^\nu, \tag{1.3c}$$

the gluonic field strength tensor. For N_c colours and N_f quark flavours, ψ is a $4N_cN_f$-dimensional spinor of quark fields, $\bar{\psi}$ the Dirac conjugate spinor, γ^μ the 4-vector of Dirac matrices, m the quark mass matrix, g the strong coupling constant, A^μ_a the gluonic fields, and f_{abc} the structure constants of the local $SU(N_c)_c$ colour symmetry. As mentioned above, the QCD Lagrangian foots on this symmetry, which means that it is invariant under transformations of the fields $\mathcal{L}(\psi, A^\nu_a) = \mathcal{L}(\Omega^\dagger\psi, \Omega^\dagger A^\nu_a \Omega)$, where

$$\Omega(X) \equiv \exp\left[i\sum_{a=1}^{8}\alpha^a(X)T_a\right] \tag{1.4}$$

describes local $SU(3)_c$ transformations. The T_a's are the generators of the symmetry group, and α^a are the corresponding parameters. This transformation of the fields is called a *gauge transformation*. Note that, in contrast to global transformations, cf. Eq.(1.8), a local transformation depends on the space-time point X. In most cases I suppress the argument of Ω for simplicity. The matrices Ω satisfies

$$\Omega^\dagger\Omega = \mathbb{1}, \quad \det\Omega = 1. \tag{1.5}$$

The chiral $U(N_f)_r \times U(N_f)_\ell$ symmetry

For massless quarks ($m = 0$ in Eq.1.3a) the Lagrangian is invariant under the global chiral symmetry. To see this, the spinor and the conjugate spinor of the quark fields are decomposed into right- and left-handed spinors

$$\psi \to \psi_r + \psi_\ell \equiv \frac{1+\gamma_5}{2}\psi + \frac{1-\gamma_5}{2}\psi. \tag{1.6}$$

Using this, the Lagrangian becomes

$$\mathcal{L} = i(\bar{\psi}_r\gamma^\mu D_\mu\psi_r + \bar{\psi}_\ell\gamma^\mu D_\mu\psi_\ell) - \frac{1}{4}F^{\mu\nu}_a F^a_{\mu\nu}. \tag{1.7}$$

Invariance under chiral symmetry means that the Lagrangian does not change, if the spinors are transformed via a global $U(N_f)_r \times U(N_f)_\ell$ symmetry transformation, $\mathcal{L}(\psi_r, \psi_\ell) = \mathcal{L}(\Omega_r\psi_r, \Omega_\ell\psi_\ell)$, where the right- and left-handed transformations are given by

$$\Omega_r \equiv \exp\left(i\sum_{a=0}^{N_f^2-1}\alpha^a_r T_a\right), \quad \Omega_\ell \equiv \exp\left(i\sum_{a=0}^{N_f^2-1}\alpha^a_\ell T_a\right), \tag{1.8}$$

$\alpha_{r,\ell}$ are the parameters, and T_a the generators of the $U(N_f)_{r,\ell}$ symmetry group. The chiral symmetry group is isomorphic to the vector and axial vector group, $U(N_f)_r \times U(N_f)_\ell \cong U(N_f)_V \times U(N_f)_A$, with $V \equiv r+\ell$, $A \equiv r-\ell$. Every unitary group can be decomposed into a direct product of a special unitary group and a complex phase, $U(N) \cong SU(N) \times U(1)$, hence the chiral group can be written as $U(N_f)_r \times U(N_f)_\ell \cong SU(N_f)_r \times SU(N_f)_\ell \times U(1)_r \times U(1)_\ell \cong SU(N_f)_V \times SU(N_f)_A \times U(1)_V \times U(1)_A$.

The $U(1)_V$ symmetry corresponds to baryon number conservation, and is always respected. In the vacuum, a non-vanishing expectation value of the quark condensate, $\langle \bar{q}_\ell \, q_r \rangle \neq 0$, spontaneously breaks the above symmetry to $SU(N_f)_V$. This gives rise to N_f^2 Goldstone bosons which dominate the low-energy dynamics of the theory. As shown by 't Hooft [tH76a, tH76b], instantons break the $U(1)_A$ symmetry explicitly to $Z(N_f)_A$ [PW84a]. (For the low-energy dynamics of QCD, however, this discrete symmetry is irrelevant.) Consequently, one of the N_f^2 Goldstone bosons becomes massive, leaving $N_f^2 - 1$ Goldstone bosons.

The $SU(N_f)_r \times SU(N_f)_\ell \times U(1)_A$ symmetry of the QCD Lagrangian is also explicitly broken by nonzero quark masses. The $N_f^2 - 1$ low-energy degrees of freedom then become pseudo-Goldstone bosons. For $M \leq N_f$ degenerate quark flavours, a $SU(M)_V$ symmetry is preserved. In nature the quark masses are not equal to zero, i.e., the chiral symmetry is only approximatively conserved. Normally, one uses models which foot on the chiral symmetry only to describe the light quarks. The two lightest quarks are the up and down quark, 1.5 MeV $\leq m_u \leq$ 4.5 MeV and 4 MeV $\leq m_d \leq$ 8 MeV. Treating these quarks as massless, i.e., using a $SU(2)_r \times SU(2)_\ell \cong O(4)$ symmetry, yields six Noether currents,

$$J^\mu_{r,a} = \bar{\psi}_r \gamma^\mu \frac{\tau_a}{2} \psi_r, \quad J^\mu_{\ell,a} = \bar{\psi}_\ell \gamma^\mu \frac{\tau_a}{2} \psi_\ell, \tag{1.9a}$$

with

$$\partial_\mu J^\mu_r = \partial_\mu J^\mu_\ell = 0 \tag{1.9b}$$

where τ_a are the three Pauli matrices [IZ85]. It is common to introduce the vector and the axial-vector currents

$$V^\mu_a \equiv J^\mu_{r,a} + J^\mu_{\ell,a} = \bar{\psi} \gamma^\mu \frac{\tau_a}{2} \psi, \quad A^\mu_a \equiv J^\mu_{r,a} - J^\mu_{\ell,a} = \bar{\psi} \gamma^\mu \gamma_5 \frac{\tau_a}{2}. \tag{1.10}$$

The corresponding conserved charges are

$$Q^V_a = \int d^3x \psi^\dagger(x) \frac{\tau_a}{2} \psi(x), \quad Q^A_a = \int d^3x \psi^\dagger(x) \gamma_5 \frac{\tau_a}{2} \psi(x). \tag{1.11}$$

To extend this, one can consider also the mass of the strange quark as "small", 80 MeV $\leq m_s \leq$ 130 MeV. Then one has to replace the three Pauli matrices by the eight Gell-Mann matrices λ_a [IZ85]. The masses of the charm, bottom, and top quarks are very large, 1.15 GeV $\leq m_c \leq$ 1.35 GeV, 4.1 GeV $\leq m_b \leq$ 4.4 GeV, and $m_t = 174.3 \pm 5.1$ GeV, hence introduction of these degrees of freedom into a chirally symmetric model is not reasonable.
In section 1.4, I present the linear σ-model with $O(N)$ symmetry, which foots on the chiral symmetry for two quark flavours.

The $Z(N_c)$ symmetry

As mentioned above, QCD is based on a local $SU(3)_c$ colour symmetry. In the following I show how to construct from this the global $Z(3)$ symmetry. A particularly simple element of the $SU(N_c)_c$ symmetry is a constant phase times the unit matrix,

$$\Omega_c \equiv \exp(i\phi)\mathbb{1}. \tag{1.12}$$

The constraint

$$\det \Omega_c = \det[\exp(i\phi)\mathbb{1}] = \exp(iN_c\phi) = \cos(N_c\phi) + i\sin(N_c\phi) \stackrel{!}{=} 1 \tag{1.13}$$

leads to a restriction of the parameter ϕ

$$\phi = \frac{2\pi}{N_c} j, \quad j = 0, 1, \ldots, (N_c - 1). \tag{1.14}$$

Hence Ω_c is just the N_c th root of unity times the unit matrix. Since j is an integer, Ω_c describes a global $Z(N_c)$ rotation (symmetry) of the fields. Indeed, we will see that this is not a symmetry of the theory with quarks, because this transformation violates the periodicities of the quark fields.
To introduce the temperature T, I work in Euclidean space-time and use the imaginary-time formalism [Das97, Kap93, LB00]. From the laws of quantum statistic, cf. [GPY81], we know that the (bosonic) gluon fields A_a^ν have to be periodic in $(0, 1/T)$,

$$A_a^\nu\left(\frac{1}{T}, \mathbf{x}\right) = A_a^\nu(0, \mathbf{x}), \tag{1.15}$$

and the (fermionic) quark spinor and conjugated spinor, ψ and $\bar{\psi}$, anti-periodic,

$$\psi\left(\frac{1}{T}, \mathbf{x}\right) = -\psi(0, \mathbf{x}), \quad \bar{\psi}\left(\frac{1}{T}, \mathbf{x}\right) = -\bar{\psi}(0, \mathbf{x}). \tag{1.16}$$

Obviously, any gauge transformation of these fields which are periodic in $(0, 1/T)$, i.e., $\Omega(\mathbf{x}, 1/T) = \Omega(\mathbf{x}, 0)$, does not change these periodicities. 't Hooft [tH78] was the first to notic that one can also consider a gauge transformation which is only periodic up to a constant equal to the identity matrix times the N th root of unity:

$$\Omega\left(\mathbf{x}, \frac{1}{T}\right) = \Omega_c, \quad \Omega(\mathbf{x}, 0) = 1. \tag{1.17}$$

Using this transformation the periodicity of the gluon fields remain

$$\Omega_c^\dagger A_a^\nu\left(\mathbf{x}, \frac{1}{T}\right)\Omega_c = A_a^\nu\left(\mathbf{x}, \frac{1}{T}\right) = A_a^\nu(\mathbf{x}, 0) \tag{1.18}$$

where one uses the fact that Ω_c, as a constant phase times a unitary matrix, commutes with the fields A_a^ν, and the relation $\Omega_c^\dagger\Omega_c = 1$. But the periodicities of the quark fields are violated

$$\Omega_c^\dagger\psi\left(\mathbf{x}, \frac{1}{T}\right) = \exp(-i\phi)\psi\left(\mathbf{x}, \frac{1}{T}\right) \neq \psi(\mathbf{x}, 0), \tag{1.19a}$$

$$\Omega_c^\dagger\bar{\psi}\left(\mathbf{x}, \frac{1}{T}\right) = \exp(-i\phi)\bar{\psi}\left(\mathbf{x}, \frac{1}{T}\right) \neq \bar{\psi}(\mathbf{x}, 0). \tag{1.19b}$$

Hence, the $Z(N_c)$ is an exact symmetry only for the pure gauge theory, i.e., without quark fields included. In section 1.4, I present a theory which is based on this symmetry, the Polyakov-loop model.

1.3 Phase transitions in QCD

In this section I discuss the possible phases of strongly interacting matter and the transitions between them. Therefore, I will briefly motivate some major concepts for the well-known example of water.

Thermodynamic systems can show different types of macroscopic behaviour (or in other words can be in different *phases*), depending on external degrees of freedom (e.g. temperature T, pressure p, chemical potential μ). Water can be in three different phases, the liquid phase, the gas phase, and the solid phase. By changing an external degree of freedom the system can change from one phase into another. Let's consider the following example of our everyday life. If one puts a pot with (liquid) water on the stove and switches the latter on, the temperature of the water increases up to a (critical) temperature $T_c = 100°$ C, where the water becomes vapour (changes the phase). The *order* of a phase transition is defined

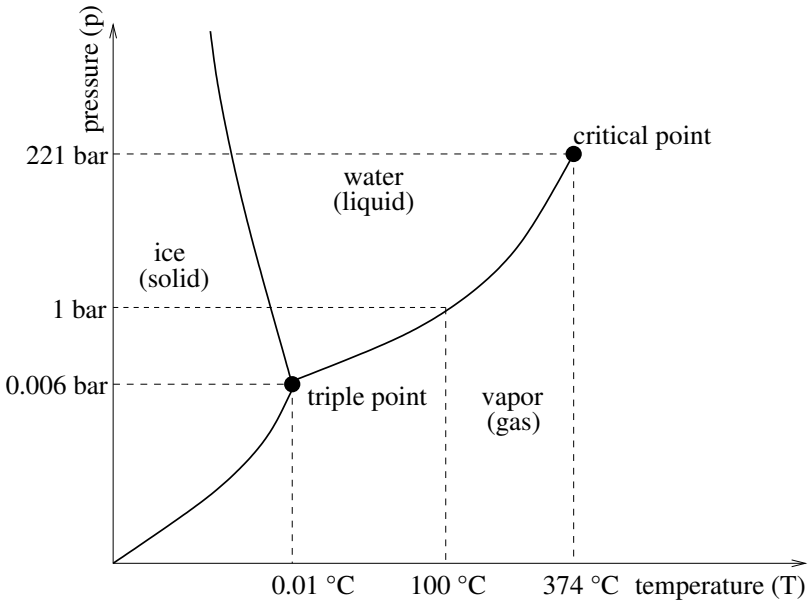

Figure 1.1: A sketch of the phase diagram of water in the pressure vs. temperature plane.

via the properties of the pressure, and its nth derivatives with respect to the temperature and/or chemical potential,

$$\left.\frac{\partial^n p}{\partial T^n}\right|_{\mu=\text{const.}}, \quad \text{and} \quad \left.\frac{\partial^n p}{\partial \mu^n}\right|_{T=\text{const.}}. \tag{1.20}$$

If the pressure is continuous, but there is a discontinuity in the first derivatives, we call this a first-order phase transition. If the pressure and its first derivatives are continuous but there is a discontinuity in its second derivatives, we call this a second-order phase transition. In principle, one can define even higher-order phase transitions, but in nature only the first- and second- (maybe third- [GW80, LM05b, LM05a, LSS81]) order phase transitions occur. If there is no discontinuity, but a rapid change in the thermodynamic quantities, we call this a crossover transition.

An appropriative way to visualise the possible phases and phase transitions of a system is a *phase diagram*. In Fig. 1.1 a sketch of the phase diagram for water is shown in the pressure vs. temperature plane. The lines represent first-order phase transitions (directly *on* the line both phases coincide). The first-order phase transition between the liquid and the gas phase becomes a second-order phase transition at a *critical point* $(p, T) = (221\ \text{bar}, 374\,^\circ\text{C})$, and for even higher

pressures $p > 221$ bar a crossover. Another remarkable feature of this diagram is the *triple point* at $(p, T) \approx (0.006\text{ bar}, 0.01\,^\circ\text{C})$ where *all* three phases coincide. The transition of the example with the pot of water is a first-order transition at $(p, T) = (1\text{ bar}, 100\,^\circ\text{C})$ in this diagram. In the next sections, we will see that most of the discussed features can also be found in the QCD phase diagram.

The quark mass dependence of the phase transition

An important parameter for the order of the phase transition in QCD is given by the mass of the quarks [m in Eq. (1.3a)]. As mentioned in Sec. 1.2 nonvanishing quark masses break the symmetry of the QCD Lagrangian explicitly. The principle of universality states that a phase is characterised by its macroscopic behaviour, which is mostly driven by the global symmetries. Therefore one way to find the order of the transition under this broken symmetry is to construct a model which respects the same (broken) global symmetry as QCD, and calculates the order in this model instead of in QCD. In this section I consider the case of vanishing chemical potential $\mu = 0$ and three (possible) quark flavours $N_f = 3$. Therefore, the mass parameters are the strange quark mass m_s and the degenerate masses of the up and down quark $m_{ud} \equiv m_u = m_d$.
The expected phase diagram in the plane of these two mass parameters is shown in Fig. 1.2. This diagram exhibits two areas of first-order phase transitions, near $m_s = m_{ud} = 0$ and $m_s = m_{ud} = \infty$, and a crossover regime between them, separated by lines of second-order phase transitions. The question marks indicate the expected position for the physical quark masses in this diagram. If one of the mass parameters is infinity (i.e., the quark is infinitely heavy) the corresponding quark flavours are thus removed from the spectrum of physical excitations. Therefore one can distinguish between four different flavour cases. First the pure gauge theory (upper right corner of Fig. 1.2) where $m_s = m_{ud} = \infty$, in this point all quarks are removed from the theory and only the gluons remains. Second, the one-flavour case $N_f = 1$ (right boundary of Fig. 1.2) where $m_s < \infty$ but $m_{ud} = \infty$, on this line only the strange degree of freedom remains in the theory. Third, the two-flavour case $N_f = 2$ (upper boundary of Fig. 1.2) where $m_s = \infty$ but $m_{ud} < \infty$, here the strange quark is removed from the theory and only the up- and down quarks remain. And finally the full three-flavour case $N_f = 3$ (the rest of the plane in Fig. 1.2) where $m_s < \infty$ and $m_{ud} < \infty$, in this area all quarks are included in the underlying theory.

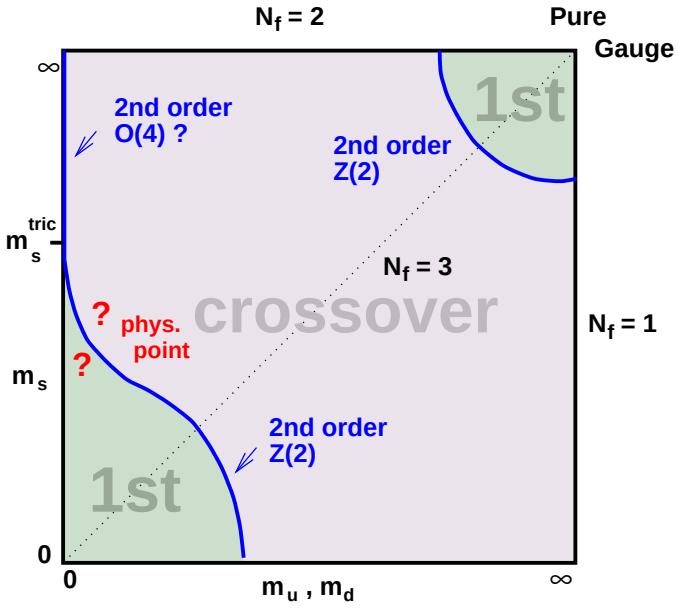

Figure 1.2: The expected phase diagram in the plane of strange vs. degenerate up and down quark masses [LP03].

One can use universality arguments to determine the order of the phase transition. According to universality, the order of the chiral transition for vanishing quark masses in QCD is *identical* to that in a theory with the same chiral symmetries as QCD. This argument was employed by Pisarski and Wilczek [PW84a] who found that for $N_f = 2$ flavours of massless quarks (upper left corner of Fig. 1.2), the transition can be of second-order, if the $U(1)_A$ symmetry is explicitly broken by instantons. It is driven first-order by fluctuations, if the $U(1)_A$ symmetry is restored at the critical temperature T_c. For $N_f = 3$ massless flavours (lower left corner of Fig. 1.2), the transition is always first-order. In this case, the term which breaks the $U(1)_A$ symmetry explicitly is a cubic invariant, and consequently drives the transition first-order. In the absence of explicit $U(1)_A$ symmetry breaking, the transition is fluctuation-induced of first-order.

For nonzero quark masses, the chiral symmetry of QCD is explicitly broken. Nonzero quark masses act like a magnetic field in spin systems, such that a second-order phase transition becomes a crossover transition. When the quark masses increase, a first-order phase transition may for a while remain of first-order, but it will ultimately become a crossover transition, too. In order to decide whether this happens for a particular choice of quark masses, universality

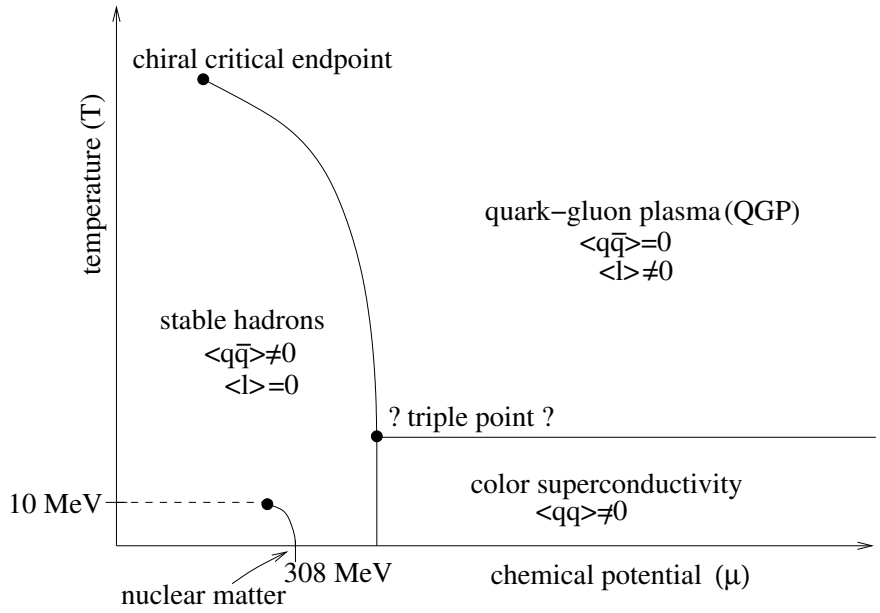

Figure 1.3: A sketch of the QCD phase diagram in the temperature vs. chemical potential plane.

arguments cannot be applied, and one has to resort to numerical calculations. For the pure gauge theory (the theory without quarks, upper right corner of Fig. 1.2) the transition is of first-order [B$^+$88, BCD$^+$88, Uka90, Uka97, Lae98, Kar00] as predicted by Svetitsky and Yaffe [SY82]. Nevertheless, recent results show that the transition is a weak first-order transition, thus it is more accurate to speak of a "nearly second-order" transition [KKLL00].

The temperature vs. chemical potential plane

In Fig. 1.3 a schematic plot of the QCD phase diagram in the temperature vs. chemical potential plane is shown. This diagram exhibits mainly three different phases, the hadronic phase, the QGP, and the colour-superconductivity phase. In the hadronic phase, the energy is small enough for stable hadrons to exist, e.g., protons, neutrons, pions, etc. As mentioned above, QCD is an asymptotically free theory, therefore for large temperatures and/or chemical potential the quarks in the hadrons become deconfined and behave more or less as free particles in a plasma, the QGP. There is probably a third phase at small temperatures and very large chemical potential, the phase of colour superconductivity, where a

quark-quark Cooper pair can be build, in analogy to the well-known electron-electron Cooper pair of electromagnetic superconductivity. Note that this phase can be separated into many other phases, e.g., the 2SC, CFL, CSL, or the polar phase, c.f. [BL84, ARW98, RSSV98, Alf01, Ris04, Sho04, RW00].

First, let's consider the transition between the hadronic phase and the QGP. The line between these two phases corresponds to a first-order phase transition which ends in the chiral critical endpoint of a second-order phase transition. The position of this chiral critical endpoint is still under investigation [FK02, FK04, Ste04, GGG05, BCPG94, AY89, HI03, AK03, E$^+$04], the latest lattice results from Fodor and Katz [FK04] found this point at $T = 162 \pm 2$ MeV and $\mu = 120 \pm 13$ MeV (indeed at nonzero chemical potential lattice QCD calculations are hampered by the fermionic sign problem and become increasingly unreliable with increasing chemical potential [dFP02]). As indicated in this plot, there are two possibilities for an order parameter of this phase transition, the quark condensate $\langle q\bar{q}\rangle$ which links the transition to the restoration of the chiral symmetry, and the expectation value of the Polyakov-loop $\langle l\rangle$ which links the transition to the restoration of the $Z(N_c)$ symmetry. In contrast to the quark condensate, the expectation value of the Polyakov-loop is zero in the hadronic phase and nonzero in the QGP, i.e., the $Z(N_c)$ symmetry is *broken* in the QGP and restored in the hadronic phase. However, note that these order parameters correspond to two very different Ansätze for the underlying symmetry. The $Z(N_c)$ symmetry is exact for infinitely heavy quarks (in the pure gauge theory), and the chiral $U(N_f)_r \times U(N_f)_\ell$ symmetry for quarks with vanishing mass. Although there are lattice QCD calculations which indicate that these two Ansätze lead to the same phase transition [Kar02], the relationship of the symmetries is still an open question in modern high energy physics, cf. e.g. [MST04, SKT04, KL99].

The stable ground state of nuclear mater at vanishing temperature is at nonzero chemical potential $\mu_0 = 308$ MeV. For smaller chemical potential, nuclear matter shows a similar behaviour to a gaseous phase and for larger the behaviour of a liquid. As the line of first-order phase transitions in the phase diagram of water, this line in the QCD phase diagram ends in an critical point of second-order (at a temperature of ~ 10 MeV).

Note that the area of colour-superconductivity is still not well understood, especially for "small" chemical potential. Maybe there is no direct phase transition between the hadronic phase and the colour superconductivity phase without passing the QGP, i.e., maybe there is no triple point between the three phases (indi-

cated by the question marks in Fig. 1.3). Or maybe there is no phase transition at all [ABR99, RW00].

1.4 Effective models of QCD

At temperatures of the order of $\sim \langle\bar{q}q\rangle^{1/3}$, the thermal excitation energy is large enough to expect the restoration of chiral symmetry. At such energy scales, the QCD coupling constant is still large, rendering perturbative calculations unreliable. Thus, one has to resort to nonperturbative methods to study chiral symmetry restoration. A first-principle approach is lattice QCD [Kar02]. Lattice QCD calculations have determined the temperature T_c for chiral symmetry restoration to be of order 150 MeV at zero quark chemical potential [LP03]. These calculations, however, face several technical problems.

The first is that they become numerically very difficult for physically realistic, i.e., small, values of the up- and down-quark masses. Although progress in this direction has been made [FK04], most studies use unphysically large values. Another problem is that, at nonzero chemical potential, lattice QCD calculations are hampered by the fermion sign problem and become increasingly unreliable for chemical potentials larger than (a factor π times) the temperature [dFP02].

An alternative nonperturbative approach to study chiral symmetry restoration is via chiral effective theories. These theories have the same global $U(N_f)_r \times U(N_f)_\ell$ symmetry as QCD but, since quark and gluons are integrated out, do not possess the local $SU(3)_c$ colour symmetry of QCD. The effective low-energy degrees of freedom are the (pseudo-) Goldstone bosons of the QCD vacuum, i.e., the pseudoscalar mesons. However, in the chirally symmetric phase these particles become degenerate with their chiral partners, the scalar mesons. Therefore, an appropriate effective theory to study chiral symmetry restoration in QCD is the linear sigma model [Lev67, GML60] which treats both scalar and pseudoscalar degrees of freedom on the same footing. The advantage of chiral effective theories over lattice QCD calculations is that their numerical treatment (within some many-body approximation scheme) is comparatively simple and that there is no problem to consider arbitrary quark chemical potential.

In the following, I introduce a reasonable effective model which respects the chiral symmetry, the linear σ-model with $O(N)$ symmetry, and an effective model which is based on the $Z(N_c)$ symmetry, the Polyakov-loop model.

The linear σ-model with $O(N)$ symmetry

The Lagrangian of the $O(N)$ linear sigma model is given by

$$\mathcal{L}(\boldsymbol{\phi}) = \frac{1}{2}\partial_\mu \boldsymbol{\phi} \cdot \partial^\mu \boldsymbol{\phi} - U(\boldsymbol{\phi}) \tag{1.21}$$

where $\boldsymbol{\phi} \equiv (\phi_1, \boldsymbol{\pi})$, with the first component ϕ_1 corresponding to the scalar σ-meson and the other components $\boldsymbol{\pi} = (\phi_2, ..., \phi_N)$ corresponding to the pseudoscalar pions. (However, note that the original σ-model introduced by Gell-Mann and Levy [GML60, IZ85] incorporates the scalar and pseudoscalar mesons as well as a fermionic isodoublet field ψ of mass zero. In the linear σ model discussed in the following, the fermionic degrees of freedom are neglected.) The function $U(\boldsymbol{\phi})$ is the tree-level potential,

$$U(\boldsymbol{\phi}) = \frac{1}{2}\mu^2 \boldsymbol{\phi} \cdot \boldsymbol{\phi} + \frac{\lambda}{N}(\boldsymbol{\phi} \cdot \boldsymbol{\phi})^2 - H\phi_1 \ , \tag{1.22}$$

where μ^2 is the bare mass and $\lambda > 0$ the four-point coupling constant. For $\mu^2 < 0$ the $O(N)$ symmetry is spontaneously broken to $O(N-1)$, leading to $N-1$ Goldstone bosons, the pions. The parameter H breaks the symmetry explicitly, giving a mass to the pion.

The parameters can be expressed in terms of the vacuum mass of the σ-meson, m_σ, the vacuum mass of the pion, m_π, and the vacuum decay constant of the pion, f_π,

$$\mu^2 = -\frac{m_\sigma^2 - 3\,m_\pi^2}{2} \ , \quad \lambda = \frac{N(m_\sigma^2 - m_\pi^2)}{8 f_\pi^2} \ , \quad H = m_\pi^2\, f_\pi \ . \tag{1.23}$$

With $m_\sigma = 600$ MeV, $m_\pi = 139.5$ MeV, and $f_\pi = 92.4$ MeV [EHO$^+$04] this leads to $H = (121.60\,\mathrm{MeV})^3, \lambda = 19.943$, and $\mu^2 = -(388.34\,\mathrm{MeV})^2$.

I assume translational invariance so that one may consider the effective potential V instead of the effective action Γ, cf. Sec. 1.5. For translationally invariant systems, these two quantities are related via

$$\Gamma[\bar{\sigma}, \bar{\boldsymbol{\pi}}, \bar{S}, \bar{P}] = -\frac{\Omega_3}{T}\, V[\bar{\sigma}, \bar{\boldsymbol{\pi}}, \bar{S}, \bar{P}] \ , \tag{1.24}$$

where Ω_3 is the 3-volume of the system, and $\bar{\sigma}, \bar{\boldsymbol{\pi}}, \bar{S}, \bar{P}$ are the expectation values of the one- and two-point functions for the scalar and pseudoscalar fields in the presence of external sources [CJT74]. I am interested in the case where these sources are zero, i.e., in the stationary points of Γ or V. Because the vacuum of

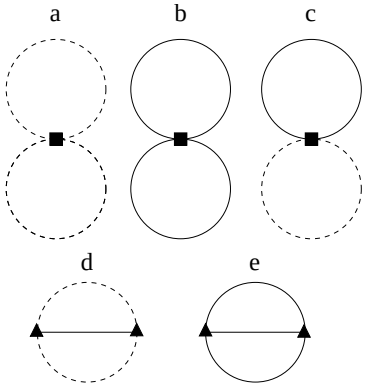

Figure 1.4: The set of two-particle irreducible diagrams considered in the linear σ model with $O(N)$ symmetry. The diagrams a,b, and c are the double-bubble diagrams, and d and e are the sunset diagrams. A full line denotes the full propagator for the σ-meson and a dashed line the full propagator for the pion. The four-particle vertex $\sim \lambda$ is represented by a square and the three-particle vertex $\sim \lambda\sigma$ by a triangle.

QCD has even parity, the expectation values of the pseudoscalar fields are zero, $\bar{\boldsymbol{\pi}} = 0$, and I shall simply omit the dependence of V on $\bar{\boldsymbol{\pi}}$ in the following.
Then, the effective potential for the $O(N)$ model in the CJT formalism, discussed in Sec. 1.5, reads [RRR03, LR00]

$$\begin{aligned} V[\bar{\sigma}, \bar{S}, \bar{P}] &= U(\bar{\sigma}) + \frac{1}{2}\int_Q \Big[\ln \bar{S}^{-1}(Q) + S^{-1}(Q;\bar{\sigma})\,\bar{S}(Q) - 1\Big] \\ &+ \frac{N-1}{2}\int_Q \Big[\ln \bar{P}^{-1}(Q) + P^{-1}(Q;\bar{\sigma})\,\bar{P}(Q) - 1\Big] \\ &+ V_2[\bar{\sigma}, \bar{S}, \bar{P}]\ , \end{aligned} \tag{1.25}$$

where $U(\bar{\sigma})$ is the tree-level potential (1.22), evaluated at $\boldsymbol{\phi} = (\bar{\sigma}, 0, \ldots, 0)$. At tree-level the one-point expectation value can be calculated analytically

$$\bar{\sigma} = f_\pi = \sqrt{-\frac{N\mu^2}{4\lambda}}\,\frac{2}{\sqrt{3}}\cos\frac{\theta}{3}, \quad \theta = \arccos\left[\frac{HN}{8\lambda}\left(-\frac{12\lambda}{N\mu^2}\right)^{3/2}\right]. \tag{1.26}$$

The quantities S^{-1} and P^{-1} are the inverse tree-level propagators for scalar and pseudoscalar mesons,

$$S^{-1}(K;\bar{\sigma}) = -K^2 + m_\sigma^2(\bar{\sigma})\ , \tag{1.27a}$$

$$P^{-1}(K;\bar{\sigma}) = -K^2 + m_\pi^2(\bar{\sigma})\ , \tag{1.27b}$$

where the tree-level masses read

$$m_\sigma^2(\bar{\sigma}) = \mu^2 + \frac{12\,\lambda}{N}\,\bar{\sigma}^2\,, \tag{1.28a}$$

$$m_\pi^2(\bar{\sigma}) = \mu^2 + \frac{4\,\lambda}{N}\,\bar{\sigma}^2\,. \tag{1.28b}$$

As explained in Sec. 1.5, the functional V_2 in Eq. (1.25) is the sum of all 2PI diagrams. The standard Hartree-Fock approximation is defined by restricting this sum to the three double-bubble diagrams shown in Figs. 1.4 a, b, and c,

$$V_2^a[\bar{P}] \equiv (N+1)(N-1)\,\frac{\lambda}{N}\left[\int_Q \bar{P}(Q)\right]^2\,, \tag{1.29a}$$

$$V_2^b[\bar{S}] \equiv 3\,\frac{\lambda}{N}\left[\int_Q \bar{S}(Q)\right]^2\,, \tag{1.29b}$$

$$V_2^c[\bar{S},\bar{P}] \equiv 2\,(N-1)\frac{\lambda}{N}\int_Q \bar{S}(Q)\int_L \bar{P}(L)\,. \tag{1.29c}$$

Later, we will see that, in order to include the nonzero decay width of the particles, one has to go beyond the Hartree-Fock approximation by additionally including the sunset diagrams of Figs. 1.4 d and e. These diagrams have an explicit dependence on $\bar{\sigma}$,

$$V_2^d[\bar{\sigma},\bar{S},\bar{P}] \equiv \frac{1}{2}\,2(N-1)\left(\frac{4\lambda\bar{\sigma}}{N}\right)^2\int_L\int_Q \bar{S}(L)\bar{P}(Q)\bar{P}(L+Q)\,, \tag{1.30a}$$

$$V_2^e[\bar{\sigma},\bar{S}] \equiv \frac{1}{2}\,3!\left(\frac{4\lambda\bar{\sigma}}{N}\right)^2\int_L\int_Q \bar{S}(L)\bar{S}(Q)\bar{S}(L+Q)\,. \tag{1.30b}$$

The complete expression for V_2 is obtained by the sum of the contributions in Eqs. (1.29) and (1.30),

$$V_2 = V_2^a + V_2^b + V_2^c + V_2^d + V_2^e\,. \tag{1.31}$$

The corresponding Dyson-Schwinger equations for the dressed propagators and the condensate equations can be derived by the minimisation of this effective potential, which will be the topic of the following chapters.

The Polyakov-loop model

In this section, I discuss how to construct an effective model, based on the $Z(N_c)$ symmetry, as discussed in Section 1.2. To find an order parameter for the pure

gauge theory with N_c colours let's first consider the Wilson line [Pol78, tH78, YS82]

$$\mathbf{L} \equiv \mathcal{P} \exp\left[ig \int_0^{1/T} A_0(\mathbf{x}, \tau) d\tau\right], \tag{1.32}$$

where A_0 denotes the temporal component of the gauge field in the fundamental representation, g the gauge coupling, and $\mathcal{P}$ denotes path ordering with respect to imaginary time τ. The thermal Wilson line transforms under local $SU(N_c)$ transformations as:

$$\mathbf{L}(\mathbf{x}) \longrightarrow \Omega^\dagger\left(\mathbf{x}, \frac{1}{T}\right) \mathbf{L}(\mathbf{x}) \Omega^\dagger(\mathbf{x}, 0). \tag{1.33}$$

An order parameter for the $Z(N_c)$ symmetry is given by the trace over the Wilson line

$$\ell = \frac{1}{N_c} \text{ tr } \mathcal{P} \exp\left[ig \int_0^{1/T} A_0(\vec{x}, \tau)\, d\tau\right] \ . \tag{1.34}$$

Its expectation value, $\ell_0(T)$, vanishes when $T < T_c$, and is nonzero above T_c. Indeed, by asymptotic freedom, $\ell_0 \to 1$ as $T \to \infty$. The simplest guess for a potential for the Polyakov-loop is:

$$V(\ell) = -\frac{b_2}{2}|\ell|^2 + \frac{1}{4}\left(|\ell|^2\right)^2, \qquad (N_c = 2)\ . \tag{1.35}$$

The Polyakov-loop model [Pis00, Pis02, DP01, DP02b, DP02a, SDJ01] is a mean-field theory for ℓ. In a mean-field analysis all coupling constants are taken as constant with temperature, except for the mass term, $\sim b_2|\ell|^2$. About the transition, condensation of ℓ is driven by changing the sign of the two-point coupling: $b_2 > 0$ above T_c [$b_2(T) \to 1$ for $T \to \infty$], and < 0 below T_c.

For two colours, (1.35) is a mean-field theory for a second-order deconfining transition [ES99, ES97, EMSZ96, EKR95, EFR$^+$89]. The ℓ field is real, and so the potential defines a mass: $(m_\ell/T)^2 = (1/Z_s)\partial^2 V/\partial \ell^2$, where Z_s is the wave function renormalisation constant for ℓ [Wir02, DO03]. The mass is measured from the two-point function of Polyakov-loops in coordinate space, $\propto (1/r)\exp(-m_\ell\, r)$ as $r \to \infty$.

For three colours, ℓ is a complex valued field, and a term cubic in ℓ appears in $V(\ell)$,

$$V(\ell) = -\frac{b_2}{2}|\ell|^2 - \frac{b_3}{3}\frac{\ell^3 + \ell^{*3}}{2} + \frac{1}{4}\left(|\ell|^2\right)^2, \qquad (N_c = 3)\ . \tag{1.36}$$

At very high temperature, the favoured vacuum is perturbative, with $\ell_0 \approx 1$, times $Z(3)$ rotations. One then chooses $b_3 > 0$ so that in the $Z(3)$ model, there is

always one vacuum with a real, positive expectation value for ℓ_0. This produces a first-order deconfining transition, where ℓ_0 jumps from 0 at T_c^- to $\ell_c = 2b_3/3$ at T_c^+ [DP01, DP02b, DP02a]; T_c is given by $b_2(T_c) = -2b_3^2/9$. The ℓ field has two masses, from its real (m_ℓ) and imaginary ($\widetilde{m}_\ell$) parts. At T_c^+, $\sqrt{Z_s} m_\ell/T = \ell_c$. The mass for the imaginary part of ℓ is $\sqrt{Z_s}\widetilde{m}_\ell(T)/T \propto \sqrt{b_3\ell}$; at T_c^+, $\widetilde{m}_\ell/m_\ell = 3$, twice the value expected from a perturbative analysis of the loop-loop correlation function, obtained by expanding ℓ from Eq. (1.34) to order A_0^3 [DP02d, DP02c]. This mass ratio receives corrections if five-point and six-point couplings are included in the effective Lagrangian [DP02d, DP02c] but those are not crucial for the following discussion. One notes that, in principle, all of the above coupling constants could be determined on the lattice. The lattice regularization requires non-perturbative renormalization of the Polyakov-loop in order to define the proper continuum limit of ℓ [KKPZ02, PP04, Zan03, DHL$^+$04].

Within the above mean-field theory, dynamical quarks act like a "background magnetic field" which breaks the $Z(3)$ symmetry explicitly, and a term linear in ℓ also appears in $V(\ell)$ [BU83, GK84, MO95, A$^+$99]:

$$V(\ell) = -b_1 \frac{\ell + \ell^*}{2} - \frac{b_2}{2}|\ell|^2 - \frac{b_3}{3}\frac{\ell^3 + \ell^{*3}}{2} + \frac{1}{4}\left(|\ell|^2\right)^2, \qquad (N_c = 3,\ m_\pi < \infty)\ . \tag{1.37}$$

Hence, as m_π decreases from infinity, $b_1(m_\pi)$ turns on. The normalisation of $b_2(T)$ for $T \to \infty$ is such that $\ell_0 \to 1$, i.e., $b_2(T = \infty) = 1 - b_1 - b_3$.

In Chapter II, the Polyakov-loop model is used to study the QCD phase transition.

1.5 The Cornwall-Jackiw-Tomboulis formalism

At nonzero temperature T, ordinary perturbation theory in terms of the coupling constant g breaks down in the sense that one can no longer order different contributions according to powers of g [DJ74]. This is because the new energy scale introduced by the temperature can conspire with the typical momentum scale p of a process so that gT/p is no longer of order g, but can be of order 1 [BP90a, BP90b]. Consequently, all terms of order gT/p have to be taken into account which requires the resummation of certain classes of diagrams.

A convenient resummation method is provided by the extension of the Cornwall-Jackiw-Tomboulis (CJT) formalism [CJT74] to nonzero temperatures and chemical potentials. The CJT formalism is equivalent to the Φ-functional approach of Luttinger and Ward [LW60] and Baym [Bay62]. It generalises the concept

of the effective action $\Gamma[\bar{\phi}]$ for the expectation value $\bar{\phi}$ of the one-point function in the presence of external sources to that for the effective action $\Gamma[\bar{\phi}, \bar{G}]$ for one and two-point functions, $\bar{\phi}$ and $\bar{G}$, in the presence of external sources. (For an extension of this approach to three- and more-point functions, see [NC75, Kle82, Car04, Ber04].)

The starting point for the CJT formalism is the generating functional for Green's functions [CJT74]

$$Z[J,K] \;=\; e^{W[J,K]} = \int \mathcal{D}\phi \exp\left\{ I[\phi] + \phi J + \frac{1}{2}\phi K \phi \right\}, \tag{1.38}$$

where $I[\phi] \equiv \int_X \mathcal{L}$ is the classical action, $W[J,K]$ the generating functional for connected Green's functions, and with the short-hand notations

$$\phi J \;\equiv\; \int_X \phi(X) J(X), \tag{1.39a}$$

$$\phi K \phi \;\equiv\; \int_{X,Y} \phi(X) K(X,Y) \phi(Y). \tag{1.39b}$$

The expectation values for the one- and two-point functions in the presence of the external sources, $\bar{\phi}$ and $\bar{G}$, are given by

$$\bar{\phi}(X) \;\equiv\; \frac{\delta W[J,K]}{\delta J(X)}, \tag{1.40a}$$

$$\bar{G}(X,Y) \;\equiv\; \frac{\delta^2 W[J,K]}{\delta J(X) \delta J(Y)}. \tag{1.40b}$$

Note that the derivative with respect to K is

$$\frac{\delta W[J,K]}{\delta K(X,Y)} = \frac{1}{2}[\bar{G}(X,Y) + \bar{\phi}(X)\bar{\phi}(Y)]. \tag{1.41}$$

The aim is now to eliminate the sources in favour of the one- and two point functions with a double Legendre transformation

$$\Gamma[\bar{\phi}, \bar{G}] = W[J,K] - \bar{\phi} J - \frac{1}{2}\bar{\phi} K \bar{\phi} - \frac{1}{2}\bar{G} K, \tag{1.42}$$

where $\bar{G}K \equiv \int_{XY} \bar{G}(X,Y) K(X,Y)$. Minimisation of this functional gives the expectation values of the one- and two-point function in the absence of the external sources, φ and $\mathcal{G}$,

$$\left.\frac{\delta \Gamma[\bar{\phi}, \bar{G}]}{\delta \bar{\phi}(X)}\right|_{\bar{\phi}=\varphi, \bar{G}=\mathcal{G}} \;=\; 0, \tag{1.43a}$$

$$\left.\frac{\delta \Gamma[\bar{\phi}, \bar{G}]}{\delta \bar{G}(X,Y)}\right|_{\bar{\phi}=\varphi, \bar{G}=\mathcal{G}} \;=\; 0. \tag{1.43b}$$

The last equation corresponds to the Dyson-Schwinger equation for the full dressed propagator. In the CJT formalism, one uses the following effective action [CJT74]

$$\Gamma[\bar{\phi},\bar{G}] = I[\bar{\phi}] - \frac{1}{2}\mathrm{Tr}\,\ln(\bar{G}^{-1}) - \frac{1}{2}\mathrm{Tr}(G^{-1}\bar{G}-1) + \Gamma_2[\bar{\phi},\bar{G}], \tag{1.44}$$

where,

$$G^{-1}(X,Y;\bar{\phi}) = -\left.\frac{\delta^2 I[\phi]}{\delta\phi(X)\delta\phi(Y)}\right|_{\phi=\bar{\phi}}, \tag{1.45}$$

is the tree-level propagator, and $\Gamma_2[\bar{\phi},\bar{G}]$ the sum of all two-particle irreducible (2PI) vacuum diagrams with internal lines given by $\bar{G}$. I'm interested in the case where the fields are translationally invariant, so that one may consider the effective potential V instead of the effective action. For translationally invariant systems, these two quantities are related via $\Gamma[\bar{\phi},\bar{G}] = -\Omega_3/T\,V[\bar{\phi},\bar{G}]$, where Ω_3 is the 3-volume of the system, thus

$$V[\bar{\phi},\bar{G}] = U(\bar{\phi}) + \frac{1}{2}\int_k \ln\bar{G}^{-1}(k) + \frac{1}{2}\int_k [G^{-1}(k;\bar{\phi})\bar{G}(k) - 1] + V_2[\bar{\phi},\bar{G}], \tag{1.46}$$

where

$$V_2[\bar{\phi},\bar{G}] = -T\Gamma_2[\bar{\phi},\bar{G}]/\Omega_3. \tag{1.47}$$

The stationary conditions in Eqs. (1.43), can now be expressed in terms of the effective potential

$$\left.\frac{\delta V[\bar{\phi},\bar{G}]}{\delta\bar{\phi}}\right|_{\bar{\phi}=\varphi,\bar{G}=\mathcal{G}} = 0, \tag{1.48a}$$

$$\left.\frac{\delta V[\bar{\phi},\bar{G}]}{\delta\bar{G}(K)}\right|_{\bar{\phi}=\varphi,\bar{G}=\mathcal{G}} = 0. \tag{1.48b}$$

Together with Eq. (1.46), the last stationary condition gives the Dyson-Schwinger equation

$$\mathcal{G}^{-1}(k) = G^{-1}(k;\varphi) + \Pi(k), \tag{1.49}$$

where

$$\Pi(k) \equiv 2\left.\frac{\delta V_2[\bar{\phi},\bar{G}]}{\delta\bar{G}(k)}\right|_{\bar{\phi}=\varphi,\bar{G}=\mathcal{G}}, \tag{1.50}$$

is the self-energy. Note that the thermodynamic pressure is (up to a sign) identical to the effective potential [Riv88]

$$p = -V[\varphi,\mathcal{G}]. \tag{1.51}$$

1.6 The aim of this work

The main focus of my thesis is QCD and its phase transitions as discussed in the introduction.

In chapter II, I present a study I've done with Adrian Dumitru and Jörg Ruppert [DRR04] about the phase transition temperature of QCD, and its dependence on the quark (or pion) mass. In the first part of this chapter, I use the linear σ-model with $O(N)$ symmetry (cf. Sec. 1.4), within the CJT formalism (cf. Sec. 1.5), which links the transition to chiral symmetry restoration. The parameters of this model depend on the vacuum mass of the pion and σ-meson and the vacuum value of the decay constant of the pion. From lattice QCD calculations we know the dependence of these values on the quark mass, and hence one can determine the dependence of the chiral phase transition (especially the transition temperature) on the quark mass. In the second part of this chapter, I use the Polyakov-loop model (cf. Sec. 1.4), which links the transition to the restoration of $Z(N_c)$ symmetry. The aim of this part is to find how "strong" one has to break the $Z(3)$ symmetry in order to reproduce the transition temperature (given by lattice QCD calculations).

In chapter III, I present a study I've done with my Ph.D. advisor Dirk Rischke and Jörg Ruppert [RRR05] about the improvement of the standard Hartree-Fock approximation by including nonzero decay width effects. In the standard Hartree-Fock approximation one treats all particles as stable quasiparticles, which means that the spectral densities of these particles are just delta-functions with zero decay width, $\Gamma = 0$. Obviously, this is a reasonable approximation for all particles with small decay width, i.e., the pion with a decay with of $\Gamma_\pi \sim 8$ eV in vacuum, but not for broad particles, like the σ-meson with a vacuum decay width of $\Gamma_\sigma \sim (600 - 1000)$ MeV. The decay width is proportional to the imaginary part of the self-energy of the particle $\Gamma \sim \mathrm{Im}\Pi$. In the standard Hartree-Fock approximation only real-valued tadpole diagrams (cf. Fig. 3.1 b, c, and 3.2 a, c) are taken into account. I improve this scheme by taking additionally into account the cut sunset diagrams (cf. Fig. 3.1 d, e, and 3.2 d), which have a real *and* an imaginary part. Beside the imaginary part, another major difference between these two types of diagrams is that the cut sunset diagram is a functional of an external four momentum vector $K = (\omega, \mathbf{k})$ (where ω is the energy and $\mathbf{k}$ the momentum of the particle). Hence, the Dyson-Schwinger equations for the full propagators and the condensate equations become integral

equations one has to solve on an energy-momentum grid. In this chapter, my focus is to study the influence of the inclusion of nonzero decay width effects, therefore, as a first approximation, I simply neglect the real part arising from these cut sunset diagrams.

Finally, in chapter IV, I present a work [Röd05] I've done to study the effects of the (in chapter III neglected) 4-momentum dependent real parts of the cut sunset diagrams in the linear σ-model with $O(N)$ symmetry. I do this not in the full Hartree-Fock but in the Hartree approximation. The difference between these both approximation is that all terms of order $\sim 1/N$ are neglected on the level of the condensate and Dyson-Schwinger equations in the Hartree approximation. This leads to a vanishing imaginary part of the pion self-energy, hence to a vanishing pion decay width. The decay width of the σ-meson remains nonzero. Besides the effects of the real part of the cut sunset diagram, I study in this chapter the influence of the "choice" of the vacuum mass of the σ-meson. As mentioned above, the parameters depend on the vacuum mass of the σ-meson mass, which is not well defined, $m_\sigma = (400 - 1200)$ MeV, because of the very large (vacuum) decay width of the σ-meson. Therefore, I compare the results for $m_\sigma = 400$, 600, and 800 MeV, in the case of explicit chiral symmetry breaking $m_\pi \neq 0$ and the chiral limit $m_\pi = 0$.

Conventions

I denote 4-vectors by capital letters, $X \equiv (x_0, \mathbf{x})$, with $\mathbf{x}$ being a 3-vector of modulus $x \equiv |\mathbf{x}|$. The imaginary-time formalism is used to compute quantities at nonzero temperature. Integrals over 4-momentum $K = (\omega, \mathbf{k})$ are denoted as

$$\int_K f(K) \equiv T \sum_{n=-\infty}^{\infty} \int \frac{d^3k}{(2\pi)^3} f(-i\omega_n, \mathbf{k}) \,, \tag{1.52}$$

where T is the temperature and $\omega_n = 2\pi n T$, $n = 0, \pm 1, \pm 2, \ldots$ are the bosonic Matsubara frequencies. My units are $\hbar = c = k_B = 1$. The metric tensor is $g^{\mu\nu} = \mathrm{diag}(+, -, -, -)$.

–II–

The quark mass dependence of the transition temperature

2.1 Motivation

Lattice QCD calculations at finite temperature and with dynamical fermions are presently performed for quark masses exceeding their physical values; for a recent review see [LP03]. To date, pion masses as low as ≈ 400 MeV are feasible [KLP01], about three times the physical pion mass. When comparing effective theories to first-principles numerical data obtained on the lattice it is therefore important to fix the parameters (coupling constants, vacuum expectation values and so on) such as to match the values of physical observables, e.g. of m_π, to those of the lattice calculations. For example, the QCD equation of state in the confined phase appears to be described reasonably well by that of a hadron resonance gas model, *after extrapolating* the physical spectrum of hadrons and resonances to that from the lattice [KRT03, KLP01]. Thus, lattice data on the dependence of various observables on the quark (or pion) mass constrain effective theories for the QCD phase transition at finite temperature and could provide relevant information on the driving degrees of freedom.

In the following, I analyse the dependence of the *chiral* symmetry restoration temperature on the vacuum mass of the pion using a linear sigma model in section 2.2. The linear sigma model provides an effective Lagrangian approach to low-energy QCD near the chiral limit [PW84b, RW93]. It incorporates the global flavour symmetry, assuming that "colour" can be integrated out. For example, it allows one to discuss the order of the $N_f = 2 + 1$ chiral phase transition as

a function of the quark masses [PW84b, RW93, LRSB00, MMOP94, MOPP92, Gol83, GGP94].

Instead of working up from zero quark mass, one could start with the quark masses taken to infinity, that is, with a pure gauge theory. Then, one can discuss the *deconfinement* transition at finite temperature within an effective Lagrangian for the Polyakov loop with global $Z(N_c)$ symmetry [YS82, Pis02, DP01, DP02b, DP02a, SDJ01, OM00, MMO02, MST04, Fuk04] (N_c is the number of colours). For finite pion mass, the symmetry is broken explicitly, and the phase transition (or crossover) temperature is shifted, relative to the pure gauge theory where pions are infinitely heavy. In section 2.3., I determine the endpoint of the line of first-order transitions for three colours, and extract the magnitude of the explicit $Z(3)$ breaking from lattice data on ΔT_c.

Pion Mass and Decay Constant in Vacuum

As discussed in Sec. 1.2, the Lagrangian of QCD with the quark mass matrices set to zero is invariant under independent rotations of the N_f right- and left-handed quark fields. It exhibits a global $SU(N_f)_r \times SU(N_f)_\ell$ symmetry, leading to $2(N_f^2-1)$ conserved currents. Those are N_f^2-1 vector currents, $V_i^\mu = \bar\psi\gamma^\mu\lambda_i\psi\ /2$, and N_f^2-1 axial currents, $A_i^\mu = \bar\psi\gamma^\mu\gamma_5\lambda_i\psi\ /2$, with λ_i the generators of $SU(N_f)$, normalised according to tr $\lambda_i\lambda_j = 2\delta_{ij}$. The $SU(N_f)_V$ subgroup of vector transformations is preserved in the vacuum [VW84], while the $SU(N_f)_A$ is broken spontaneously by a non-vanishing chiral condensate $\langle\bar q_R q_L\rangle \neq 0$, leading to non-conservation of the axial currents.

In reality, of course, even $SU(N_f)_V$ is broken explicitly by the non-vanishing quark mass matrix. Nevertheless, since $m_u \simeq m_d$, the $SU(2)_V$ symmetry is almost exact in QCD. The small explicit breaking of $SU(2)_A$ is responsible for the non-vanishing pion mass, as given by the Gell-Mann-Oakes-Renner relation

$$m_\pi^2 = \frac{1}{f_\pi^2}\, m_q\, \langle\bar q q\rangle\ . \tag{2.1}$$

I neglect isospin breaking effects here, and so assume that $m_u = m_d \equiv m_q$. $\langle\bar q q\rangle$ denotes the sum of the vacuum expectation values of the operators $\bar u_R u_L$ and $\bar d_R d_L$, and their complex conjugates. The proportionality constant f_π is the pion decay constant. It should be noted that (2.1) is only valid at tree level, and that loop effects induce an implicit dependence of both f_π and $\langle\bar q q\rangle$ on m_q. For small

m_q, this dependence can be computed in chiral perturbation theory [GL89]. For example, at next-to-leading order,

$$m_\pi^2 = M^2 \left[1 - \frac{1}{2}\left(\frac{M}{4\pi F}\right)^2 \log\frac{\Lambda_3^2}{M^2}\right] , \tag{2.2a}$$

$$f_\pi = F \left[1 + \left(\frac{M}{4\pi F}\right)^2 \log\frac{\Lambda_4^2}{M^2}\right] , \tag{2.2b}$$

where M and F are the couplings of the effective theory (equivalent to m_q and $\langle\bar{q}q\rangle$), and Λ_3 and Λ_4 are two renormalization-group invariant scales. These relations link the behaviour of f_π to that of m_π, the mass of a physical state. (In what follows, I use m_π to vary the strength of explicit symmetry breaking rather than using directly the scale-dependent quark masses).

More accurate results than Eqs. (2.2a,2.2b) can perhaps be obtained by computing quark propagators for various quark masses on the lattice. Ref. [CH03] analysed the propagators for gauge-field configurations generated with the standard Wilson gauge action ("quenched QCD"), using overlap fermions with exact chiral symmetry. They obtained a parametrisation of both m_π and f_π in terms of the mass m_q of u and d quarks (see section 2 in [CH03]) which allows to express f_π as a function of m_π. Their data covers an interval of 0.4 GeV $\lesssim m_\pi \lesssim$ 1 GeV, and 0.15 GeV $\lesssim \sqrt{2}f_\pi \lesssim$ 0.22 GeV.

2.2 Results: The linear σ-model with $O(N)$ symmetry

In this section, I discuss chiral symmetry restoration at nonzero temperature, and in particular the dependence of the symmetry restoration temperature on the pion mass. For simplicity, I restrict myselfe here to the two-flavour case. My emphasis is not on the order of the transition as the strange quark mass is varied but rather on how the temperature at which the transition occurs (be it either a true phase transition or just a crossover) depends on the pion mass. Such dependence arises from two effects. First, of course, due to explicit symmetry breaking occurring when $m_\pi > 0$. Second, due to the "indirect" dependence of spontaneous symmetry breaking, i.e., of the condensate $\langle\bar{q}q\rangle$ resp. f_π, on the pion mass (through pion loops, see previous section).

In the following I use the counter-term renormalization scheme as discussed in section V.B in [LR00]. In this scheme a mass renormalization scale μ is introduced

and the couplings then depend on that scale. However, choosing

$$\mu_{ren}^2 = \exp\left[\frac{m_\sigma^2(\ln\, m_\sigma^2 - 1) - m_\pi^2(\ln\, m_\pi^2 - 1)}{m_\sigma^2 - m_\pi^2}\right], \tag{2.3}$$

the four-point coupling $\lambda(\mu) = \lambda_{\rm tree}$ retains its tree-level (classical) value [LR00]. In other words, this renormalization prescription evolves the renormalization scale μ_{ren} in such a way as to keep λ constant.

Explicitly, this leads to the following expressions for the couplings [LR00]:

$$\lambda = \frac{1}{2}\frac{m_\sigma^2 - m_\pi^2}{f_\pi^2}, \quad H = f_\pi\left(m_\sigma^2 - 2\lambda f_\pi^2\right), \quad m^2 = -\frac{1}{2}\left(m_\sigma^2 - 3m_\pi^2\right) - 6\lambda Q_\mu(m_\pi), \tag{2.4}$$

where

$$Q_\mu(M) \equiv \frac{1}{(4\pi)^2}\left[M^2 \ln\frac{M^2}{\mu_{ren}^2} - M^2 + \mu_{ren}^2\right]. \tag{2.5}$$

These equations determine the couplings in vacuum in terms of m_π, f_π and m_σ. The dependence of f_π and m_π on the quark mass is taken from the data of ref. [CH03] shown in figure 2.1. Roughly, for $m_\pi : 0.4$ GeV $\to 1$ GeV, f_π increases by about 50 %, leading to an increase of the explicit symmetry breaking term H by a factor of 10. I also require the dependence of m_σ on m_π, which I take from a computation with standard Wilson fermions [K$^+$04b], shown in figure 2.2. Those authors find that m_σ is essentially a linear function of m_π^2. I checked how my results in Fig. 2.3 depend on this assumption by using, alternatively, a linear dependence $m_\sigma = m_\pi + \text{const.}$, with $m_\sigma = 0.6$ GeV for $m_\pi = 0.14$ GeV. I found essentially the same dependence of T_c on m_π.

At nonzero temperature, one uses the effective potential for composite operators, as discussed in Sec. 1.5, to determine the masses and the scalar condensate in the Hartree-Fock approximation. This approximation is defined by only taking into account the double-bubble diagrams shown in Figs. 1.4 d and e in the effective potential V. The gap equations for the condensate and the masses are given by minimisation of this potential. The expectation values of the one- and two-point functions in the absence of external sources, σ and $\mathcal{S}$, $\mathcal{P}$, are determined from the stationary points of V,

$$\left.\frac{\delta V}{\delta\bar\sigma}\right|_{\bar\sigma=\sigma,\bar S=\mathcal{S},\bar P=\mathcal{P}} = 0, \left.\frac{\delta V}{\delta\bar S}\right|_{\bar\sigma=\sigma,\bar S=\mathcal{S},\bar P=\mathcal{P}} = 0, \left.\frac{\delta V}{\delta\bar P}\right|_{\bar\sigma=\sigma,\bar S=\mathcal{S},\bar P=\mathcal{P}} = 0, \tag{2.6}$$

leading to the gap equations for the chiral condensate σ, and the effective masses of the σ-meson and the pions, M_σ and M_π,

$$H = \sigma\left[M_\sigma^2 - 2\lambda\sigma^2\right], \tag{2.7a}$$

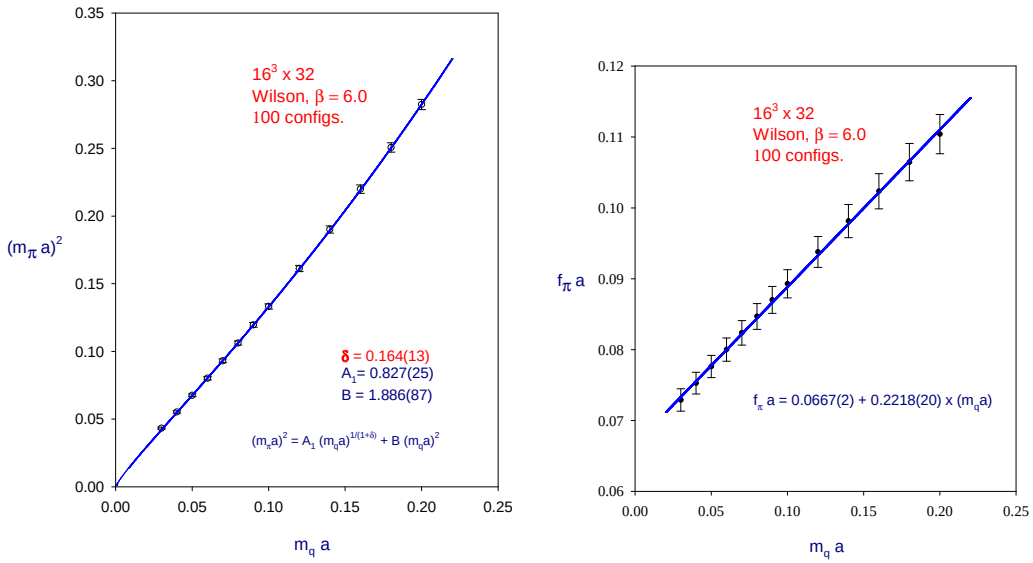

Figure 2.1: The pion mass squared $(m_\pi a)^2$ (left), and the pion decay constant $f_\pi a$ (right) versus the bare mass, where $a = 0.505$ GeV is the lattice spacing [CH03].

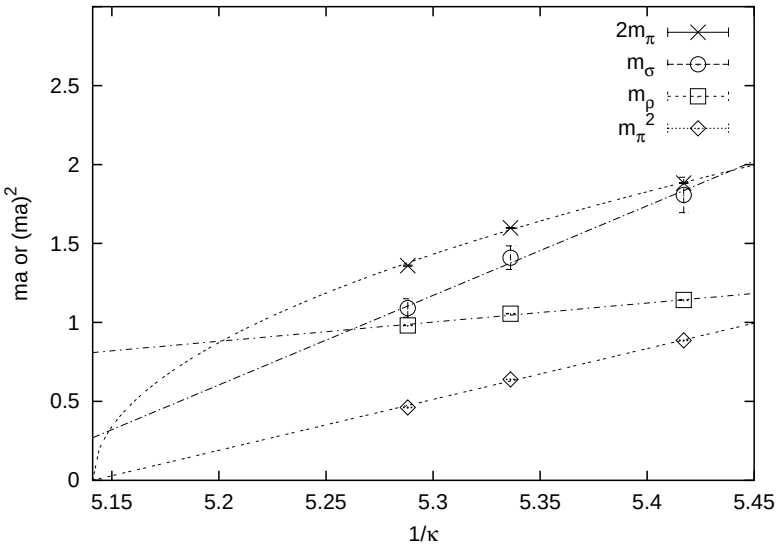

Figure 2.2: The (squared) meson masses: m_π^2, m_ρ, m_σ, and $2m_\pi$ in lattice units as a function of the inverse hopping parameter [K+04b]. The chiral limit is given by $1/\kappa_c \approx 5.13$.

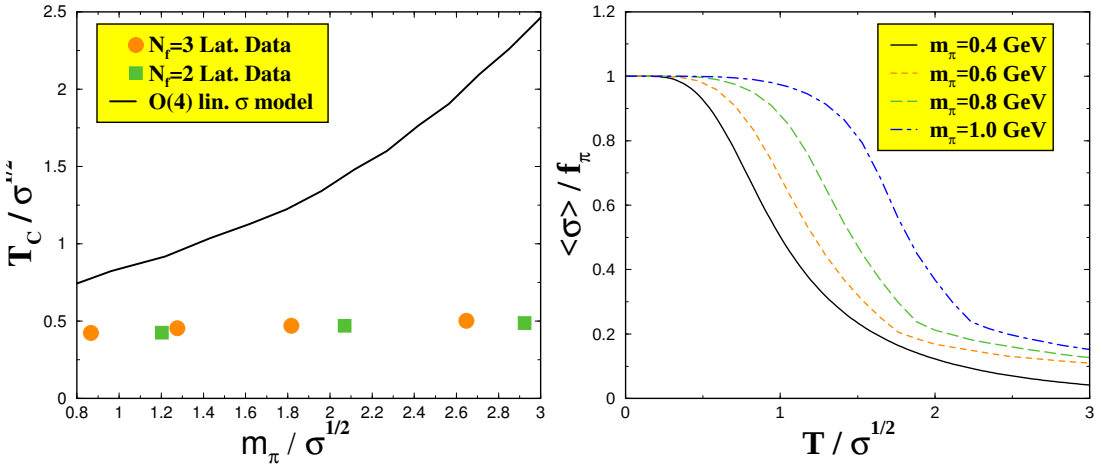

Figure 2.3: Left: The crossover temperature T_c as a function of the (vacuum) pion mass as obtained from the linear sigma model with $O(4)$ symmetry in comparison to lattice data [KLP01] for two and three flavours. The scale for both T_c and m_π is set by the zero-temperature string tension in the pure gauge theory, $\sqrt{\sigma} \simeq 0.425$ GeV. Right: The scalar condensate, $\langle\sigma\rangle$, as a function of temperature for various pion masses.

$$M_\sigma^2 = m^2 + 3\lambda\left\{\sigma^2 + [Q_T(M_\sigma) + Q_\mu(M_\sigma)] + [Q_T(M_\pi) + Q_\mu(M_\pi)]\right\}, \quad (2.7b)$$

$$M_\pi^2 = m^2 + \lambda\left\{\sigma^2 + [Q_T(M_\sigma) + Q_\mu(M_\sigma)] + 5[Q_T(M_\pi) + Q_\mu(M_\pi)]\right\}, \quad (2.7c)$$

where the nonzero-temperature contribution of the tadpole diagram is given by

$$Q_T(m) \equiv \frac{1}{2\pi^2}\int_0^\infty dq[\omega(q)]^{-1} f[\omega(q)], \quad (2.8)$$

where $f(\omega) \equiv 1/[\exp(\omega/T) - 1]$ is the Bose-Einstein distribution function and $\omega(q) \equiv \sqrt{q^2 + m^2}$ the quasiparticle energy. The self-consistent solution of the above gap equations for a given vacuum pion mass determines the temperature dependence of the scalar condensate as the order parameter of chiral symmetry restoration. For explicitly broken chiral symmetry, $H > 0$, the transition in this approach is a crossover. I define the crossover temperature T_c by the peak of $\partial\sigma/\partial T$. The dependence of T_c on m_π is depicted in Fig. 2.3 (left), where I have also shown lattice results obtained with two and three degenerate quark flavours, respectively [KLP01] (the $N_f = 2$ data with standard action, the $N_f = 3$ data with improved p4-action). Driven by the increase of both f_π and H with m_π, the linear sigma model predicts a rather rapid rise of T_c with the pion mass, as compared to the data which is nearly flat on the scale of the figure. While lattice data

indicate a rather weak dependence of T_c on the quark mass (see also ref. [B$^+$97]), models with spontaneous symmetry breaking in the vacuum naturally predict a rather steep rise of T_c with the VEV $\sigma_{\rm vac} = f_\pi$, which itself increases with the quark (or pion) mass. My findings here are in qualitative agreement with those from ref. [BJW99] who employed nonperturbative flow equations to compute the effective potential for two-flavour QCD within the linear sigma model. They also find a steeper slope of $T_c(m_\pi)$ than indicated by the lattice, even though their analysis appears to predict a somewhat weaker increase of f_π with m_π than the data of [CH03], which I employ here.

Fig. 2.3 also shows the temperature dependence of the σ condensate (right). With m_σ a linear function of m_π^2 [K$^+$04b], the width of the crossover is approximately independent of the pion mass for 0.4 GeV $\lesssim m_\pi \lesssim$ 1 GeV, while I found considerable broadening when m_σ is linear in m_π (not shown). The chiral susceptibility $\partial\sigma/\partial T$ at its maximum is ≈ 0.25, i.e., the crossover is in fact quite broad for the range of m_π considered. Since this is at variance with lattice data on QCD thermodynamics (pressure and energy density as functions of temperature, see e.g. the review in [LP03]), one might argue that the crossover is in fact not driven by the order parameter field but by heavier degrees of freedom [KRT03, KLP01, GL89]. Such degrees of freedom could reduce the pion-mass dependence of the transition substantially: using three-loop chiral perturbation theory (i.e., the nonlinear model), Gerber and Leutwyler find [GL89] that T_c increases rapidly from $\approx$ 190 MeV in the chiral limit (using their set of couplings) to $\approx$ 240 MeV for physical pion mass. However, when heavy states are included (in the dilute gas approximation), then T_c increases less rapidly, from $\approx$ 170 MeV in the chiral limit to $\approx$ 190 MeV for physical pion mass.

2.3 Results: The Polyakov-loop model

In this section I consider the Polyakov-loop model as introduced in Sec. 1.4. As discussed, the effective potential for three colours with explicit breaking of the $Z(3)$ symmetry is given by,

$$V(\ell) = -b_1 \frac{\ell + \ell^*}{2} - \frac{b_2}{2}|\ell|^2 - \frac{b_3}{3}\frac{\ell^3 + \ell^{*3}}{2} + \frac{1}{4}\left(|\ell|^2\right)^2 , \qquad (N_c = 3,\ m_\pi < \infty) \ . \tag{2.9}$$

First, I consider the case where b_1 is very small, and take the term linear in ℓ as a perturbation; then the weakly first-order phase transition of the pure gauge theory persists (in what follows, the critical temperature in the pure gauge theory with $b_1 = 0$ will be denoted T_c^*). The critical temperature is determined from

$$b_2(T_c) = -\frac{2}{9}b_3^2\left(1 + \frac{27}{2}\frac{b_1}{b_3^3}\right) + \mathcal{O}(b_1^2) \ . \tag{2.10}$$

The order parameter jumps at T_c, from

$$\ell_0(T_c^-) = \frac{9}{2}\frac{b_1}{b_3^2} + \mathcal{O}(b_1^2) \ , \tag{2.11}$$

to

$$\ell_0(T_c^+) = \frac{2}{3}b_3 - \frac{9}{2}\frac{b_1}{b_3^2} + \mathcal{O}(b_1^2) \ . \tag{2.12}$$

Note that numerically $\ell_0(T_c^-)$ could be much larger than b_1 if the phase transition in the pure gauge theory is weak and so the correlation length $\xi = 1/m_\ell$ near T_c is large (i.e., if b_3 is small), as indeed appears to be the case for $N_c = 3$ colours [KKLL00]. In other words, it could be that on the lattice ℓ quickly develops a non-vanishing expectation value at T_c^- already for rather large quark (or pion) masses, but this does not automatically imply a large explicit symmetry breaking (see also Fig. 2.4 below).

From Eq. (2.10) one can estimate the shift of T_c induced by letting $m_\pi < \infty$. Writing the argument of b_2 in that equation as $T_c^* + \Delta T_c$ and expanding to first-order in ΔT_c one obtains

$$\begin{aligned} \frac{\Delta T_c}{T_c^*} &= -3\,\frac{b_1}{b_3}\,\left(T\frac{\partial b_2}{\partial T}\right)^{-1}_{T=T_c^*} + \mathcal{O}(b_1^2) \\ &= -\frac{2}{3}\,\ell_0(T_c^-)\,b_3\left(T\frac{\partial b_2}{\partial T}\right)^{-1}_{T=T_c^*} + \mathcal{O}(b_1^2) \ . \end{aligned} \tag{2.13}$$

The shift in T_c with decreasing pion mass is proportional to the expectation value of the Polyakov-loop just below T_c; all other factors on the right-hand side of Eq. (2.13) do not depend on b_1 or m_π. Numerical values for b_3 and for $b_2(T)$ were obtained in [DP01, DP02b, SDJ01, SDL02] by fitting the effective potential (1.36) to the pressure and energy density of the pure gauge theory with three colours; those are $b_3 \approx 0.9$ and $b_3^2/[T_c^* \partial b_2(T_c^*)/\partial T] \approx 1$, to within 10%. I therefore expect that numerically $\Delta T_c/T_c^*$ is roughly equal to $\ell_0(T_c^-)$.

The Eqs. (2.11,2.12) seem to indicate that the discontinuity of ℓ_0 at T_c vanishes, i.e., that the phase transition turns into a crossover, at a pion mass such that $b_1(m_\pi) = 2b_3^3/27$. However, one cannot really extend the $\mathcal{O}(b_1)$ estimates to the endpoint of the line of first-order transitions because it applies, near T_c, only if $-4b_2(T_c) \ll b_3^2$, which translates into $b_1 \ll b_3^3/108$, see Eq. (2.10). To find the endpoint of the line of first-order transitions I solve numerically for the global minimum of (2.9) as a function of b_2, for given b_1, see Fig. 2.4 (left). The numerical solution is "exact" and does not assume that b_1 is small. I employ $b_3 = 0.9$ to properly account for the small latent heat of the pure gauge theory [DP01, DP02b, DP02a, SDJ01, DP02c, DP02d, SDL02]. Also, for $b_1 = 0$, this b_3 corresponds to $\ell_c = 0.6$, which is close to the expectation value of the renormalised (fundamental) loop for the $N_c = 3$ pure gauge theory [KKPZ02, PP04, Zan03, DHL$^+$04].

Clearly, for very small b_1 the order parameter ℓ_0 jumps at some $b_2^c \equiv b_2(T_c)$, i.e., the first-order phase transition persists. (The abscissa is normalised by $|b_2(T_c^*)| = 2b_3^2/9$.) I find that the discontinuity vanishes at $b_1^c = 0.026(1)$, so there is no true phase transition for $b_1 > b_1^c$. Nevertheless, I define b_2^c even in the crossover regime via the peak of $\partial \ell_0(b_2)/\partial b_2$. The shift of b_2^c with increasing b_1 can now be converted into the shift of T_c itself by expanding about T_c^*:

$$\frac{\Delta T_c}{T_c^*} = \Delta b_2^c \left(T \frac{\partial b_2}{\partial T} \right)^{-1}_{T=T_c^*} , \tag{2.14}$$

as already discussed above. I also note that from Fig. 2.4 (left) the susceptibility for the Polyakov-loop at its maximum is $\partial \ell_0/\partial b_2 \simeq 3.5$, 2, 1.5 for $b_1 = 0.06$, 0.1, and 0.126, respectively. That is, the crossover is rather sharp for the values of b_1 shown in the figure.

Explicit breaking of the Z(3) symmetry of the gauge theory has previously been studied in [GK84, MO95, A$^+$99], and has been identified as the essential factor in determining the endpoint of deconfining phase transitions. Moreover, while the term $\sim b_1$ quickly washes out the transition, those studies showed that along

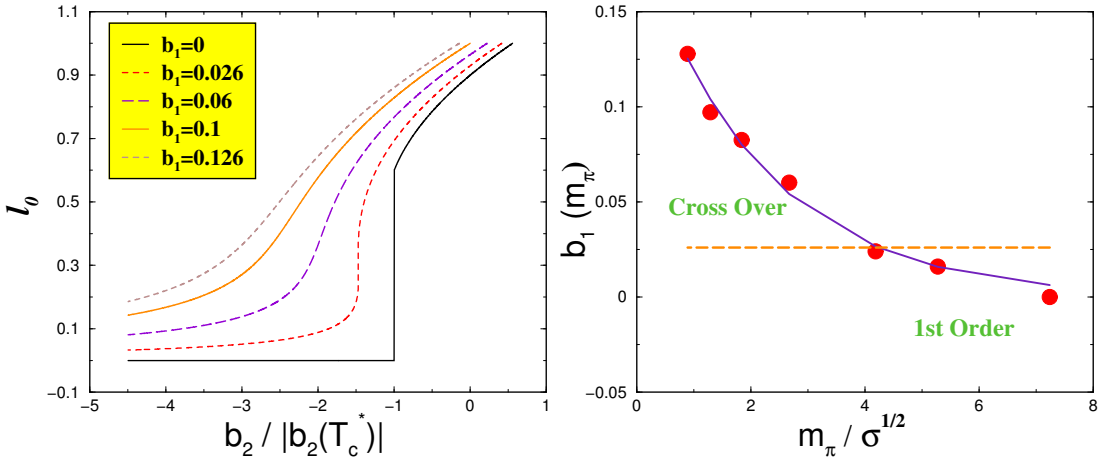

Figure 2.4: Left: The expectation value for the Polyakov-loop, $\ell_0(b_2(T))$, for various values of the explicit symmetry breaking coupling, b_1. All curves terminate at $\ell_0 = 1 \Leftrightarrow T = \infty$. Right: b_1 as a function of m_π, obtained by matching to three-flavour lattice data for $T_c(m_\pi)$. The solid line corresponds to an exponential increase of b_1 with decreasing m_π, see text. The broken horizontal line displays the endpoint of the line of first-order phase transitions in terms of b_1; the intersection with the $b_1(m_\pi)$ curve then gives the corresponding pion mass.

the line of first-order transitions the shift of T_c (or, alternatively, of the critical coupling β_c) is moderate, which agrees with my findings. However, the numerical values for the critical "external field" at the endpoint obtained in [MO95, A$^+$99] from actual Monte-Carlo simulations can not be compared directly to my estimate for b_1^c because I work here with the renormalised (continuum-limit) loop, not the bare loop. Ref. [KLP01] studied finite-temperature QCD with $N_f = 3$ flavours and various quark masses on the lattice (with improved p4-action), and determined the critical (or crossover) temperature as a function of the pion mass. Using Eq. (2.14) one can match $\Delta T_c/T_c^*$ to the data from [KLP01] to determine $b_1(m_\pi)$. In other words, I extract the function $b_1(m_\pi)$ required to match the effective Lagrangian (2.9) to $T_c(m_\pi)$ found on the lattice. The result is shown in Fig. 2.4 on the right. (Again, the pion mass is normalised to the zero-temperature string tension in the pure gauge theory, $\sqrt{\sigma} \simeq 0.425$ GeV.) Evidently, the $\approx 33\%$ reduction of T_c from $m_\pi = \infty$ (pure gauge theory) to $m_\pi/\sqrt{\sigma} \approx 1$ requires only small explicit breaking of the $Z(3)$ symmetry for the Polyakov-loop ℓ: I find that $b_1 < 0.15$ even for the smallest pion masses available on the lattice. This is due to the rather

weak first-order phase transition of the pure gauge theory with $N_c = 3$ colours, reflected by the strong dip of the string tension in the confined phase near T_c^- and of the Polyakov-loop screening mass m_ℓ in the deconfined phase near T_c^+ [KKLL00]; cf. also the discussion in [Pis00, Pis02, DP01, DP02b, DP02a, DP02c, DP02d].
Moreover, $b_1(m_\pi)$ appears to follow the expected behaviour $\sim \exp(-m_\pi)$. The exponential fit shown by the solid line corresponds to $b_1(m_\pi) = a \exp(-b\, m_\pi/\sqrt{\sigma})$, with $a = 0.19$ and $b = 0.47$. Surprisingly, by naive extrapolation one obtains a pretty small explicit symmetry breaking even in the chiral limit, $b_1 \approx 0.2$.
Finally, the endpoint of the line of first-order transitions at $b_1^c = 0.026$ (indicated by the dashed horizontal line) intersects the curve $b_1(m_\pi)$ at $m_\pi/\sqrt{\sigma} \approx 4.2$. For heavier pions the theory exhibits a first-order deconfining phase transition, which then turns into a crossover for $m_\pi \lesssim 4.2\ \sqrt{\sigma} \approx 1.8$ GeV ($\hat{=}\, m_q \approx 0.9$ GeV). According to my estimate, the endpoint of the line of first-order transitions occurs at $\Delta T_c/T_c^* \approx 12\%$, which is slightly less than a previous (qualitative) estimate of 26% from ref. [OM00].
Of course, so far my analysis is restricted to pion masses $m_\pi/\sqrt{\sigma} \gtrsim 1$. On the other hand, one might cross a chiral critical point for some pion mass $m_\pi/\sqrt{\sigma} < 1$ [GGP94]. Attempting a fit with the model (2.9) beyond that point would then lead to deviations from $b_1 \sim \exp(-m_\pi)$.

–III–

The improved Hartree-Fock approximation

3.1 Motivation

In this section I consider the linear σ-model with $O(N)$ symmetry (cf. Sec. 1.4) within the CJT formalism (cf. Sec. 1.5). Of course, it is practically impossible to solve the exact theory (i.e. to include all possible diagrams in the effective potential), therefore one has to solve the model within a many-body approximation scheme. The most popular among these many-body approximation schemes is the Hartree-Fock approximation. In this case, Γ_2 [cf. Eq. (1.44)] solely contains diagrams of so-called "double-bubble" topology, cf. Fig. 1.4 a–c. Note that, in Refs. [Pet99, LR00, LRSB00, RRR03], this scheme has been termed "Hartree" approximation. However, since the exchange contributions with respect to internal indices are in fact included, it is more appropriate to call it "Hartree-Fock" approximation. Neglecting the exchange contributions leads to the actual Hartree approximation which, in the case of the $O(N)$ model, has also been termed "large-N" approximation [Pet99, LR00]. In the Hartree-Fock approximation, the self-energies, which according to Eq. (1.50) are obtained by cutting lines in the diagrams for Γ_2, only consist of "tadpole" diagrams, cf. Figs. 3.1 b,c, and 3.2 a,c. For the chiral effective theories, such as the $U(N_f)_r \times U(N_f)_\ell$ and $O(N)$ models, this approximation scheme has been studied in great detail [BG77, BK96, RM98, AC97, Pet99, LR00, LRSB00, RRR03]. The Hartree-Fock approximation is a very simple approximation scheme, since tadpole self-energies do not have an imaginary part and, consequently, all particles are stable quasi-

particles. Moreover, since tadpoles are independent of energy and momentum, the Dyson-Schwinger equations for the propagators reduce to fix-point equations for the in-medium masses.

There are, however, several problems with the Hartree-Fock approximation related to the truncation of Γ_2. For instance, in the case of the $O(N)$ model, it does not correctly reproduce the order of the chiral symmetry restoring phase transition and it violates Goldstone's theorem in the sense that the Goldstone bosons do not remain massless for nonzero temperatures $0 < T < T_c$. Several ways to remedy this shortcoming have been suggested. The simplest one is to neglect subleading contributions in $1/N$, leading to the Hartree (or large-N, see discussion above) approximation [Pet99, LR00]. Here, the Goldstone bosons remain massless for $T < T_c$ and the transition is of second-order, as expected from universality class arguments [PW84a]. Another possibility to restore Goldstone's theorem is via so-called "external" propagators [ABW98, vHK02a, vHK02c, vHK02b, AAB$^+$02]. These objects are obtained from the Hartree-Fock propagators by additionally resumming all diagrams pertaining to the Random Phase Approximation (RPA), with internal lines given by the Hartree-Fock propagators. Another way to restore the second-order nature of the chiral phase transition is to include so-called "two-particle point-irreducible" (2PPI) contributions to Γ_2 [VC92, Ver01, BM03]. In this work, I am not concerned with these formal shortcomings of the Hartree-Fock approximation: I focus exclusively on the case realized in nature where chiral symmetry is already explicitly broken by (small) nonzero quark masses, such that the pion is no longer a Goldstone boson and assumes a mass $m_\pi \simeq 139.5$ MeV [EHO$^+$04]. My goal in this work is to include the nonzero decay width of the particles in a self-consistent many-body approximation scheme. To this end, one has to go beyond the Hartree-Fock approximation and add other diagrams to Γ_2 which, upon cutting lines according to Eq. (1.50), yield self-energies with nonzero imaginary part. The most simple of such diagrams, and the ones considered in the following, are those of the so-called "sunset" topology, cf. Fig. 1.4 d,e, leading to the self-energy diagrams shown in Figs. 3.1 d,e and 3.2 d.

The self-energies arising from the sunset diagrams in Γ_2 depend on the energy and the momentum of the incoming particle. Therefore, the Dyson-Schwinger equations no longer reduce to fix-point equations for the in-medium masses. Since the self-energies now have a nonzero imaginary part, implying a finite lifetime of the corresponding particles, the spectral densities are no longer delta-functions. It is therefore convenient to rewrite the Dyson-Schwinger equations for the propaga-

tors into a set of self-consistent integral equations for the spectral densities which has to be solved numerically.

3.2 The Dyson-Schwinger and the condensate equations

In this section I discuss the application of the improved Hartree-Fock approximation to the $O(N)$ model. The linear σ model with $O(N)$ symmetry and its effective potential is already introduced in Chapter 1.4. As mentioned above, in the standard Hartree-Fock approximation one takes into account only the three possible double-bubble diagrams, V_2^a, V_2^b, and V_2^c of Eqs. 1.29, in the effective potential. As explained, in order to include the nonzero decay width of the particles one has to go beyond the standard Hartree-Fock approximation by additionally including the two sunset diagrams, V_2^d and V_2^e of Eqs. 1.30. The complete expression for V_2 is obtained by the sum of all contributions,

$$V_2 = V_2^a + V_2^b + V_2^c + V_2^d + V_2^e \; . \tag{3.1}$$

The expectation values of the one- and two-point functions in the absence of external sources, σ and $\mathcal{S}$, $\mathcal{P}$, are determined from the stationary points of V,

$$\left.\frac{\delta V}{\delta\bar{\sigma}}\right|_{\bar{\sigma}=\sigma,\bar{S}=\mathcal{S},\bar{P}=\mathcal{P}} = 0 \; , \quad \left.\frac{\delta V}{\delta\bar{S}}\right|_{\bar{\sigma}=\sigma,\bar{S}=\mathcal{S},\bar{P}=\mathcal{P}} = 0 \; , \quad \left.\frac{\delta V}{\delta\bar{P}}\right|_{\bar{\sigma}=\sigma,\bar{S}=\mathcal{S},\bar{P}=\mathcal{P}} = 0 \; , \tag{3.2}$$

leading to an equation for the scalar condensate σ,

$$H = \mu^2\,\sigma + \frac{4\lambda}{N}\,\sigma^3 + \frac{4\lambda}{N}\,\sigma \int_Q \left[3\,\mathcal{S}(Q) + (N-1)\,\mathcal{P}(Q)\right] + \left.\frac{\delta V_2}{\delta\bar{\sigma}}\right|_{\bar{\sigma}=\sigma,\bar{S}=\mathcal{S},\bar{P}=\mathcal{P}} \; , \tag{3.3a}$$

where

$$\begin{aligned}\left.\frac{\delta V_2}{\delta\bar{\sigma}}\right|_{\bar{\sigma}=\sigma,\bar{S}=\mathcal{S},\bar{P}=\mathcal{P}} \;=\; & \left(\frac{4\lambda}{N}\right)^2 \sigma \left[2(N-1)\int_L\int_Q \mathcal{S}(L)\mathcal{P}(Q)\mathcal{P}(L+Q)\right. \\ & \left. + 3!\int_L\int_Q \mathcal{S}(L)\mathcal{S}(Q)\mathcal{S}(L+Q)\right] \; ,\end{aligned} \tag{3.3b}$$

and to the Dyson-Schwinger equations for the scalar and pseudoscalar propagators,

$$\mathcal{S}^{-1}(K;\sigma) \;=\; S^{-1}(K;\sigma) + \Sigma[K;\sigma] \; , \tag{3.3c}$$

$$\mathcal{P}^{-1}(K;\sigma) \;=\; P^{-1}(K;\sigma) + \Pi[K;\sigma] \; . \tag{3.3d}$$

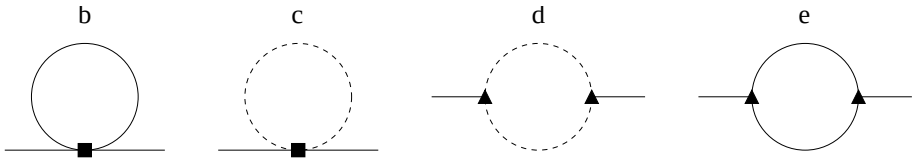

Figure 3.1: The self-energy of the σ-meson. The diagrams b and c are tadpole contributions generated by cutting an internal σ-line in the double-bubble diagrams b and c in Fig. 1.4. The diagrams d and e are one-loop contributions generated by cutting an internal σ-meson line in the sunset diagrams d and e of Fig. 1.4. Lines and vertices as in Fig. 1.4.

Here I introduced the self-energies of the scalar and pseudoscalar fields,

$$\Sigma = \Sigma^a + \Sigma^b + \Sigma^c + \Sigma^d + \Sigma^e \ , \quad \Pi = \Pi^a + \Pi^b + \Pi^c + \Pi^d + \Pi^e \ , \tag{3.4}$$

with

$$\Sigma^a \equiv 2\,\frac{\delta V_2^a}{\delta\bar{S}}\bigg|_{\bar\sigma=\sigma,\bar S=\mathcal{S},\bar P=\mathcal{P}} = 0 \ , \tag{3.5a}$$

$$\Sigma^b \equiv 2\,\frac{\delta V_2^b}{\delta\bar{S}}\bigg|_{\bar\sigma=\sigma,\bar S=\mathcal{S},\bar P=\mathcal{P}} = \frac{4\lambda}{N}\,3\int_Q \mathcal{S}(Q) \ , \tag{3.5b}$$

$$\Sigma^c \equiv 2\,\frac{\delta V_2^c}{\delta\bar{S}}\bigg|_{\bar\sigma=\sigma,\bar S=\mathcal{S},\bar P=\mathcal{P}} = \frac{4\lambda}{N}(N-1)\int_Q \mathcal{P}(Q) \ , \tag{3.5c}$$

$$\Sigma^d[K;\sigma] \equiv 2\,\frac{\delta V_2^d}{\delta\bar{S}}\bigg|_{\bar\sigma=\sigma,\bar S=\mathcal{S},\bar P=\mathcal{P}} = \left(\frac{4\lambda\sigma}{N}\right)^2 2(N-1)\int_Q \mathcal{P}(K-Q)\mathcal{P}(Q) \ , \tag{3.5d}$$

$$\Sigma^e[K;\sigma] \equiv 2\,\frac{\delta V_2^e}{\delta\bar{S}}\bigg|_{\bar\sigma=\sigma,\bar S=\mathcal{S},\bar P=\mathcal{P}} = \left(\frac{4\lambda\sigma}{N}\right)^2 3\cdot 3!\int_Q \mathcal{S}(K-Q)\mathcal{S}(Q) \tag{3.5e}$$

and

$$\Pi^a \equiv \frac{2}{N-1}\,\frac{\delta V_2^a}{\delta\bar{P}}\bigg|_{\bar\sigma=\sigma,\bar S=\mathcal{S},\bar P=\mathcal{P}} = \frac{4\lambda}{N}\,(N+1)\int_Q \mathcal{P}(Q) \ , \tag{3.6a}$$

$$\Pi^b \equiv \frac{2}{N-1}\,\frac{\delta V_2^b}{\delta\bar{P}}\bigg|_{\bar\sigma=\sigma,\bar S=\mathcal{S},\bar P=\mathcal{P}} = 0 \ , \tag{3.6b}$$

$$\Pi^c \equiv \frac{2}{N-1}\,\frac{\delta V_2^c}{\delta\bar{P}}\bigg|_{\bar\sigma=\sigma,\bar S=\mathcal{S},\bar P=\mathcal{P}} = \frac{4\lambda}{N}\int_Q \mathcal{S}(Q) \ , \tag{3.6c}$$

$$\Pi^d[K;\sigma] \equiv \frac{2}{N-1}\,\frac{\delta V_2^d}{\delta\bar{P}}\bigg|_{\bar\sigma=\sigma,\bar S=\mathcal{S},\bar P=\mathcal{P}} = \left(\frac{4\lambda\sigma}{N}\right)^2 4\int_Q \mathcal{P}(K-Q)\mathcal{S}(Q) \ , \tag{3.6d}$$

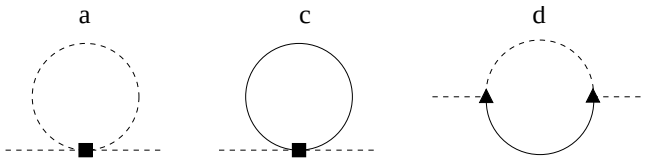

Figure 3.2: The self-energy of the pion. The diagrams a and c are tadpole contributions generated by cutting an internal pion line in the double-bubble diagrams a and c in Fig. 1.4. The diagram d is the one-loop contribution generated by cutting an internal pion line in the sunset diagram d in Fig. 1.4. Lines and vertices as in Fig. 1.4.

$$\Pi^e \equiv \frac{2}{N-1}\,\frac{\delta V_2^e}{\delta \bar{P}}\bigg|_{\bar{\sigma}=\sigma,\bar{S}=\mathcal{S},\bar{P}=\mathcal{P}} = 0\,. \tag{3.6e}$$

The calculation of the self-energy contributions Eqs. (3.5) and (3.6) corresponds to opening internal lines in the diagrams of Fig. 1.4. Employing this procedure to the double-bubble diagrams leads to the tadpole contributions for the self-energies of the σ-meson (see Figs. 3.1 b, c) and the pion (see Figs. 3.2 a, c). This defines the standard Hartree-Fock approximation. Additionally, the sunset diagrams of Figs. 1.4 d, e lead to the one-loop contributions shown in Figs. 3.1 d, e and 3.2 d. The latter contributions depend on the energy and the momentum of the particles and lead to nonvanishing imaginary parts for the self-energies. The explicit calculation of the self-energies (3.5) and (3.6) is discussed in Appendix A.1. The next step is to rewrite the set of Dyson-Schwinger equations (3.3c) and (3.3d) in terms of a set of integral equations for the spectral densities. In general, the spectral densities for the σ-meson and the pion are defined as

$$\rho_\sigma(\omega,\mathbf{k}) \equiv 2\,\mathrm{Im}\,\mathcal{S}(\omega+\mathrm{i}\eta,\mathbf{k};\sigma)\,, \tag{3.7a}$$

$$\rho_\pi(\omega,\mathbf{k}) \equiv 2\,\mathrm{Im}\,\mathcal{P}(\omega+\mathrm{i}\eta,\mathbf{k};\sigma)\,. \tag{3.7b}$$

If the imaginary parts of the self-energies are zero, as in the standard Hartree-Fock approximation, all particles are stable quasiparticles, i.e., their spectral densities become delta-functions with support on the quasiparticle mass shell,

$$\rho_\sigma(\omega,\mathbf{k}) = 2\pi\,Z_\sigma[\omega_\sigma(\mathbf{k}),\mathbf{k}]\,\{\delta[\omega-\omega_\sigma(\mathbf{k})]-\delta[\omega+\omega_\sigma(\mathbf{k})]\}\,, \tag{3.8a}$$

$$\rho_\pi(\omega,\mathbf{k}) = 2\pi\,Z_\pi[\omega_\pi(\mathbf{k}),\mathbf{k}]\,\{\delta[\omega-\omega_\pi(\mathbf{k})]-\delta[\omega+\omega_\pi(\mathbf{k})]\}\,, \tag{3.8b}$$

where $\omega_{\sigma,\pi}(\mathbf{k})$ are the quasiparticle energies for σ-meson and pions, defined by the positive solutions of

$$\omega_\sigma^2(\mathbf{k}) = k^2 + m_\sigma^2(\sigma) + \mathrm{Re}\,\Sigma[\omega_\sigma(\mathbf{k}),\mathbf{k};\sigma]\,, \tag{3.9a}$$

$$\omega_\pi^2(\mathbf{k}) \;=\; k^2 + m_\pi^2(\sigma) + \mathrm{Re}\,\Pi[\omega_\pi(\mathbf{k}),\mathbf{k};\sigma]\;, \tag{3.9b}$$

and

$$Z_\sigma[\omega_\sigma(\mathbf{k}),\mathbf{k}] \;\equiv\; \left|\frac{\partial \mathcal{S}^{-1}(K;\sigma)}{\partial k_0}\right|^{-1}_{k_0=\omega_\sigma(\mathbf{k})}\;, \tag{3.10a}$$

$$Z_\pi[\omega_\pi(\mathbf{k}),\mathbf{k}] \;\equiv\; \left|\frac{\partial \mathcal{P}^{-1}(K;\sigma)}{\partial k_0}\right|^{-1}_{k_0=\omega_\pi(\mathbf{k})}\;, \tag{3.10b}$$

are the wave-function renormalization factors on the quasi-particle mass shell. Since the real parts of the self-energies are even functions of energy, these factors are also even in $\omega_{\sigma,\pi}(\mathbf{k})$. In the standard Hartree-Fock approximation, the (real parts of the) self-energies do not depend on K^μ, such that

$$\omega_\sigma(k) = \sqrt{k^2 + M_\sigma^2(\sigma)}\;, \quad \omega_\pi(k) = \sqrt{k^2 + M_\pi^2(\sigma)}\;, \tag{3.11}$$

where

$$M_\sigma^2(\sigma) \equiv m_\sigma^2(\sigma) + \mathrm{Re}\,\Sigma(\sigma)\;, \quad \mathrm{M}_\pi^2(\sigma) \equiv \mathrm{m}_\pi^2(\sigma) + \mathrm{Re}\,\Pi(\sigma)\;, \tag{3.12}$$

are the effective σ-meson and pion masses, and

$$Z_\sigma[\omega_\sigma(k)] = \frac{1}{2\omega_\sigma(k)}\;, \quad Z_\pi[\omega_\pi(k)] = \frac{1}{2\omega_\pi(k)}\;. \tag{3.13}$$

For nonvanishing imaginary parts of the self-energies the spectral densities assume the following form:

$$\rho_\sigma(\omega,\mathbf{k}) \;=\; -\frac{2\,\mathrm{Im}\,\Sigma(\omega,\mathbf{k};\sigma)}{[\omega^2 - k^2 - m_\sigma^2(\sigma) - \mathrm{Re}\,\Sigma(\omega,\mathbf{k};\sigma)]^2 + [\mathrm{Im}\,\Sigma(\omega,\mathbf{k};\sigma)]^2}, \tag{3.14a}$$

$$\rho_\pi(\omega,\mathbf{k}) \;=\; -\frac{2\,\mathrm{Im}\,\Pi(\omega,\mathbf{k};\sigma)}{[\omega^2 - k^2 - m_\pi^2(\sigma) - \mathrm{Re}\,\Pi(\omega,\mathbf{k};\sigma)]^2 + [\mathrm{Im}\,\Pi(\omega,\mathbf{k};\sigma)]^2}. \tag{3.14b}$$

The general calculation of the imaginary parts of the self-energies is discussed in Appendix A.1. It turns out that they do not depend on the direction of 3-momentum $\mathbf{k}$, but only on the modulus k. The tadpole diagrams of Figs. 3.1 b, c (for the σ-meson) and Figs. 3.2 a, c (for the pion) do not have an imaginary part. Thus [see Appendix, Eq. (A.18)],

$$\begin{aligned}\mathrm{Im}\,\Sigma(\omega,\mathrm{k};\sigma) \;&=\; \mathrm{Im}\,\Sigma^{\mathrm{d}}(\omega,\mathrm{k};\sigma) + \mathrm{Im}\,\Sigma^{\mathrm{e}}(\omega,\mathrm{k};\sigma) \\ &=\; \left(\frac{4\lambda\sigma}{N}\right)^2 \frac{1}{2(2\pi)^3}\frac{1}{k}\int_{-\infty}^{\infty} d\omega_1\, d\omega_2\, [1 + f(\omega_1) + f(\omega_2)]\delta(\omega - \omega_1 - \omega_2)\end{aligned}$$

$$
\begin{aligned}
&\times \int_0^\infty dq_1\, q_1\, dq_2\, q_2\, \Theta\left(|q_1-q_2| \le k \le q_1+q_2\right) \\
&\times \left[2(N-1)\,\rho_\pi(\omega_1,q_1)\rho_\pi(\omega_2,q_2) + 3\cdot 3!\,\rho_\sigma(\omega_1,q_1)\rho_\sigma(\omega_2,q_2)\right], \qquad (3.15a)\\
\mathrm{Im}\,\Pi(\omega,\mathrm{k};\sigma) &= \mathrm{Im}\,\Pi^{\mathrm{d}}(\omega,\mathrm{k};\sigma) \\
&= \left(\frac{4\lambda\sigma}{N}\right)^2 \frac{1}{2(2\pi)^3}\frac{1}{k}\int_{-\infty}^{\infty} d\omega_1\, d\omega_2\, [1+f(\omega_1)+f(\omega_2)]\delta(\omega-\omega_1-\omega_2) \\
&\times \int_0^\infty dq_1\, q_1\, dq_2\, q_2\, \Theta\left(|q_1-q_2| \le k \le q_1+q_2\right) \\
&\times 4\,\rho_\sigma(\omega_1,q_1)\rho_\pi(\omega_2,q_2)\ , \qquad (3.15b)
\end{aligned}
$$

where $f(\omega) = [\exp(\omega/T)-1]^{-1}$ is the Bose-Einstein distribution function. These expressions are not ultraviolet divergent and thus do not need to be renormalised. For the real parts, I employ the following approximation. One only takes into account the Hartree-Fock contributions, arising from the tadpole diagrams Figs. 3.1 b, c (for the σ-meson) and Figs. 3.2 a, c (for the pion). As discussed above, these contributions do not depend on energy and momentum. The real parts of the diagrams in Figs. 3.1 d, e and 3.2 d are functions of energy and momentum and are much harder to compute, involving an additional numerical integration as compared to the respective imaginary parts (3.15). Therefore, in the present first step where I focus exclusively on the effects of a nonzero decay width, I neglect them. Consequently [see Appendix, Eq. (A.9)],

$$
\begin{aligned}
\mathrm{Re}\,\Sigma(\sigma) &= \mathrm{Re}\,\Sigma^{\mathrm{b}}(\sigma) + \mathrm{Re}\,\Sigma^{\mathrm{c}}(\sigma) \\
&= \frac{4\lambda}{N}\frac{4}{(2\pi)^3}\int_0^\infty d\omega\, dq\, q^2\, f(\omega)\ \left[3\,\rho_\sigma(\omega,q) + (N-1)\,\rho_\pi(\omega,q)\right], \qquad (3.16a)\\
\mathrm{Re}\,\Pi(\sigma) &= \mathrm{Re}\,\Pi^{\mathrm{a}}(\sigma) + \mathrm{Re}\,\Pi^{\mathrm{c}}(\sigma) \\
&= \frac{4\lambda}{N}\frac{4}{(2\pi)^3}\int_0^\infty d\omega\, dq\, q^2\, f(\omega)\ \left[\rho_\sigma(\omega,q) + (N+1)\,\rho_\pi(\omega,q)\right]. \qquad (3.16b)
\end{aligned}
$$

Since the real parts do not depend on energy and momentum, they only modify the masses of the σ-meson and the pion, cf. Eq. (3.12). Note that I only consider the temperature-dependent contributions in Eqs. (3.16). The omitted vacuum parts are ultraviolet divergent and have to be renormalised. The proper way to perform renormalization within the CJT-formalism was first presented in Refs. [vHK02a, vHK02c, vHK02b]. In the standard Hartree-Fock approximation for the $O(N)$ model, this leads to the same equations that one obtains applying the renormalization procedure of Ref. [LR00]. In that paper, the dependence of the results on the renormalization scale was studied in detail. It was found that simply neglecting the vacuum parts instead of applying the proper renormalization

procedure leads only to quantitative, but not to qualitative changes in the results. Since I am interested in the effect of nonzero imaginary parts for the self-energies and not in issues of renormalization, I simply neglect the vacuum parts. This prescription is also used to compute the tadpole and the sunset contributions in Eq. (3.3a) for the condensate.

After obtaining real and imaginary parts (3.16) and (3.15), respectively, one inserts them in the expressions (3.8) (if the imaginary part is zero) or (3.14) (if the imaginary part is nonzero) for the spectral densities. These spectral densities can then be used to again evaluate the real and imaginary parts of the self-energies. This defines an iterative scheme to self-consistently solve for the spectral densities as a function of energy and momentum. A convenient starting point for this scheme is the standard Hartree-Fock approximation, i.e., neglecting the imaginary parts altogether.

The self-consistently computed spectral densities obey a sum rule [LB00],

$$\int_{-\infty}^{\infty} \frac{d\omega}{2\pi}\, \omega\, \rho_{\sigma,\pi}(\omega, \mathbf{k}) = 1 \; . \tag{3.17}$$

In my calculation, there are two reasons why this sum rule may be violated. One is because I neglected the real parts of the self-energy diagrams in Figs. 3.1 d, e and 3.2 d. The other is due to the numerical realization of the above described iterative scheme. Numerically, one has to solve for the spectral density on a finite, discretized grid in energy-momentum space. If the imaginary part of the self-energy becomes very small, the spectral density converges towards a delta function. The support of the delta function may be located between grid sites, which causes a loss of spectral strength, which in turn violates the sum rule.

My prescription to restore the validity of the sum rule is the following. One first checks whether the imaginary part is smaller than the grid spacing (in my calculations, 10 MeV in both energy and momentum direction) at the location of the quasiparticle mass shell, $\omega = \omega_{\sigma,\pi}(k)$. If this is the case, one adds a sufficiently wide numerical realization of the delta function, $\delta_{\rm num}$, to the original spectral density, $\rho(\omega, k) \to \rho(\omega, k) + c \cdot \delta_{\rm num}[\omega - \omega_{\sigma,\pi}(k)]$, where c is a constant that is adjusted so that the sum rule is fulfilled on our energy-momentum grid,

$$\int_{-\omega_{\rm max}}^{\omega_{\rm max}} \frac{d\omega}{2\pi}\, \omega\, \rho_{\sigma,\pi}(\omega, \mathbf{k}) = 1 \; , \tag{3.18}$$

where $\omega_{\rm max}$ is the maximum energy on the energy-momentum grid.

On the other hand, if the imaginary part turns out to be sufficiently large, I presume that a possible violation of the sum rule (3.18) arises from neglecting

the real parts of the self-energy diagrams in Figs. 3.1 d, e and 3.2 d. In this case, one multiplies the spectral density by a constant, $\rho \to c' \cdot \rho$, where c' is adjusted so that the sum rule (3.18) is fulfilled. (By comparing the results to the case $c' = 1$, I found that this somewhat *ad hoc* correction procedure does not lead to major quantitative changes.)

Restricting the sum rule to a finite range in energy as in Eq. (3.18), however, causes the following problem. If the decay width of the particles is very large and consequently the spectral density a rather broad distribution around the quasiparticle mass shell, there will be parts which lie outside the energy-momentum grid. I could estimate the magnitude of this physical effect if I knew the behaviour of the spectral density at energies $\omega > \omega_{\max}$. This is possible at zero temperature (with the help of Weinberg's sum rules), but not at nonzero temperature. Here, I simply assume that this effect is sufficiently small to be neglected, i.e., I assume that a possible violation of the sum rule (3.18) is due to the two above mentioned artifacts and accordingly perform the correction of the spectral density.

Another physical effect which causes a loss of spectral strength is if the quasiparticle energy $\omega_{\sigma,\pi}(k) > \omega_{\max}$. In this case, I do not perform the correction of the spectral density as described above. This occurs at large momenta k, close to the edge of the energy-momentum grid. I checked that, in the numerical calculation of the integrals in Eqs. (3.15), the integrands become sufficiently small in this region, so that the imaginary parts are not sensitive to this effect.

This concludes the discussion of the improvement of the standard Hartree-Fock approximation by self-consistently including nonzero decay widths.

3.3 Results

In this section I present the numerical results for the $O(4)$ linear sigma model obtained in the Hartree-Fock approximation improved by including nonzero decay widths, as discussed in Sec. 3.2. The condensate σ is shown in the left part of Fig. 3.3 as a function of temperature for the standard and the improved Hartree-Fock approximation. The qualitative behaviour is similar in the two approximations: the condensate drops significantly with temperature indicating the restoration of chiral symmetry. Since I consider the case of explicit $O(4)$ symmetry breaking by taking $H \neq 0$ in Eq. (1.22), the chiral phase transition is a crossover transition. Nevertheless, one can define a transition temperature,

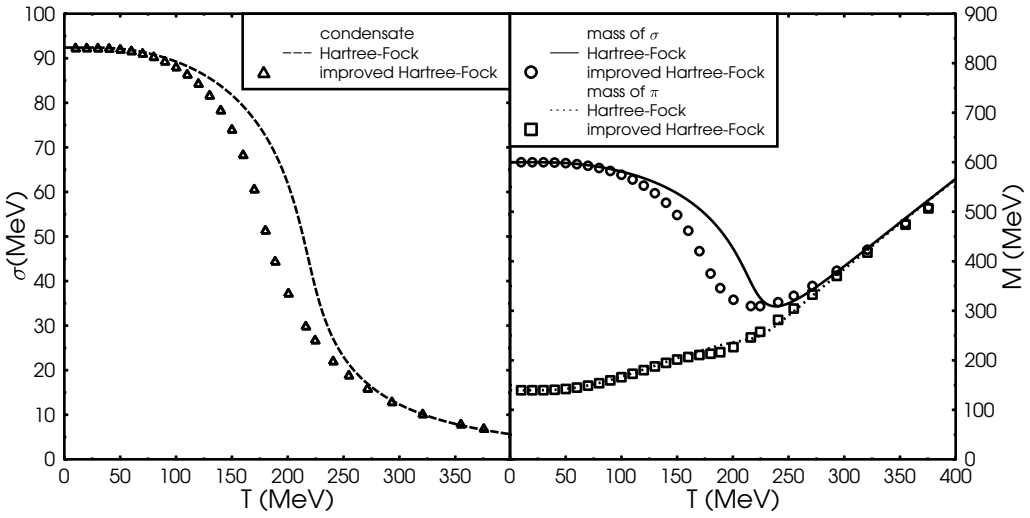

Figure 3.3: The values for the condensate (left panel) and the effective masses of the σ-meson and the pion, (right panel) as functions of temperature. The values are calculated in the standard Hartree-Fock approximation (dashed and solid lines) and in the improved Hartree-Fock approximation (symbols) as discussed in Sec. 3.2.

T_χ, as the temperature where the chiral susceptibility $\partial\sigma/\partial T$ assumes a maximum. Quantitatively, the inclusion of a nonzero decay width lowers T_χ by about 20% as compared to the standard Hartree-Fock approximation. The transition temperature $T_\chi \simeq 175$ MeV agrees within error bars with recent lattice results, $T_\chi \simeq 172 \pm 5$ MeV for the two-flavour case [LP03]. (Note, however, that the latter value is extracted from an extrapolation to the chiral limit, while my results are for the case of explicit symmetry breaking, i.e., for nonzero quark masses.)

For the solution of the condensate equation (3.3a) the relative magnitude of the contribution from the sunset diagrams, Eq. (3.3b), is negligibly small, of order $\sim 10^{-4}$, and thus can be safely neglected. In turn, not having to compute the integrals pertaining to the double loop, cf. Eq. (A.24), considerably speeds up the computation.

In the right part of Fig. 3.3, I show the effective masses $M_\sigma \equiv m_\sigma^2 + \mathrm{Re}\,\Sigma$ and $M_\pi \equiv m_\pi^2 + \mathrm{Re}\,\Pi$ of the σ-meson and the pion as functions of temperature in both approximation schemes. Since the decay width of the pion remains comparatively small, cf. Fig. 3.4, the mass of the pion does not change appreciably when taking the nonzero decay width into account. On the other hand, the large

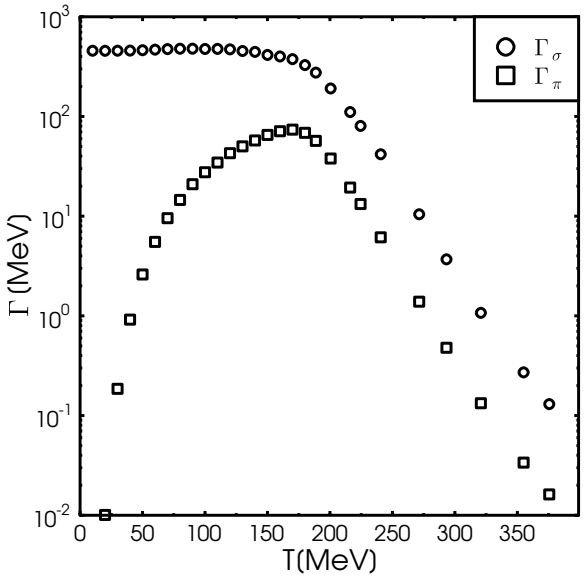

Figure 3.4: The decay width of the σ-meson, $\Gamma_\sigma = \mathrm{Im}\Sigma(\omega_\sigma)/\omega_\sigma$, and the pion, $\Gamma_\pi = \mathrm{Im}\Pi(\omega_\pi)/\omega_\pi$, in the improved Hartree-Fock approximation as a function of the temperature at momentum $k = 325$ MeV.

decay width of the σ-meson at temperatures below T_χ, cf. Fig. 3.4, does influence the mass: in this range of temperatures the mass exhibits a stronger decrease with temperature in the improved Hartree-Fock approximation. At large temperatures $T > T_\chi$, the decay width of the σ-meson becomes negligibly small, cf. Fig. 3.4, and the mass approaches the value computed in the standard Hartree-Fock approximation. Both σ-meson and pion masses approach each other above T_χ, indicating the restoration of chiral symmetry.

In Fig. 3.4 I show the decay widths of σ-mesons and pions, defined as [Wel83, LB00]

$$\Gamma_\sigma(k) \equiv \frac{\mathrm{Im}\,\Sigma[\omega_\sigma(\mathrm{k}),\mathrm{k};\sigma]}{\omega_\sigma(k)}\,, \quad \Gamma_\pi(k) \equiv \frac{\mathrm{Im}\,\Pi[\omega_\pi(\mathrm{k}),\mathrm{k};\sigma]}{\omega_\pi(k)}\,, \tag{3.19}$$

where $\omega_{\sigma,\pi}(k)$ is the energy on the quasi-particle mass shell, cf. Eq. (3.9). At small temperatures, due to the possible decay of a σ-meson into two pions, the decay width of the former is large, of the order of its mass. Note that the value $\Gamma_\sigma \simeq 460$ MeV obtained here at $T = 0$ is completely determined by the parameters m^2, λ, and H of the $O(4)$ model, i.e., without adjusting any additional parameter. It is reasonably close to the experimentally measured value $\Gamma_\sigma \sim (600 - 1000)$ MeV [EHO$^+$04]. The σ decay width increases with tempera-

ture up to a maximum of about 500 MeV at a temperature $T \simeq 100$ MeV and then decreases rapidly. The decay width of the pion vanishes at $T = 0$. It increases at nonzero temperature and assumes a maximum at about $T \simeq 180$ MeV. At this temperature the decay width is about half of the corresponding pion mass. It decreases rapidly at higher temperature. Although the decay widths of both particles decrease at high temperatures, they do not become degenerate, the decay width of the σ-meson remains about a factor of 8 larger than that of the pion. This difference can be traced to the symmetry factors multiplying the one-loop self-energies for the σ-meson and pion, cf. Eqs. (3.15). For the σ-meson, there is a factor $2(N-1)$ in front of the pion loop and a factor $3 \cdot 3!$ in front of the σ-loop, so that the overall factor is $\sim 2(N-1)+3 \cdot 3! = 24$. For the pion, there is only a mixed σ-pion loop with a symmetry factor 4. From this simple argument one already expects that the decay width of the σ-meson is about a factor of 6 larger than that of the pion. The remaining difference comes from the fact that the self-consistently computed spectral densities of σ-meson and pion under the integrals in Eqs. (3.15) are also different, cf. Fig. 3.7.

One might argue that, at asymptotically large temperatures, effects from chiral symmetry breaking can no longer play a role and the decay widths, as well as the spectral densities, of σ-meson and pion should become degenerate. This is true in the chiral limit, where there is a thermodynamic phase transition between the phases of broken and restored chiral symmetry, and where $\sigma \equiv 0$ in the latter phase. Here, however, I consider the case of explicitly broken chiral symmetry, where $\sigma > 0$, even when the temperature is very large. Since the decay widths are proportional to σ^2, they also do not vanish at large temperature. The difference in the symmetry factors for the self-energies of σ-mesons and pions then leads to different values for the decay widths and spectral densities.

The self-consistently calculated spectral densities of the σ-meson and the pion as functions of the external energy ω and momentum k are shown in Fig. 3.5 and Fig. 3.6 for different temperatures, $T = 80$, 160, 240, and 320 MeV. For a detailed discussion, let us fix the momentum at $k = 325$ MeV and consider the spectral densities as functions of energy ω for different temperatures, cf. Fig. 3.7. At all temperatures, the pion spectral density (dotted line) exhibits a pronounced peak on the mass shell, at $\omega_\pi(k) = \sqrt{k^2 + M_\pi^2(\sigma)}$. When the temperature is below 200 MeV, such that $M_\pi \simeq m_\pi = 139.5$ MeV, cf. Fig. 3.3, the peak is located at $\omega_\pi(325\,\mathrm{MeV}) \simeq 350$ MeV. Above $T \sim 200$ MeV, M_π increases significantly with temperature, and the position of the peak shifts towards larger energies,

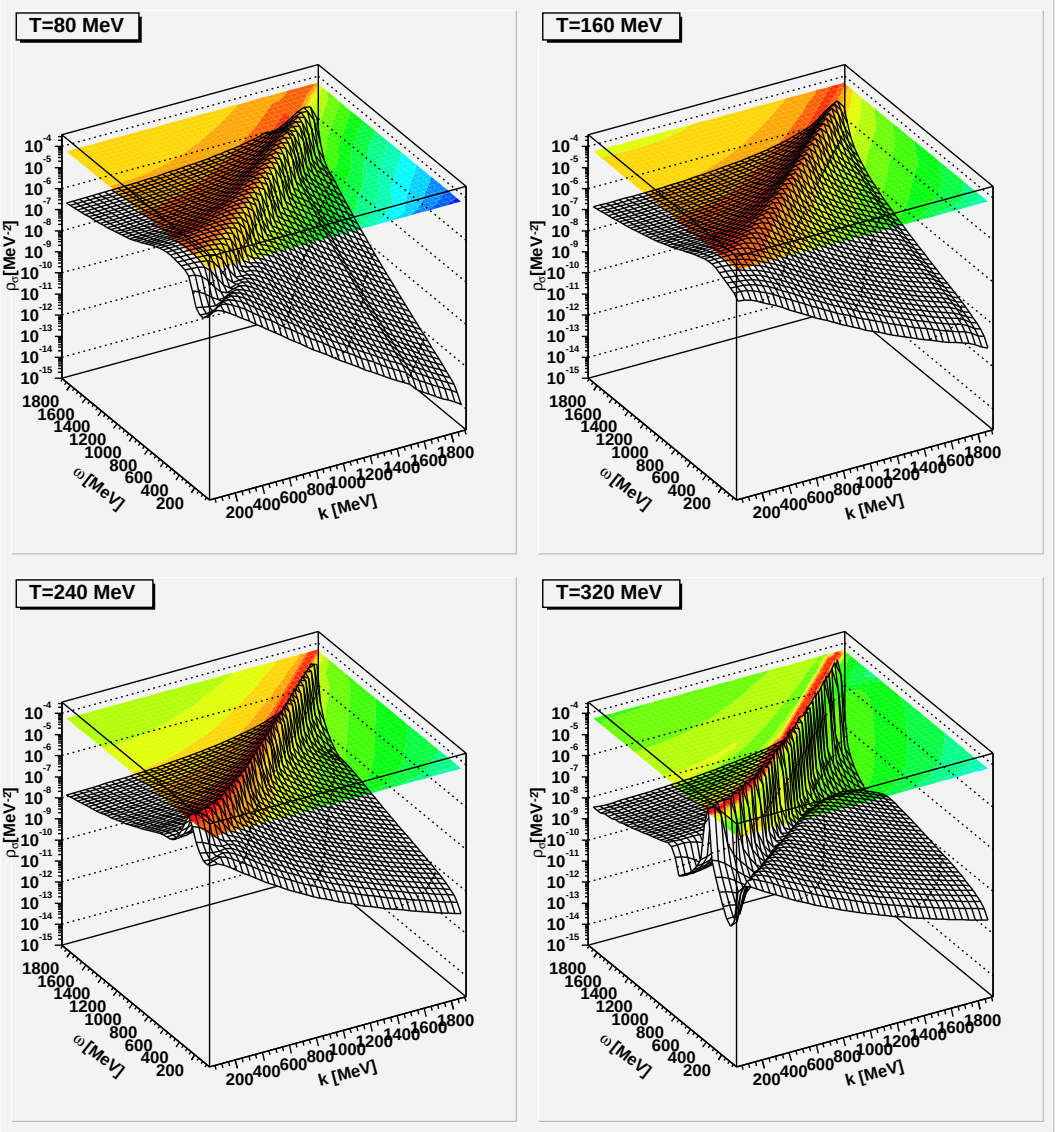

Figure 3.5: The spectral density of the σ-meson as a function of energy ω and momentum k at temperatures 80, 160, 240, and 320 MeV.

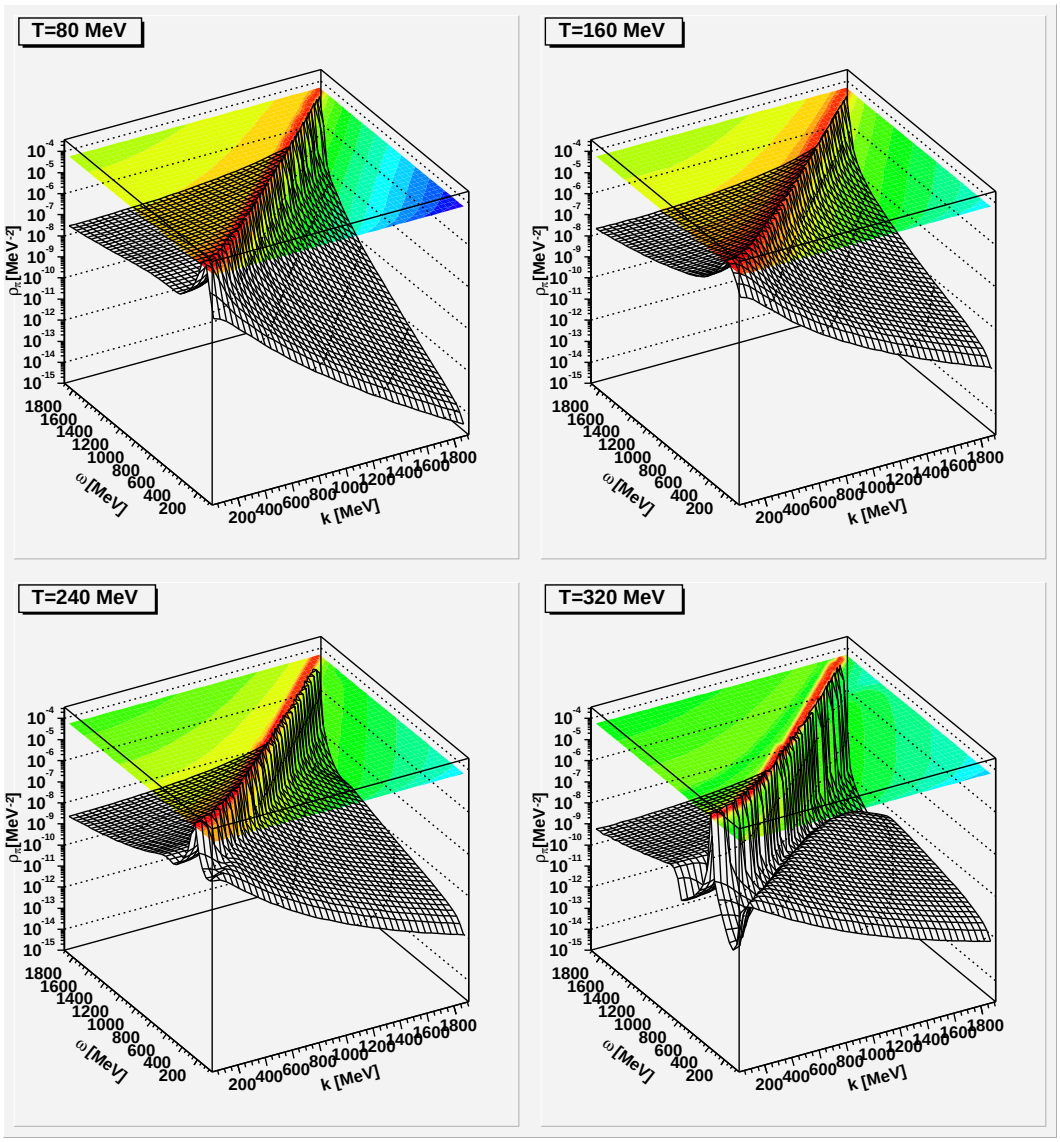

Figure 3.6: The spectral density of the pion as a function of energy ω and momentum k at temperatures 80, 160, 240, and 320 MeV.

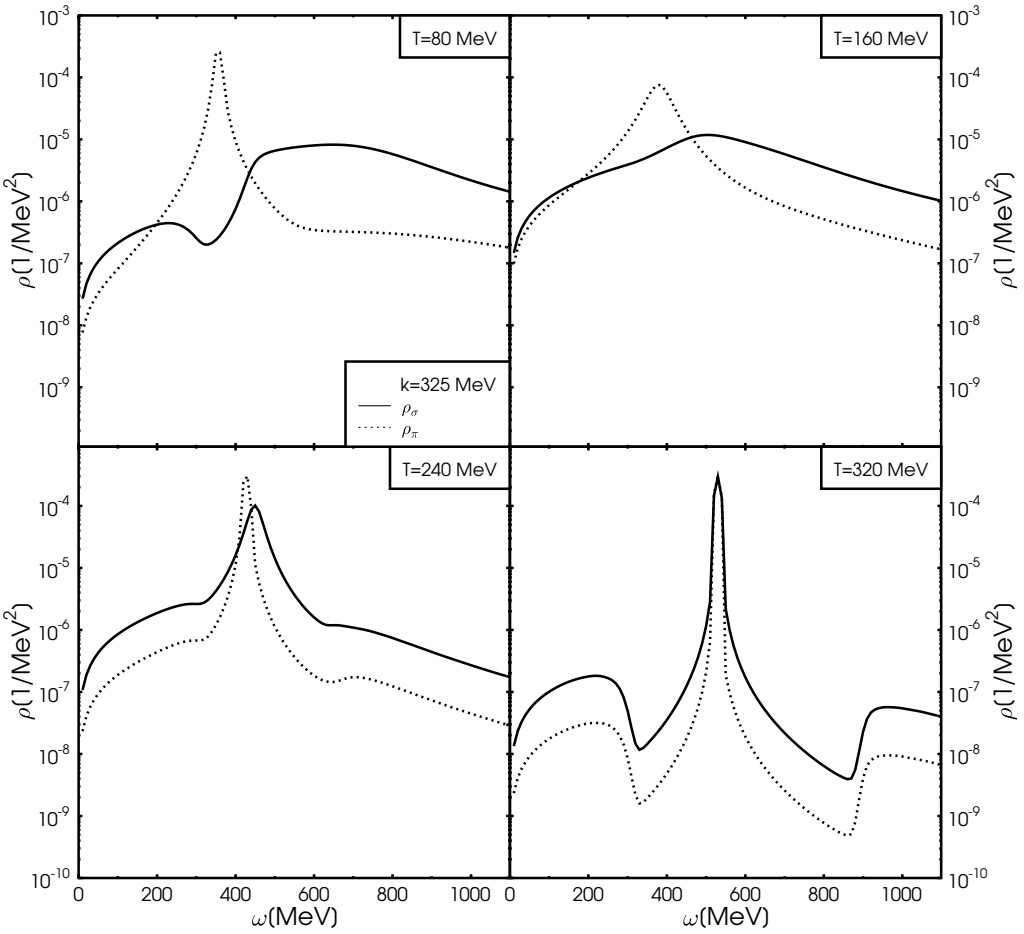

Figure 3.7: The spectral density of the σ-meson and pion as a function of energy ω at temperatures 80, 160, 240, and 320 MeV. The momentum is $k = 325$ MeV.

$\omega_\pi(325\,\mathrm{MeV}) \simeq 500$ MeV. The broadening of the peak is due to scattering of the pion off σ-mesons in the medium.

In contrast to the pion spectral density, for temperatures below ~ 170 MeV the σ spectral density (full line) does not exhibit a peak at the mass shell, $\omega_\sigma(k) = \sqrt{k^2 + M_\sigma^2(\sigma)}$. The reason is that $\omega_\sigma(k)$ is still sufficiently large to allow for the decay into two pions. Consequently, in this temperature range the σ spectral density is very broad. On the other hand, for temperatures above ~ 170 MeV, where $\omega_\sigma(k)$ drops below $2\,M_\pi$, the two-pion decay channel is closed and the σ spectral density develops a distinct peak, whose width is due to scattering of the σ-mesons off pions and other σ-mesons in the medium.

Two other features of the spectral densities shown in Fig. 3.7 are noteworthy. The first is the region below the light-cone, $K^2 = \omega^2 - k^2 < 0$, where the mesons are Landau-damped. The second is the two-particle decay threshold. For $\sigma \to \pi\pi$, this threshold is located at $\omega \sim 2\,M_\pi$, for $\sigma \to \sigma\sigma$, it is at $\omega \sim 2\,M_\sigma$, and for $\pi \to \sigma\pi$ at $\omega \sim M_\sigma + M_\pi$. The threshold is most clearly seen at large temperatures, e.g. $T = 320$ MeV, when both particles become degenerate in mass, $M_\sigma \simeq M_\pi \sim 400$ MeV, and the threshold is at $\omega \sim 900$ MeV.

–IV–

The improved Hartree approximation

4.1 Motivation

In the standard Hartree (or Hartree-Fock) approximation of the $O(N)$ model, one only takes into account the double-bubble diagrams. In these approximations the self-energies of the particles are only real valued, therefore no decay width effects are included. The difference between the Hartree and the Hartree-Fock approximation is, that in the Hartree approximation all terms of order $\sim 1/N$ are neglected on the level of the Dyson-Schwinger and the condensate equations. In the last chapter I presented the so-called improved Hartree-Fock approximation, which takes additionally into account sunset type diagrams. This leads to 4-momentum dependent real and imaginary parts in the Dyson-Schwinger equations. Indeed, in Chapter III, I neglected the 4-momentum dependent *real* parts of the Dyson-Schwinger equations for simplicity. In the present Chapter, I include them, although in the Hartree approximation [Röd05]. This leads to a vanishing imaginary part of the pion self-energy (because it is of order $\sim 1/N$), i.e., the spectral density of the pion is just a delta function. As shown in chapter III, the inclusion of the pion decay width does not lead to a major change of the results, therefore this is still a good approximation for the pion. The contributions from the $\sigma \to 2\sigma$ decay, in the self-energy of the σ-meson, is also of order $\sim 1/N$, and vanishes, but (a part of) the contribution from the $\sigma \to 2\pi$ decay remains. Therefore, its spectral density has a nonzero width, as expected for the σ-meson with a very large (vacuum) decay width, $\Gamma_\sigma = (600 - 1000)$ MeV. In the following, I

σ-meson vacuum mass	explicit chiral symmetry breaking $m_\pi = 139.5\,\mathrm{MeV}, f_\pi = 92.4\,\mathrm{MeV}$ $H = (121.6\,\mathrm{MeV})^3$	chiral limit $m_\pi = 0\,\mathrm{MeV}, f_\pi = 90\,\mathrm{MeV}$ $H = 0$
$m_\sigma = 400\,\mathrm{MeV}$	$\lambda = 8.230$ $\mu^2 = -(225.41\,\mathrm{MeV})^2$	$\lambda = 9.877$ $\mu^2 = -(282.84\,\mathrm{MeV})^2$
$m_\sigma = 600\,\mathrm{MeV}$	$\lambda = 19.043$ $\mu^2 = -(388.34\,\mathrm{MeV})^2$	$\lambda = 22.222$ $\mu^2 = -(424.264\,\mathrm{MeV})^2$
$m_\sigma = 800\,\mathrm{MeV}$	$\lambda = 36.341$ $\mu^2 = -(539.27\,\mathrm{MeV})^2$	$\lambda = 39.506$ $\mu^2 = -(565.685\,\mathrm{MeV})^2$

Table 4.1: The masses and decay constants at vanishing temperature and the corresponding parameter sets for the $O(4)$ linear sigma model for the two symmetry breaking patterns studied here.

call this the improved Hartree approximation.
As discussed in Sec. 1.4, the parameter H is given as a function of the vacuum mass m_π, and the vacuum decay constant f_π of the pion : $H = m_\pi^2 f_\pi$. In this chapter I compare the chiral limit, $m_\pi = 0$ and $f_\pi = 90$ MeV, with the case of explicit chiral symmetry breaking, $m_\pi = 139.5$ MeV and $f_\pi = 92.4$ MeV. The bare mass μ^2 and the four-point coupling λ depends additionally on the vacuum mass of the σ-meson m_σ: $\mu^2 = -(m_\sigma^2 - 3\,m_\pi^2)/2$, and $\lambda = N(m_\sigma^2 - m_\pi^2)/(8 f_\pi^2)$. As mentioned above, the decay width of the σ-meson in vacuum is very large, therefore its vacuum mass is not well defined, $m_\sigma = (400 - 1200)$ MeV [EHO$^+$04]. I compare the results for $m_\sigma = 400,\ 600$, and 800 MeV. The parameter sets of the model, for $N = 4$, are summarised in table 4.1.

4.2 The Dyson-Schwinger and the condensate equations

In the following I repeat the derivation of the condensate and the Dyson-Schwinger equations in the CJT formalism, as discussed in chapter III, and show how the equations simplify in the improved Hartree approximation. The diagrams included in the effective potential are the three double-bubble diagrams [$\sim (\int \bar{P})^2$, $\sim (\int \bar{S})^2$, and $\sim \int \bar{P} \int \bar{S}$] shown in Figs. 1.4 a, b, c, and the two sunset

diagrams ($\sim \int\int \bar{S}\bar{P}\bar{P}$ and $\sim \int\int \bar{S}\bar{S}\bar{S}$) shown in Figs. 1.4 d, e. To get the expectation values for the one- and two-point functions in the absence of external sources, σ, $\mathcal{S}$, and $\mathcal{P}$, one has to find the stationary points of the effective potential (1.25). Minimisation of the effective potential with respect to the one-point function

$$\left.\frac{\delta V}{\delta\bar{\sigma}}\right|_{\bar{\sigma}=\sigma,\bar{S}=\mathcal{S},\bar{P}=\mathcal{P}} = 0, \tag{4.1}$$

leads to an equation for the scalar condensate σ,

$$\begin{aligned} H &= \mu^2\,\sigma + \frac{4\lambda}{N}\,\sigma^3 + \frac{4\lambda}{N}\,\sigma \int_Q \left[3\,\mathcal{S}(Q) + (N-1)\,\mathcal{P}(Q)\right] \\ &+ \left(\frac{4\lambda}{N}\right)^2 \sigma \left[2(N-1)\int_L\int_Q \mathcal{S}(L)\mathcal{P}(Q)\mathcal{P}(L+Q)\right. \\ &\qquad \left. + 3!\int_L\int_Q \mathcal{S}(L)\mathcal{S}(Q)\mathcal{S}(L+Q)\right]\,. \end{aligned} \tag{4.2}$$

Using the fact that $\sigma^2 \sim N$ [cf. Eq. (1.26)], this equation becomes in the large-N limit,

$$H = \sigma\left\{\mu^2 + \frac{4\lambda}{N}\left[\sigma^2 + N\int_Q \mathcal{P}(Q)\right]\right\}. \tag{4.3}$$

The minimisation of the effective potential with respect to the two-point functions,

$$\left.\frac{\delta V}{\delta\bar{S}}\right|_{\bar{\sigma}=\sigma,\bar{S}=\mathcal{S},\bar{P}=\mathcal{P}} = 0\,, \quad \left.\frac{\delta V}{\delta\bar{P}}\right|_{\bar{\sigma}=\sigma,\bar{S}=\mathcal{S},\bar{P}=\mathcal{P}} = 0\,, \tag{4.4}$$

leads to the Dyson-Schwinger equations for the scalar and pseudoscalar propagators, $\mathcal{S}$ and $\mathcal{G}$,

$$\mathcal{S}^{-1}(K;\sigma) = S^{-1}(K;\sigma) + \Sigma(K;\sigma)\,, \tag{4.5a}$$

$$\mathcal{P}^{-1}(K;\sigma) = P^{-1}(K;\sigma) + \Pi(K;\sigma)\,. \tag{4.5b}$$

Here I introduced the self-energy of the scalar

$$\begin{aligned} \Sigma(K;\sigma) &\equiv 2\left.\frac{\delta V_2}{\delta\bar{S}}\right|_{\bar{\sigma}=\sigma,\bar{S}=\mathcal{S},\bar{P}=\mathcal{P}} \\ &= \frac{4\lambda}{N}\left[3\int_Q \mathcal{S}(Q) + (N-1)\int_Q \mathcal{P}(Q)\right] \\ &+ \left(\frac{4\lambda\sigma}{N}\right)^2\left[2(N-1)\int_Q \mathcal{P}(K-Q)\mathcal{P}(Q)\right. \\ &\qquad \left. + 3\cdot 3!\int_Q \mathcal{S}(K-Q)\mathcal{S}(Q)\right] \end{aligned} \tag{4.6a}$$

and pseudoscalar fields

$$\begin{aligned}\Pi(K;\sigma) &\equiv \frac{2}{N-1}\,\frac{\delta V_2}{\delta \bar{P}}\bigg|_{\bar{\sigma}=\sigma,\bar{S}=\mathcal{S},\bar{P}=\mathcal{P}} \\ &= \frac{4\lambda}{N}\left[\int_Q \mathcal{S}(Q) \;+(N+1)\int_Q \mathcal{P}(Q)\right] \\ &+ \left(\frac{4\lambda\sigma}{N}\right)^2 4\int_Q \mathcal{P}(K-Q)\mathcal{S}(Q)\;. \qquad (4.6b)\end{aligned}$$

In the large-N limit, all σ-meson tadpoles and a part of the pion tadpole ($\sim \int \mathcal{S}$ and $\sim \int \mathcal{P}$) vanish, and only a part of the pion term ($\sim \int \mathcal{P}\mathcal{P}$) remains,

$$\Sigma(K;\sigma) = \frac{4\lambda}{N}N\int_Q \mathcal{P}(Q) \;+\left(\frac{4\lambda\sigma}{N}\right)^2 2\,N\int_Q \mathcal{P}(K-Q)\mathcal{P}(Q)\;, \qquad (4.7a)$$

$$\Pi(K;\sigma) = \frac{4\lambda}{N}N\int_Q \mathcal{P}(Q). \qquad (4.7b)$$

The tadpole contributions have no imaginary parts, therefore

$$\mathrm{Im}\,\Sigma(\mathrm{K};\sigma) = \left(\frac{4\lambda\sigma}{N}\right)^2 2\,N\,\mathrm{Im}\int_{\mathrm{Q}} \mathcal{P}(\mathrm{K}-\mathrm{Q})\mathcal{P}(\mathrm{Q})\;, \qquad (4.8a)$$

$$\mathrm{Im}\,\Pi = 0. \qquad (4.8b)$$

The imaginary part of the σ-meson self-energy depends on the 4-momentum vector, $K=(\mathbf{k},\omega)$, but the real part can be split into terms which do not depend on K, $[\mathrm{Re}\,\Sigma]_1$, arising from the tadpole contribution, and terms which are 4-momentum dependent, $[\mathrm{Re}\,\Sigma(\mathrm{K},\sigma)]_2$, arising from the sunset diagram,

$$\mathrm{Re}\,\Sigma(\mathrm{K};\sigma) = [\mathrm{Re}\,\Sigma]_1 + [\mathrm{Re}\,\Sigma(\mathrm{K};\sigma)]_2, \qquad (4.9)$$

where

$$[\mathrm{Re}\,\Sigma]_1 = \frac{4\lambda}{N}\,N\int_Q \mathcal{P}(Q)\;, \qquad (4.10a)$$

$$[\mathrm{Re}\,\Sigma(\mathrm{K};\sigma)]_2 = \left(\frac{4\lambda\sigma}{N}\right)^2 2\,N\,\mathrm{Re}\int_{\mathrm{Q}} \mathcal{P}(\mathrm{K}-\mathrm{Q})\mathcal{P}(\mathrm{Q}). \qquad (4.10b)$$

As mentioned above, the 4-momentum dependent terms in the pion self-energy vanish in the large-N limit. The 4-momentum independent term of the real part of the pion self-energy is the same as for the σ-meson,

$$\mathrm{Re}\,\Pi = [\mathrm{Re}\,\Sigma]_1 = \frac{4\lambda}{N}\,N\int_{\mathrm{Q}} \mathcal{P}(\mathrm{Q})\;. \qquad (4.11)$$

I want to calculate the spectral density of the σ-meson, ρ_σ. To this aim, I rewrite the Dyson-Schwinger equations (4.5) and the equation for the chiral condensate (4.3) as functions of the spectral density of the pion ρ_π. In the large-N limit, the imaginary part of the pion vanishes, and therefore the spectral density is just a delta function

$$\rho_\pi(\omega, k) = \frac{\pi}{\omega_\pi(k)} \left\{\delta[\omega - \omega_\pi(k)] - \delta[\omega + \omega_\pi(k)]\right\} \ , \tag{4.12}$$

with support on the quasiparticle energy for the pion $\omega_\pi(k)$,

$$\omega_\pi(k) = \sqrt{k^2 + M_\pi^2(\sigma)} \ , \tag{4.13}$$

where I defined an effective mass for the pion M_π,

$$M_\pi^2(\sigma) \equiv m_\pi^2(\sigma) + \mathrm{Re}\,\Pi \ . \tag{4.14}$$

In the chirally broken phase ($\sigma \neq 0$) the imaginary part of the σ-meson is nonzero, therefore the spectral density assumes the following form:

$$\rho_\sigma(\omega, \mathbf{k}) = -\frac{2\,\mathrm{Im}\,\Sigma(\omega, \mathbf{k}; \sigma)}{[\omega^2 - k^2 - m_\sigma^2(\sigma) - \mathrm{Re}\,\Sigma(\omega, \mathbf{k}; \sigma)]^2 + [\mathrm{Im}\,\Sigma(\omega, \mathbf{k}; \sigma)]^2} \ . \tag{4.15}$$

In the chirally restored phase ($\sigma = 0$) the 4-momentum dependent parts of the σ-meson self-energy vanish, hence also the spectral density of the σ-meson becomes a delta function,

$$\rho_\sigma(\omega, k) = \frac{\pi}{\omega_\sigma(k)} \left\{\delta[\omega - \omega_\sigma(k)] - \delta[\omega + \omega_\sigma(k)]\right\} \ , \tag{4.16}$$

with support on the quasiparticle energy for the σ-meson $\omega_\sigma(k)$,

$$\omega_\sigma(k) = \sqrt{k^2 + M_\sigma^2(\sigma)} \ , \tag{4.17}$$

where I defined an effective mass for the σ-meson M_σ,

$$M_\sigma^2(\sigma) \equiv m_\sigma^2(\sigma) + [\mathrm{Re}\,\Sigma]_1 \ . \tag{4.18}$$

Note that in the chirally broken phase ($\sigma \neq 0$), the quasiparticle energy for the σ-meson $\omega_\sigma(\mathbf{k})$ is given by the solution of

$$\omega_\sigma^2(\mathbf{k}) - k^2 - M_\sigma^2(\sigma) - [\mathrm{Re}\,\Sigma(\omega_\sigma(\mathbf{k}), \mathbf{k}; \sigma)]_2 = 0. \tag{4.19}$$

The imaginary and the real parts of the self-energies, Eqs. (4.8a), (4.10b), and (4.11), can be written as functions of the pion spectral density. Note that for

the real parts, I only consider temperature-dependent contributions and neglect the (ultraviolet divergent) vacuum parts, which is a simple way to renormalize the integrals. The imaginary parts are not ultraviolet divergent and thus do not need to be renormalised. The 4-momentum independent term is just the standard tadpole integral, cf. Eq. (A.26),

$$\mathrm{Re}\,\Pi = [\mathrm{Re}\,\Sigma]_1 = \frac{1}{2\pi^2}\int_0^\infty dq\; q^2[\omega_\pi(q)]^{-1}\mathrm{f}[\omega_\pi(q)]. \tag{4.20}$$

The derivation of the equations for the 4-momentum dependent terms is given in appendix A.2,

$$\begin{aligned}
\mathrm{Im}\,\Sigma(\omega,\mathrm{k}) &= \left(\frac{4\lambda\sigma}{N}\right)^2 \frac{N}{8\pi}\frac{1}{k}\int_0^\infty dq\; q\,[\omega_\pi(q)]^{-1}\Theta\left(|q_0-q|\le k\le q_0+q\right) \\
&\times \{1+f[\omega_\pi(q_0)]+f[\omega_\pi(q)]\}, \qquad (4.21a)\\
[\mathrm{Re}\,\Sigma(\omega,\mathrm{k})]_2 &= \left(\frac{4\lambda\sigma}{N}\right)^2 \frac{N}{8\pi^2}\frac{1}{k}\mathrm{P}\int_0^\infty dq_1\, q_1\, dq_2\, q_2 \\
&\times \Theta\left(|q_1-q_2|\le k\le q_1+q_2\right)[\omega_\pi(q_1)\omega_\pi(q_2)]^{-1} \\
&\times \left\{\frac{f[\omega_\pi(q_1)]+f[\omega_\pi(q_2)]}{\omega_\pi(q_1)+\omega_\pi(q_2)-\omega}+\frac{f[\omega_\pi(q_1)]+f[\omega_\pi(q_2)]}{\omega_\pi(q_1)+\omega_\pi(q_2)+\omega}\right. \qquad (4.21b)\\
&\quad \left.+\frac{-f[\omega_\pi(q_1)]+f[\omega_\pi(q_2)]}{\omega_\pi(q_1)-\omega_\pi(q_2)-\omega}+\frac{-f[\omega_\pi(q_1)]+f[\omega_\pi(q_2)]}{\omega_\pi(q_1)-\omega_\pi(q_2)+\omega}\right\},
\end{aligned}$$

where $f(\omega)\equiv 1/[\exp(\omega/T)-1]$ is the Bose-Einstein distribution function, $q_0\equiv\sqrt{[\omega-\omega_\pi(q)]^2-M_\pi^2}$, and $\mathrm{P}\int\ldots$ denotes the principal value of the integral. Note that $\Theta\left(|q_1-q_2|\le k\le q_1+q_2\right)/k = 2\delta(q_1-q_2)$ in the limit $k\to 0$, which can be used to perform the q-integration, cf. Eqs. (A.38), and (A.44). An appropriate way to perform the principal value numerically is discussed in the appendix, cf. Eqs. (A.43), and (A.44).

The spectral densities have to obey a sum rule [LB00],

$$\int_{-\infty}^{\infty}\frac{\mathrm{d}\omega}{2\pi}\,\omega\,\rho_{\sigma,\pi}(\omega,\mathbf{k}) = 1\,. \tag{4.22}$$

In the improved Hartree approximation, the spectral density of the pion (4.12) is just a delta function, and normalised in such way that this sum rule is *a priori* fulfilled. As mentioned above, this is not the case for the σ-meson spectral density in the chirally broken phase. The main reason for a possible violation of the sum rule is due to neglecting terms of the order $\sim 1/N$ in the self-energy, which leads to a loss of spectral strength. I found that the inclusion of the

4-momentum dependent real part $[\mathrm{Re}\,\Sigma]_2$ is close to negligible for the validity of the sum rule. Other possible problems arise from the numerical realisation of the spectral density on a finite $\omega_{max} \times k_{max}$ energy-momentum grid, where $\omega_{max} \geq |\omega|$ and $k_{max} \geq |k|$ are the boundaries of the grid. If the imaginary part of the self-energy becomes very small, the spectral density becomes more and more a delta function, which one has to realise numerically. On the other side, if this imaginary part is very large, i.e., the width of the spectral density becomes very large, one has to use a large ω_{max}, otherwise one loses too much spectral strength for energies $\omega > \omega_{max}$. To minimise these numerical problems, I use a rather large and fine (quadratic) energy-momentum grid, with $\omega_{max} = k_{max} = 2$ GeV and a lattice spacing of 5 MeV.
As discussed in Chapter III, if the sum rule is not fulfilled, I use the following way to restore it. If the imaginary part of the σ-meson self-energy is very small, I add a numerical realisation of a delta function δ_{num} to the spectral density: $\rho'_\sigma(\omega, k) \to \rho_\sigma(\omega, k) + c_1 \cdot \delta_{\mathrm{num}}[\omega - \omega_\sigma(k)]$. If the imaginary part of the self-energy is large enough (compared with the lattice spacing) I just multiply the spectral density by a factor: $\rho'_\sigma(\omega, k) \to c_2 \cdot \rho_\sigma(\omega, k)$. The constants c_1 and c_2 are adjusted in a way that ρ'_σ fulfills the sumrule on the energy-momentum grid

$$\int_{-\omega_{max}}^{\omega_{max}} \frac{\mathrm{d}\omega}{2\pi}\, \omega\, \rho'_\sigma(\omega, \mathbf{k}) = 1 \; . \tag{4.23}$$

The numerically scheme for the improved Hartree approximation is the following. At first, one solves the standard Hartree approximation, i.e., the condensate and the Dyson-Schwinger equations, Eqs. (4.3) and (4.5) with $[\mathrm{Re}\,\Sigma]_2 = [\mathrm{Im}\,\Sigma]_2 = 0$, to obtain the chiral condensate and the effective mass of the pion, σ and M_π. With these results, one calculates the 4-momentum dependent real and imaginary parts (4.21) of the σ-meson self-energy, and finally the spectral density, Eq. (4.15) or (4.16). The decay width of the σ-meson Γ_σ is defined as [Wel83, LB00]

$$\Gamma_\sigma(k) = \frac{\mathrm{Im}\,\Sigma[\omega_\sigma(\mathrm{k}), \mathrm{k}; \sigma]}{\omega_\sigma(k)} \; . \tag{4.24}$$

4.3 Results

In this section I present the numerical results for the linear sigma model with $O(4)$ symmetry in the improved Hartree approximation as discussed in the last section, for the parameter sets given in table 4.1.

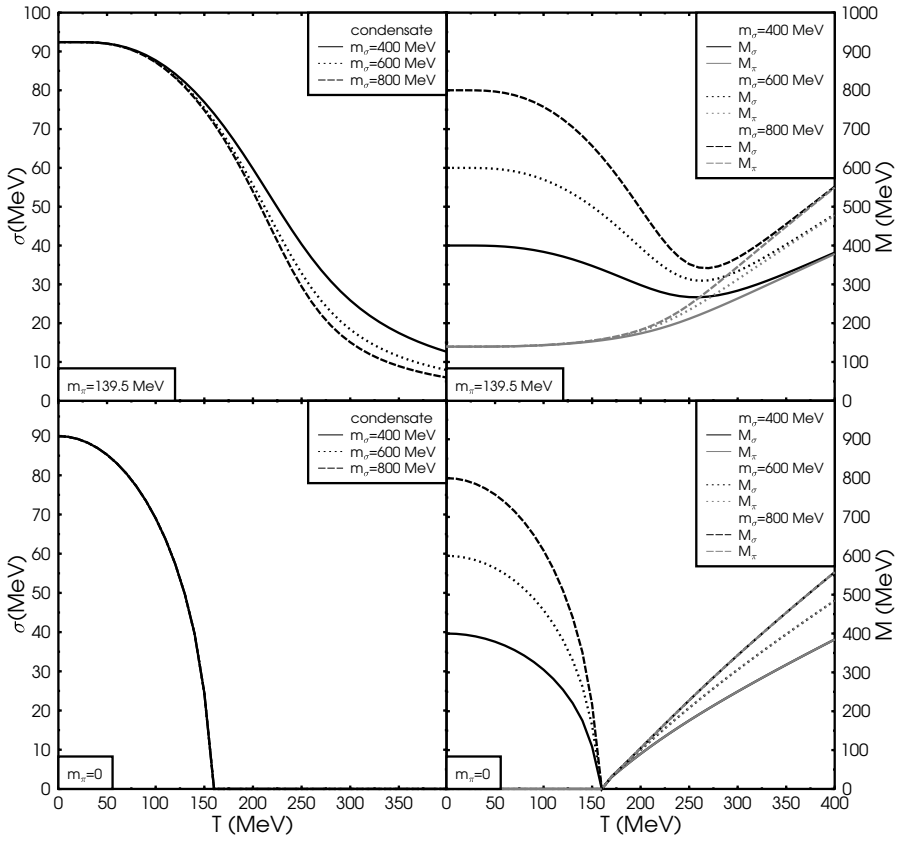

Figure 4.1: The chiral condensate σ (left column) and the effective masses of the σ-meson and the pion, M_σ and M_π (right column), as functions of temperature T and σ-meson vacuum mass m_σ. In the upper row the results with explicit chiral symmetry breaking are shown and in the lower row the results in the chiral limit.

The mass

I start the discussion of the results with the chiral condensate σ, given by the solution of Eq.(4.3), and the 4-momentum independent effective masses of the σ-meson and the pion, M_σ and M_π, as defined in Eqs. (4.18) and (4.14). Note, however, that (in the chirally broken phase, $\sigma \neq 0$) the mass of the σ-meson (the energy where the σ-meson spectral density assumes its maximum) is additionally modified by the 4-momentum dependent real part of the σ-meson self-energy $[\mathrm{Re}\,\Sigma(\mathrm{K};\sigma)]_2$ in Eq. (4.10b), which is discussed later.

In the upper row of Fig. 4.1 the results for the chiral condensate σ (left column) and the effective mass for the σ-meson and the pion, M_σ and M_π (right column),

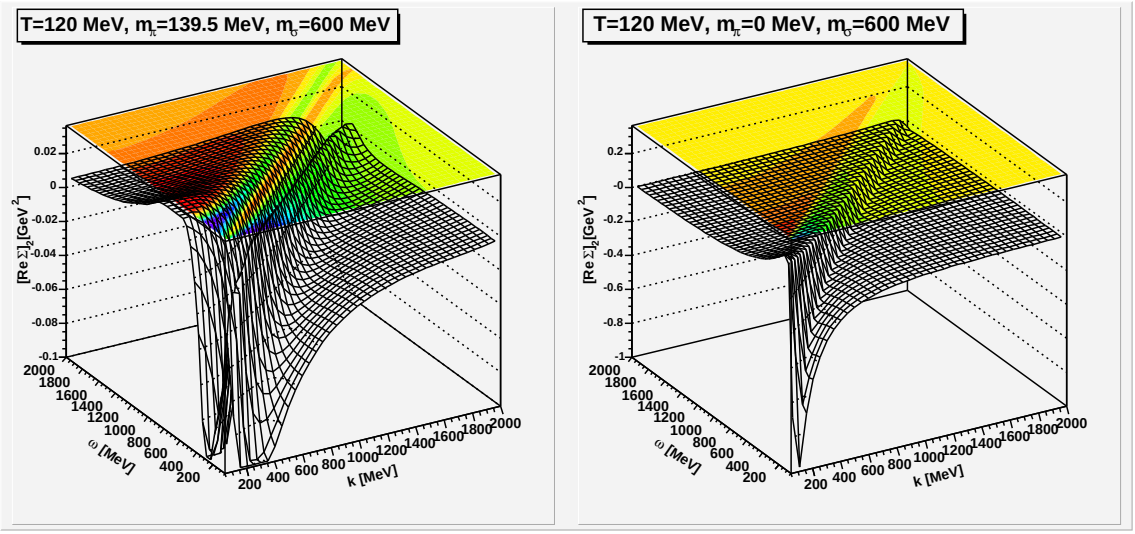

Figure 4.2: The 4-momentum dependent real part of the σ-meson self-energy $[\mathrm{Re}\,\Sigma]_2$, in the energy-momentum plane, for the case with explicit chiral symmetry breaking (left) and the corresponding result for the chiral limit (right) at a temperature of $T = 120$ MeV.

are shown as functions of T and m_σ, in the case with explicit chiral symmetry breaking. The results show the behaviour of a crossover transition. Neither the chiral condensate nor the mass of the scalar particle M_σ become equal to zero, even for high temperatures. Thus, M_σ and M_π become only approximatively degenerate for large temperatures. In the lower row of Fig. 4.1 the corresponding results for the chiral limit are presented. The results show the behaviour of a second-order phase transition. The condensate σ and the mass of the scalar particle M_σ becomes equal to zero at a critical temperature T_χ, therefore $M_\sigma = M_\pi$ for $T \geq T_\chi$. The condensate (accordingly T_χ) does not depend on the vacuum mass m_σ. This can be understood as a consequence of the condensate equation (4.3) in the chiral limit ($H = 0$),

$$0 = \mu^2 + \frac{4\lambda}{N}\left[\sigma^2 + N\int_Q \mathcal{P}(Q)\right]. \tag{4.25}$$

For $m_\pi = 0$ the integral can be performed analytically [LR00],

$$0 = -\frac{m_\sigma^2}{2} + \frac{4\lambda}{N}\sigma^2 + 4\lambda\frac{T^2}{12}. \tag{4.26}$$

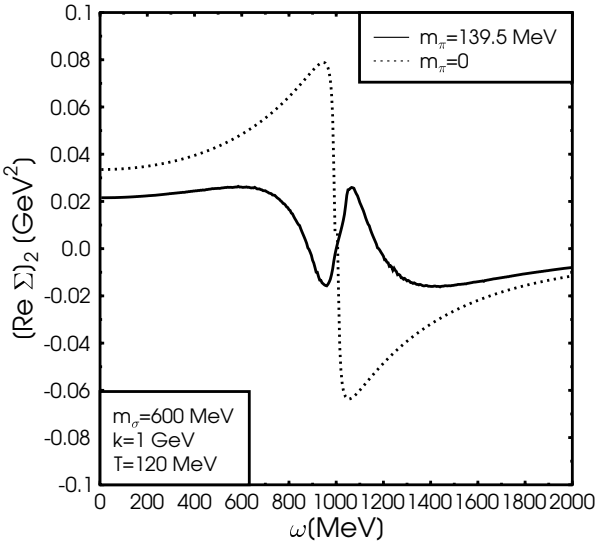

Figure 4.3: The 4-momentum dependent real part of the σ-meson self-energy $[\mathrm{Re}\,\Sigma]_2$, at a fixed momentum of $k = 1$ GeV, for the case with explicit chiral symmetry breaking (full line) and the corresponding result for the chiral limit (dotted line) at a temperature of $T = 120$ MeV.

Using (1.28a), this leads to an (m_σ-independent) equation for the condensate:

$$\sigma = \sqrt{f_\pi^2 - \frac{T^2 N}{12}} \tag{4.27}$$

that determines the critical temperature (where $\sigma = 0$) to be $T_\chi = \sqrt{12/N} f_\pi$. This agrees with the numerical results for the $O(4)$ model, $T_\chi = \sqrt{3} f_\pi \approx 160\,\mathrm{MeV}$. The 4-momentum dependent real part of the σ-meson self-energy $[\mathrm{Re}\,\Sigma]_2$ is shown in Fig. 4.2 on the whole energy-momentum plane, and in Fig. 4.3 at fixed momentum (in the middle of the grid) of $k = 1$ GeV as a function of energy. It is larger in the chiral limit as in the case with explicitly broken chiral symmetry, because $[\mathrm{Re}\,\Sigma]_2 \sim \lambda^2 \sim (\mathrm{m}_\sigma^2 - \mathrm{m}_\pi^2)^2$ is maximal for $m_\pi^2 = 0$. Note that $[\mathrm{Re}\Sigma]_2$ is small compared to the (squared) 4-momentum independent mass of the σ-meson, shown in Fig. 4.1. I come back to the influence of $[\mathrm{Re}\Sigma]_2$ in the discussion of the spectral density.

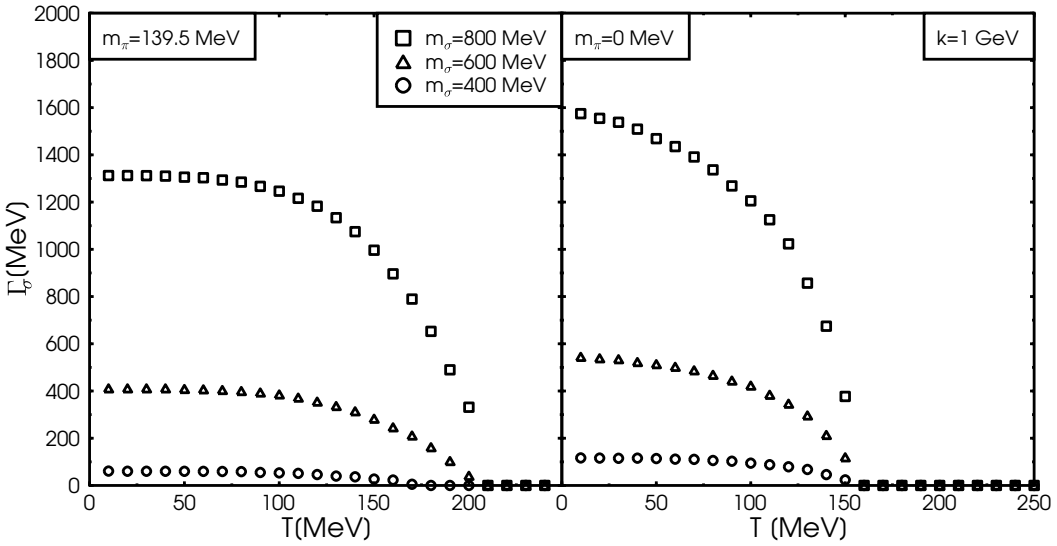

Figure 4.4: The decay width of the σ-meson Γ_σ, as a function of temperature T and σ-meson vacuum mass m_σ, at momentum $k = 1$ GeV, in the case with explicit chiral symmetry breaking (left) and the chiral limit (right).

The decay width

After calculating the (4−momentum dependent) imaginary part of the σ-meson self-energy (4.8a), the decay width Γ_σ (4.24) is calculated at the quasiparticle energy $\omega = \omega_\sigma$. The imaginary part of the self-energy, and therefore the decay width, of the pion is of order $\sim 1/N$, and therefore neglected.

In Fig. 4.4 the decay width of the σ-meson Γ_σ is shown as a function of temperature T. The qualitative behaviour is similar in all cases, but the decay width is larger in the chiral limit ($m_\pi = 0$) compared to the case with explicit chiral symmetry breaking ($m_\pi \neq 0$), because $\Gamma_\sigma \sim \mathrm{Im}\,\Sigma \sim \lambda^2 \sim (\mathrm{m}_\sigma^2 - \mathrm{m}_\pi^2)^2 \leq \mathrm{m}_\sigma^4$ [cf. Eqs. (4.8a) and (1.23)]. The decay width is a strictly monotonic decreasing function with temperature, and becomes approximately zero (equal zero) for temperatures larger than ~ 200 MeV ($T \geq T_\chi$) in the case with explicitly broken chiral symmetry (the chiral limit). This is a consequence of the (partial) restoration of the chiral symmetry, the masses of the chiral partners become (approximatively) degenerate, and therefore the phase space of the $\sigma \to 2\pi$ decay

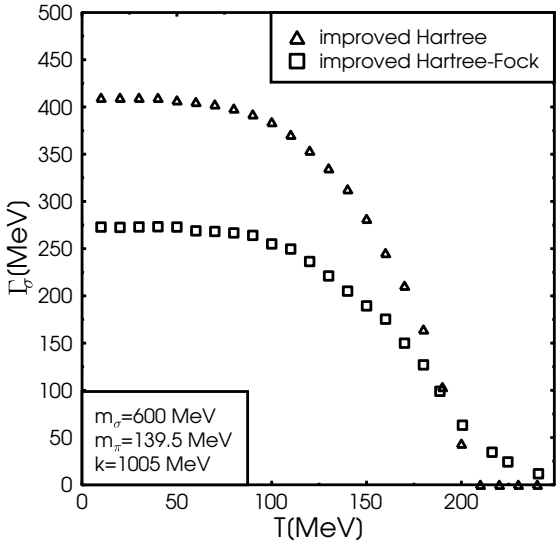

Figure 4.5: The decay width of the σ-meson Γ_σ, in the improved Hartree (triangles) and in the improved Hartree-Fock (squares) approximation, as a function of the temperature T, at momentum $k = 1005$ MeV and σ-meson vacuum mass of $m_\sigma = 600$ MeV, in the case with explicit chiral symmetry breaking.

is squeezed. The dependence on the vacuum mass of the σ-meson is significant. The reason for this is that $\Gamma_\sigma \sim \mathrm{Im}\,\Sigma \sim \mathrm{m}_\sigma^4$ which agrees reasonably with the results, $\mathrm{Im}\,\Sigma = 1 : 3 : 16$ for $m_\sigma = 400 : 600 : 800$ MeV.

In Fig. 4.5 the decay width of the σ-meson in the improved Hartree (triangles) is compared with the improved Hartree-Fock [RRR05] (squares) approximation. The main difference comes from the combinatorial factor in front of the two-pion term ($\sim \int \mathcal{PP}$) in the imaginary part of the self-energy [cf. Eqs. (4.6a) with (4.8a)]. A part of this contribution is of order $\sim 1/N$, and neglected in the Hartree approximation. Therefore, this factor is $2 \cdot N = 8$ in the improved Hartree, and $2 \cdot (N-1) = 6$ in the improved Hartree-Fock approximation, which would lead to a decay width which is an factor ≈ 1.33 larger in the improved Hartree approximation. The remaining difference, shown in the plot, comes from the σ-meson term ($\sim 3 \cdot 3! \int \mathcal{SS}$) in Eq. (4.8a), which vanishes in the large-N limit.

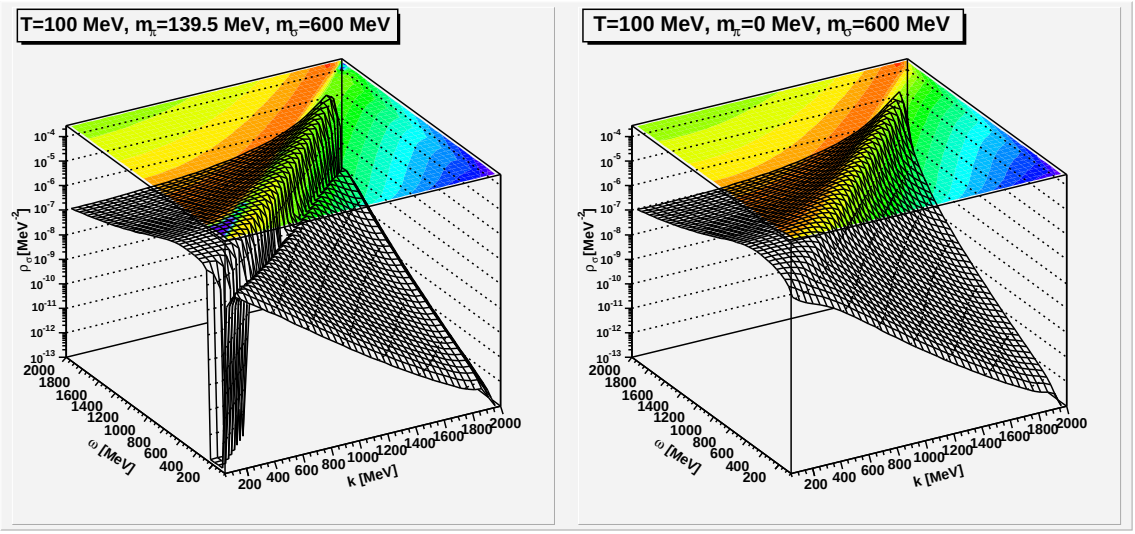

Figure 4.6: The spectral density of the σ-meson ρ_σ, as a function of energy ω, momentum k, and σ-meson vacuum mass m_σ at a temperature of $T = 100$ MeV, in the case with explicit chiral symmetry breaking (left) and in the chiral limit (right).

The spectral density

Finally, after solving the coupled condensate and Dyson-Schwinger equations self-consistently, Eqs. (4.3) and (4.5), the spectral density of the σ-meson ρ_σ is given in the chiral broken phase ($\sigma \neq 0$) by Eq. (4.15), and in the restored phase ($\sigma = 0$) by Eq. (4.16).

In Fig. 4.6 the spectral density is plotted as a function of energy and momentum, and in Fig. 4.7 at fixed momentum (as for the real part in the middle of the grid) of $k = 1$ GeV. In Fig. 4.7 all possible parameter sets (cf. table 4.1) are compared. The spectral density does not exhibit a pronounced peak at the mass-shell energy $\omega_\sigma = \sqrt{k^2 + M_\sigma^2}$. The reason for this is that the energy of the σ-meson ω_σ is large enough to decay into two pions. As discussed above, the decay width of this process is large and becomes even larger for increasing m_σ, as shown in the plot. A remarkable difference between the chiral limit (right) and the case with explicit chiral symmetry breaking (left) is that $\rho_\sigma \approx 0$ around $\omega \approx 1$ GeV in the case with explicit symmetry breaking but not in the chiral limit. This effect can be traced back to the threshold energy for $\sigma \to 2\pi$, which is $\omega = 2M_\pi$, and therefore zero in the chiral limit but not in the case with explicit chiral symmetry breaking. For $\omega < k$ the σ-meson is Landau-damped.

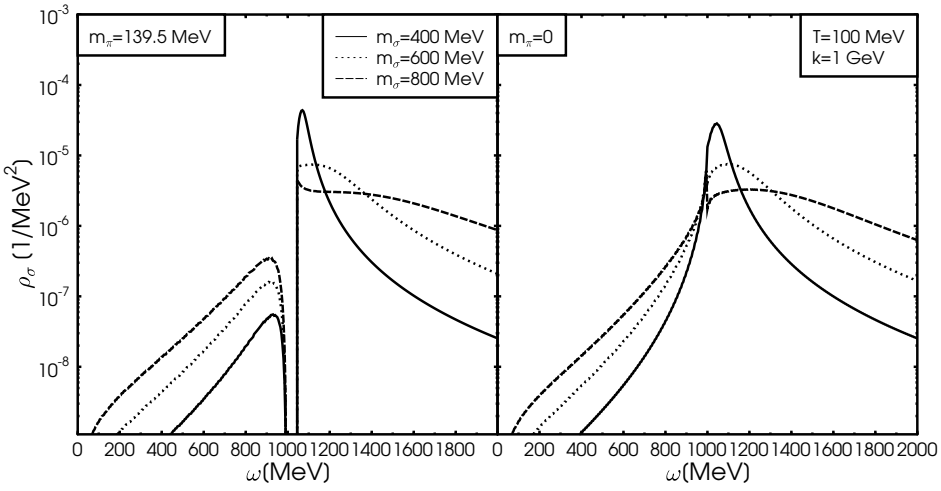

Figure 4.7: The spectral density of the σ-meson ρ_σ, as a function of energy ω, and σ-meson vacuum mass m_σ, at a momentum of $k = 1$ GeV and a temperature of $T = 100$ MeV, in the case with explicit chiral symmetry breaking (left) and in the chiral limit (right).

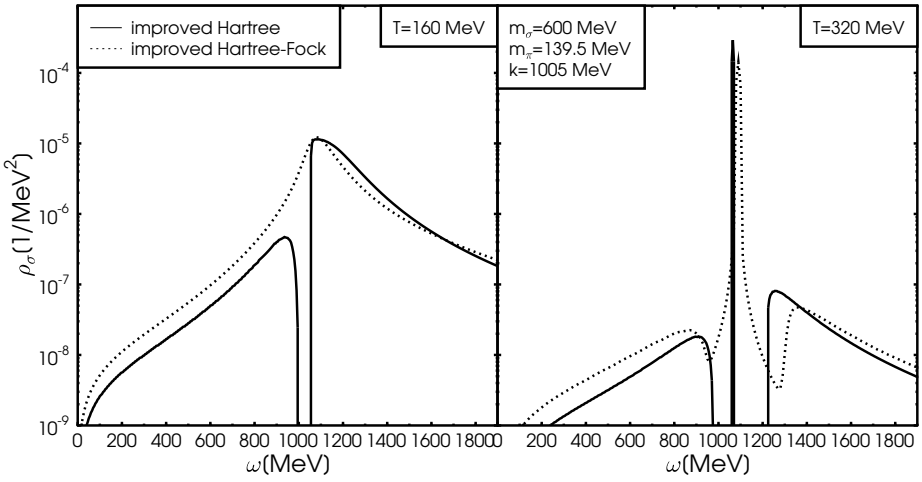

Figure 4.8: The spectral density of the σ-meson ρ_σ, as a function of energy ω, at a momentum of $k = 1$ GeV, and a vacuum σ-meson mass of $m_\sigma = 600$MeV, in the case with explicit chiral symmetry breaking. The results are shown for the improved Hartree (full line) and the improved Hartree-Fock (dotted line) approximation at temperatures of $T = 160$ MeV (left), and 320 MeV (right).

To illustrate the effects of neglecting terms of order $\sim 1/N$, I compare in Fig. 4.8 the results from the improved Hartree (full lines) with the results from the improved Hartree-Fock [RRR05] (dotted lines) approximation. The results are shown in the low-temperature regime, $T = 160$ MeV (left), and in the high-temperature regime, $T = 320$ MeV (right). In the improved Hartree-Fock approximation one does not neglect the $\sim 1/N$ terms in the imaginary part of the self-energy, which leads to a nonzero width of the pion spectral density, and therefore to a washed-out σ-meson spectral density.

Another major difference between the improved Hartree and Hartree-Fock approximation is that the 4-momentum dependent real parts are neglected in the latter one. However, as mentioned, the differences in Fig. 4.8 can be mainly traced back to the the neglected terms of order $\sim 1/N$. To quantify the difference arising from the 4-momentum dependent real parts, I calculate the relative change between the spectral density with and without $[\mathrm{Re}\Sigma]_2$, averaged over the energy-momentum grid, $\langle \mathrm{diff} \rangle \equiv \langle |(\rho_{\mathrm{W}} - \rho_{\mathrm{WO}})/\rho_{\mathrm{W}}| \rangle_{k,\omega}$, where ρ_{W} is the standard spectral density given by Eq. (4.15), ρ_{WO} the spectral density given by Eq. (4.15) with $[\mathrm{Re}\Sigma]_2 \equiv 0$, and $\langle \ldots \rangle_{k,\omega}$ denotes the average over the energy-momentum grid. This mean value is $\langle \mathrm{diff} \rangle = 5.61 \pm 2.90\%$ for $T = 160$ MeV, and $\langle \mathrm{diff} \rangle = 0.44 \pm 0.01\%$ for $T = 320$ MeV.

–V–

Conclusions & Outlook

In the following I briefly discuss the major results from the last three chapters and explain what is planned in the future.

Chapter II: The quark mass dependence of the transition temperature [DRR04]

Three-colour QCD exhibits a (weakly) first-order deconfining phase transition at a temperature $T_c/\sqrt{\sigma} \approx 0.63$ in the limit of infinitely heavy quarks ($\sqrt{\sigma} \approx 0.425$ GeV denotes the string tension at $T = 0$ in this theory). Near T_c, the screening mass for the fundamental Polyakov-loop ℓ drops substantially [KKLL00], and so one might hope to capture the physics of the phase transition using some effective Lagrangian for ℓ [YS82, Pis02, DP01, DP02b, DP02a, SDJ01, OM00, MMO02, MST04, Fuk04].

For finite quark masses, a term linear in ℓ appears which breaks the $Z(3)$ center-symmetry explicitly. This reduces the deconfinement temperature, with $\Delta T_c/T_c^*$ on the order of the expectation value of the Polyakov-loop at T_c^-, cf. Eq. (2.13). At some point then, the line of first-order deconfinement phase transitions ends [GGP94, GK84, MO95, A$^+$99, B$^+$90], see Fig. 5.1. I have provided a quantitative estimate of this point, $m_\pi \simeq 4.2\ \sqrt{\sigma} \approx 1.8$ GeV($\hat{=} m_q \approx 0.9$ GeV) and $T_c \simeq 240$ MeV for $N_f = 3$ degenerate flavours, by matching the effective Lagrangian for the Polyakov-loop to lattice data on $T_c(m_\pi)$ [KLP01]. Assuming that $b_1 \propto N_f$ [A$^+$99] shifts "D" to $m_\pi \simeq 1.4$ GeV for $N_f = 2$ and to 0.8 GeV for $N_f = 1$.

Going to even smaller quark (or pion) masses leaves a crossover between the low-temperature and high-temperature regimes of QCD. The dependence of the

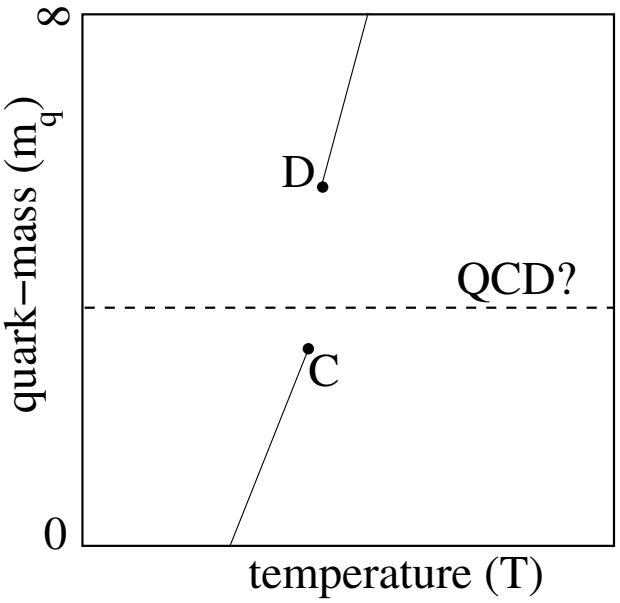

Figure 5.1: Schematic phase diagram in the temperature vs. quark mass plane. C is the chiral critical point, D the deconfining critical point.

crossover temperature T_c on the pion mass appears to be well described by a small explicit breaking of the $Z(3)$ center symmetry, $b_1 \sim \exp(-m_\pi)$, down to $m_\pi/\sqrt{\sigma} \simeq 1$, which is the smallest pion mass covered by the lattice data of Ref. [KLP01]. On the other hand, a linear sigma model leads to a stronger dependence of T_c on m_π than seen in the data.

In turn, in the chiral limit, and for $N_f = 3$ flavours, one expects a first-order *chiral* phase transition [PW84b, GGP94, B$^+$90]. The linear sigma model should then be an appropriate effective Lagrangian for low-energy QCD [PW84b, RW93, LRSB00, MMOP94, MOPP92, Gol83, GGP94]. The first-order chiral phase transition ends in a critical point "C" if either the mass of the strange quark or those of all three quark flavours increase. Given that the explicit symmetry breaking term for the Polyakov-loop remains rather small when extrapolated to $m_\pi \to 0$, that is $b_1 \to 0.2$, I speculate that "C" might be rather close to the chiral limit. Indeed, recent lattice estimates for $N_f = 3$ place "C" at $m_\pi \simeq 290$ MeV [KLS01] for standard staggered fermion action and $N_t = 4$ lattices; improved (p4) actions predict values as low as $m_\pi \simeq 67$ MeV [K$^+$04a].

Of course, the question arises why, for pion masses down to $\simeq 400$ MeV, the QCD crossover is described rather naturally by a slight "perturbation" of the

$m_\pi = \infty$ limit, in the form of an explicit breaking of the global $Z(N_c)$ symmetry for the Polyakov-loop. Physically, the reason is the flatness of the potential for ℓ in the pure gauge theory at T_c, see e.g. the figures in [DP01, DP02b, SDL02], which causes the sharp drop of the screening mass for ℓ near T_c^+ [KKLL00]. This is natural, given that finite-temperature expectation values of Polyakov-loops at $N_c = 3$ are close to those at $N_c = \infty$ [DHL$^+$04], where the potential at T_c becomes entirely flat [GW80, KSS82, DHL$^+$04]. Hence, a rather small "tilt" of the potential (due to explicit symmetry breaking) quickly washes out the deconfining phase transition of the pure gauge theory, and causes a significant shift ΔT_c of the crossover temperature already for small b_1. If so, then for $N_c \to \infty$, at the Gross-Witten point, the endpoint "D" should be located at $b_1 = 0$; the discontinuity for the Polyakov-loop at T_c, which in a mean-field model for the pure gauge theory is 1/2 at $N_c = \infty$ [DHL$^+$04, GW80, KSS82], then vanishes for arbitrarily small explicit symmetry breaking. This has previously been noted by Green and Karsch [GK84] within a mean-field model. If confirmed by lattice Monte-Carlo studies, one might improve the understanding of the degrees of freedom driving the QCD crossover for pion masses above the chiral critical point "C".

Chapter III: The improved Hartree-Fock approximation [RRR05]

In chapter III, I have studied the $O(N)$ linear sigma model at nonzero temperature within a self-consistent many-body resummation scheme. This scheme extends the standard Hartree-Fock approximation by including nonzero decay widths of the particles. In the standard Hartree-Fock approximation, the self-energies of the particles consist of tadpole diagrams which have no imaginary part. Consequently, all particles are stable quasi-particles. In order to obtain a nonzero decay width, one has to include diagrams in the self-energy, which have a nonzero imaginary part corresponding to decay and, in a medium, scattering processes.

In order to incorporate the nonzero decay width in a self-consistent way, I apply the Cornwall-Jackiw-Tomboulis formalism. The standard Hartree-Fock approximation is obtained by considering only double-bubble diagrams in the 2PI effective action, leading to the (energy- and momentum-independent) tadpole contributions in the 1PI self-energies. In order to extend the Hartree-Fock approximation, I additionally take into account diagrams of sunset topology in the 2PI effective action. This has the consequence that the 1PI self-energies obtain

additional energy- and momentum-dependent one-loop contributions which have a nonzero imaginary part. The spectral densities of σ-mesons and pions are then computed as solutions of a self-consistent set of Dyson-Schwinger equations for the σ-meson and pion two-point functions, coupled to a fix-point equation for the chiral condensate. I only take into account the imaginary parts of the new one-loop contributions. I made sure that the spectral densities obey a standard sum rule by adjusting their normalisation, if necessary.
I found that the temperature T_χ for chiral symmetry restoration is about 20% smaller as compared to the Hartree-Fock approximation when including nonzero particle decay widths. My value $T_\chi \simeq 175$ MeV agrees reasonably well with lattice results [LP03]. I computed the decay widths of σ-mesons and pions as a function of temperature. The vacuum value for the σ-meson decay width comes out to be in the experimentally observed range, without adjusting a parameter of the model. It stays approximately constant up to temperatures $\sim T_\chi$ and then decreases sharply with temperature. The pion decay width grows from zero at $T = 0$ to a value ~ 100 MeV at $T \sim T_\chi$, and then also decreases with temperature. I also investigated the spectral densities of σ-mesons and pions as functions of energy and momentum for temperatures in the range of $T = 80$ to 320 MeV. Below the chiral phase transition, the spectral density of the σ-meson is broad, due to the possible decay into two pions. It develops a peak at the quasi-particle mass shell above the chiral phase transition, when this decay channel is closed. On the other hand, the spectral density of the pion always exhibits a distinct peak at the quasi-particle mass shell. The width of this peak is due to scattering off σ-mesons in the medium. Above the chiral phase transition, the spectral densities of σ-mesons and pions become degenerate in shape.

Chapter IV: The improved Hartree approximation [Röd05]

In chapter IV, I systematically improved the standard Hartree (or large-N) approximation of the $O(N)$ linear sigma model by taking into account, additionally to the double-bubble diagrams, the sunset diagrams in the effective potential of the CJT formalism. This leads to 4-momentum dependent real and imaginary parts of the Dyson-Schwinger equations. In contrast to chapter III, I didn't neglect the 4-momentum dependent real parts, to study their influences to the results. I solve these and the equation of the condensate selfconsistently in the chiral limit ($m_\pi = 0$), and in the case with explicitly broken chiral symmetry

($m_\pi \neq 0$), to get the decay width and the spectral density of the σ-meson.
First, I presented the results for the real parts of the Dyson-Schwinger equations and the condensate equation. The 4-momentum independent parts, i.e., the effective masses and the chiral condensate exhibit a crossover transition in the case with explicit chiral symmetry breaking and a second-order phase transition in the chiral limit, which agrees with the predictions made by Pisarski and Wilczek [PW84a]. I found, that the 4-momentum dependent real part of the self-energy is rather small compared to the (squared) 4-momentum independent effective masses. It is larger in the chiral limit, simply because $[\mathrm{Re}]_2 \sim \lambda^2 \sim (\mathrm{m}_\sigma^2 - \mathrm{m}_\pi^2)^2$ is maximal for $m_\pi^2 = 0$.
The decay width shows qualitatively the same behaviour in all cases. It is a decreasing function with temperature and becomes (approximatively) zero in the high-temperature regime. Nevertheless, quantitatively it depends strongly on the choice of the vacuum mass of the σ-meson, by reason that $\Gamma_\sigma \sim \mathrm{Im}\,\Sigma \sim \lambda^2 \sim \mathrm{m}_\sigma^4$. Also, the decay widths are larger in the chiral limit, due to the fact that $\Gamma_\sigma \sim \lambda^2 \sim (m_\sigma^2 - m_\pi^2)^2$.
In the low-temperature regime, the spectral density of the σ-meson is a very broad function in energy (and becomes even broader for larger vacuum mass m_σ) due to the $\sigma \to 2\pi$ decay. In the high-temperature regime, the spectral density becomes more and more a delta function. Remarkable is the fact that ρ_σ becomes zero in a certain energy interval, in the case with explicit chiral symmetry breaking but not in the chiral limit. This can be traced back to the threshold energy for $\sigma \to 2\pi$, which is $2m_\pi$, and therefore zero in the chiral limit but not in the other case. For $\omega < k$ the σ-meson is Landau-damped. The influence of the 4-momentum dependent real part of the self-energy to the spectral density is rather small and does not change the results qualitatively.

Outlook

The present studies can be continued along several lines:

- Throughout this thesis I used the linear σ model with $O(4)$ symmetry, which is isomorphic to the linear σ model with $SU(2) \times SU(2)$ symmetry. Both models contains only mesons composed from the lightest two quarks (the up and down quarks), but the $O(4)$ model is the limit of the $SU(2) \times SU(2)$ model with maximally broken $U(1)_A$ symmetry, which leads to the fact that the η and the a_0 mesons become infinitely heavy, and hence cannot be describted by this theory, cf. [RRR03]. It would be exciting to study the influence of nonzero decay width effects also for these mesons, and additionally for mesons with strange and maybe also charm degrees of freedom. The scalar (s) and pseudoscalar (ps) mesons contained in the linear σ models are summarized in the following table:

	$O(4)$	$SU(2)_r \times SU(2)_\ell$	$SU(3)_r \times SU(3)_\ell$	$SU(4)_r \times SU(4)_\ell$
s	σ	$a_0^\pm, a_0^0$	$\kappa^\pm, \kappa^0, \bar{\kappa}^0, f_0$	$D_0^\pm, D_0^0, \bar{D}_0^0, D_{s,0}^\pm, \chi_{c,0}$
ps	$\pi^\pm, \pi^0$	η	$K^\pm, K^0, \bar{K}^0, \eta'$	$D^\pm, D^0, \bar{D}^0, D_s^\pm, \eta_c$

- In chapter II, the chiral critical point (denoted by "C" in figure 5.1) is at $m_q = 0$, because only the 2-flavor case is discussed. Extending the model by the strange degree of freedom would allow us to give an estimate for the position of this point in the whole quark mass plane, discussed in Sec. 1.3, cf. Fig. 1.2.

- So far only the scalar and pseudoscalar mesons are taking into account. The inclusion of baryonic degrees of freedom into a framework, similar to that discussed in Chapters III or IV, is still under investigation [Bec05]. Also, the inclusion of vector mesons [RR05, Ste] is under investigation, and is of particular importance, since in-medium changes in the spectral properties of vector mesons are reflected in the dilepton spectrum [RR05] which, in turn, is experimentally observable in heavy-ion collisions at GSI-SIS, CERN-SPS and BNL-RHIC energies.

- As disussed, a major advantage of effective models over lattice QCD calculations is that no problems with a nonzero chemical potential occur [VVO02, COVV05]. Including the chemical potential in the framework of the improved Hartree or Hartree-Fock approximation would us allow to

study, e.g., the influence of nonzero decay width effects on the chiral critical endpoint in the $T - \mu-$plane shown in figure 1.3 (cf. e.g. [SMMR01]).

- Up to now, I neglected the ultraviolet divergent vacuum parts of the integrals, i.e., I just used trivial renormalization. One should check what happens if one use a "real" renormalization scheme (e.g. the cut-off or counter-term scheme, cf. [LR00]).

- The influence of the 4-momentum dependent real parts of the self-energy in the improved Hartree approximation is very small, nevertheless, one should check its influence also in the full Hartree-Fock approximation.

–Appendix A–

The calculation of the diagrams

A.1 In the improved Hartree-Fock approximation

In this Appendix I discuss the calculation of the three types of diagrams (see Fig. A.1) contributing to the self-energies and the condensate equation. To evaluate them explicitly, I use standard techniques of thermal field theory, see for example Refs. [Das97, Kap93, LB00, Lan97, LvW87, vW].

The tadpole diagram

In the following I discuss the calculation of the tadpole diagram in Fig. A.1 a as a functional of the spectral density. In the imaginary-time formalism it is given

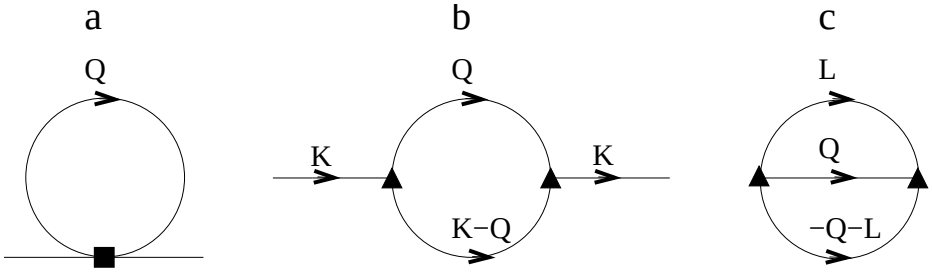

Figure A.1: The general topology of the tadpole diagram a, the cut sunset diagram b, and the sunset diagram c.

by

$$\mathcal{T} \equiv T \sum_n \int \frac{d^3q}{(2\pi)^3} \Delta(-i\omega_n, \mathbf{q}) \tag{A.1}$$

where T is the temperature, and Δ is either the σ-meson or pion propagator. The first step is to perform the sum over the Matsubara frequencies. To this aim I introduce the mixed representation of the propagator

$$\Delta(-i\omega_n, \mathbf{q}) = \int_0^{1/T} d\tau \exp(-i\omega_n \tau) \Delta(\tau, \mathbf{q}), \tag{A.2}$$

with

$$\Delta(\tau, \mathbf{q}) = \int_{-\infty}^{\infty} \frac{d\omega}{2\pi} \left[\Theta(\tau) + f(\omega)\right] \rho(\omega, \mathbf{q}) \exp(-\omega\tau) \ , \tag{A.3}$$

where $f(\omega) = [\exp(\omega/T) - 1]^{-1}$ is the Bose-Einstein distribution function. With the identity

$$T \sum_n \exp(-i\omega_n \tau) = \sum_{m=-\infty}^{\infty} \delta\left(\tau - \frac{m}{T}\right) \ , \tag{A.4}$$

the Matsubara sum can be performed analytically

$$\begin{aligned}
\mathcal{T} &= T \sum_n \int \frac{d^3q}{(2\pi)^3} \int_0^{1/T} d\tau \exp(-i\omega_n \tau) \Delta(\tau, \mathbf{q}) \\
&= \int \frac{d^3q}{(2\pi)^3} \int_0^{1/T} d\tau \Delta(\tau, \mathbf{q}) \left[\delta(\tau) + \delta\left(\tau - \frac{1}{T}\right)\right] \\
&= \int \frac{d^3q}{(2\pi)^3} \frac{1}{2} \left[\Delta(0, \mathbf{q}) + \Delta\left(\frac{1}{T}, \mathbf{q}\right)\right] \\
&= \int \frac{d^3q}{(2\pi)^3} \Delta(0, \mathbf{q}) \ ,
\end{aligned} \tag{A.5}$$

where use has been made of the KMS condition $\Delta(\tau, \mathbf{q}) \equiv \Delta(\tau - 1/T, \mathbf{q})$. With Eq. (A.3) I finally have

$$\mathcal{T} = \int_{-\infty}^{\infty} \frac{d\omega}{2\pi} \int \frac{d^3q}{(2\pi)^3} \left[\frac{1}{2} + f(\omega)\right] \rho(\omega, \mathbf{q}) \ . \tag{A.6}$$

Due to isotropy of space, the spectral density of a scalar particle cannot depend on the direction of $\mathbf{q}$, thus the angular integration can be carried out:

$$\mathcal{T} = 4\pi \int_{-\infty}^{\infty} \frac{d\omega}{2\pi} \int_0^{\infty} \frac{d\,q}{(2\pi)^3} q^2 \left[\frac{1}{2} + f(\omega)\right] \rho(\omega, q) \ . \tag{A.7}$$

Using the fact that the spectral density for bosonic degrees of freedom is an odd function of the energy, $\rho(\omega) = -\rho(-\omega)$,

$$\begin{aligned} \mathcal{T} &= 4\pi \int_0^\infty \frac{d\omega}{2\pi} \frac{dq}{(2\pi)^3}\, q^2 [f(\omega) - f(-\omega)]\rho(\omega, q) \\ &= 4\pi \int_0^\infty \frac{d\omega}{2\pi} \frac{dq}{(2\pi)^3}\, q^2 \left[1 + 2f(\omega)\right] \rho(\omega, q) \ . \end{aligned} \tag{A.8}$$

Subtracting the divergent vacuum contribution I obtain:

$$\mathcal{T} = \frac{4}{(2\pi)^3} \int_0^\infty d\omega\, dq\, q^2\, f(\omega)\, \rho(\omega, q) \ . \tag{A.9}$$

The cut sunset diagram

In this section I calculate the imaginary part of the cut sunset diagram of Fig. A.1 b. In the imaginary-time formalism the cut sunset diagram is given by

$$\begin{aligned} \mathcal{C}(-i\omega_m, \mathbf{k}) &\equiv \int_Q \Delta_1(K - Q)\, \Delta_2(Q) \\ &= T \sum_n \int \frac{d^3q}{(2\pi)^3} \Delta_1(-i(\omega_m - \omega_n), \mathbf{k} - \mathbf{q}) \Delta_2(-i\omega_n, \mathbf{q}) \ , \end{aligned} \tag{A.10}$$

where Δ_1, Δ_2 are the propagators of σ-mesons and/or pions. The major difference between the tadpole diagram, discussed in the last section, and this diagram is the fact that it explicitly depends on the external four-momentum, $K^\mu \equiv (-i\omega_m, \mathbf{k})$. Analogously to the last section one introduces the mixed representation [see Eq. (A.2)] of the propagators Δ_1 and Δ_2

$$\begin{aligned} \mathcal{C}(-i\omega_m, \mathbf{k}) = T \sum_n \int \frac{d^3q}{(2\pi)^3} \quad & \int_0^{1/T} d\tau_1 \exp[-i(\omega_m - \omega_n)\tau_1] \Delta_1(\tau_1, \mathbf{k} - \mathbf{q}) \\ \times \quad & \int_0^{1/T} d\tau_2 \exp(-i\omega_n \tau_2) \Delta_2(\tau_2, \mathbf{q}) \ . \end{aligned} \tag{A.11}$$

The summation over the Matsubara frequencies leads to a delta function [cf. Eq. (A.4)]

$$\mathcal{C}(-i\omega_m, \mathbf{k}) = \int \frac{d^3q}{(2\pi)^3} \int_0^{1/T} d\tau \exp(-i\omega_m \tau) \Delta_1(\tau, \mathbf{k} - \mathbf{q}) \Delta_2(\tau, \mathbf{q}) \ . \tag{A.12}$$

Introduction of the spectral densities [see Eq. (A.3)] for both propagators in the mixed representation leads to

$$\mathcal{C}(-i\omega_m, \mathbf{k}) = \int \frac{d^3q}{(2\pi)^3} \int_0^{1/T} d\tau \exp(-i\omega_m \tau)$$

$$\times \int_{-\infty}^{\infty} \frac{d\omega_1}{2\pi}[1+f(\omega_1)]\rho_1(\omega_1,\mathbf{k}-\mathbf{q})\exp(-\omega_1\tau)$$
$$\times \int_{-\infty}^{\infty} \frac{d\omega_2}{2\pi}[1+f(\omega_2)]\rho_2(\omega_2,\mathbf{q})\exp(-\omega_2\tau)\ . \qquad \text{(A.13)}$$

The integration over τ can be performed analytically. Employing the identity

$$\left[\exp\left(-\frac{\omega_1+\omega_2}{T}\right)-1\right]\,[1+f(\omega_1)][1+f(\omega_2)] = -1-f(\omega_1)-f(\omega_2)\ , \qquad \text{(A.14)}$$

the expression can be rewritten as

$$\mathcal{C}(-i\omega_m,\mathbf{k}) = \int_{-\infty}^{\infty}\frac{d\omega_1}{2\pi}\,\frac{d\omega_2}{2\pi}\frac{1+f(\omega_1)+f(\omega_2)}{i\omega_{\rm m}+\omega_1+\omega_2}\int\frac{d^3q}{(2\pi)^3}\,\rho_1(\omega_1,\mathbf{k}-\mathbf{q})\rho_2(\omega_2,\mathbf{q})\ . \qquad \text{(A.15)}$$

Using the fact that the spectral densities do not depend on the direction of momentum and

$$\int\frac{d^3x}{(2\pi)^3}f(|\mathbf{y}-\mathbf{x}|)g(x) = \frac{2\pi}{y}\frac{1}{(2\pi)^3}\int_0^\infty dx_1\,x_1\,dx_2\,x_2\,f(x_1)g(x_2)$$
$$\times\ \Theta\left(|x_1-x_2|\le y\le x_1+x_2\right)\ , \qquad \text{(A.16)}$$

one can perform one angular integration, yielding

$$\mathcal{C}(-i\omega_m,\mathbf{k}) = \int_{-\infty}^{\infty}\frac{d\omega_1}{2\pi}\,\frac{d\omega_2}{2\pi}\,\frac{1+f(\omega_1)+f(\omega_2)}{i\omega_{\rm m}+\omega_1+\omega_2}$$
$$\times\ \frac{2\pi}{k}\frac{1}{(2\pi)^3}\int_0^\infty dq_1\,q_1\,dq_2\,q_2\,\rho_1(\omega_1,q_1)\rho_2(\omega_2,q_2)$$
$$\times\ \Theta\left(|q_1-q_2|\le k\le q_1+q_2\right)\ . \qquad \text{(A.17)}$$

The imaginary part of the retarded cut sunset diagram can be extracted using analytical continuation, $-i\omega_m\to\omega+i\epsilon$, and the Dirac identity $\mathrm{Im}1/(\mathrm{x}+\mathrm{i}\epsilon) = -\pi\delta(\mathrm{x})$,

$$\mathrm{Im}\,\mathcal{C}(\omega,\mathbf{k}) = \frac{1}{2(2\pi)^3}\frac{1}{k}\int_{-\infty}^{\infty}d\omega_1\,d\omega_2[1+f(\omega_1)+f(\omega_2)]\,\delta(\omega-\omega_1-\omega_2) \qquad \text{(A.18)}$$
$$\times\ \int_0^\infty dq_1\,q_1\,dq_2\,q_2\,\Theta\left(|q_1-q_2|\le k\le q_1+q_2\right)\,\rho_1(\omega_1,q_1)\,\rho_2(\omega_2,q_2).$$

This integral is finite and therefore does not require renormalization.

The sunset diagram

In the imaginary-time formalism the sunset diagram shown in Fig. A.1 c is given by the following expression:

$$\mathcal{S} = T^2\sum_{n,m}\int\frac{d^3l}{(2\pi)^3}\,\frac{d^3q}{(2\pi)^3}\Delta_1(-i\omega_m,\mathbf{l})\Delta_2(-i\omega_n,\mathbf{q})\Delta_3(-i(-\omega_n-\omega_m),-\mathbf{q}-\mathbf{l})\ . \qquad \text{(A.19)}$$

I introduce the mixed representation, see Eq. (A.2), for the three propagators Δ_1, Δ_2, and Δ_3. One can perform the Matsubara sums employing Eq. (A.4). In the mixed representation one introduces the spectral densities ρ_1, ρ_2, and ρ_3 in order to perform the τ integration analytically. Employing the identity

$$\begin{aligned} & \left[\exp\left(-\frac{\omega_1+\omega_2+\omega_3}{T}\right)-1\right]\left[1+f(\omega_1)\right]\left[1+f(\omega_2)\right]\left[1+f(\omega_3)\right] \\ = \; & -1-f(\omega_1)-f(\omega_2)-f(\omega_3)-f(\omega_1)f(\omega_2)-f(\omega_1)f(\omega_3)-f(\omega_2)f(\omega_3), \end{aligned} \tag{A.20}$$

for the Bose-Einstein distribution functions I obtain

$$\begin{aligned} \mathcal{S} &= \int_{-\infty}^{\infty}\frac{d\omega_1}{2\pi}\frac{d\omega_2}{2\pi}\frac{d\omega_3}{2\pi} \\ &\times \frac{1+f(\omega_1)+f(\omega_2)+f(\omega_3)+f(\omega_1)f(\omega_2)+f(\omega_1)f(\omega_3)+f(\omega_2)f(\omega_3)}{\omega_1+\omega_2+\omega_3} \\ &\times \int\frac{d^3l}{(2\pi)^3}\frac{\mathrm{d}^3q}{(2\pi)^3}\,\rho_1(\omega_1,\mathbf{l})\rho_2(\omega_2,\mathbf{q})\rho_3(\omega_3,-\mathbf{q}-\mathbf{l})\;. \end{aligned} \tag{A.21}$$

Using the fact that the spectral densities do not depend on the direction of momentum, the angular integrals can be carried out with the result

$$\begin{aligned} \mathcal{S} &= \frac{2}{(2\pi)^7}\int_{-\infty}^{\infty}d\omega_1\,d\omega_2\,d\omega_3\int_0^{\infty}dq_1\,q_1\,dq_2\,q_2\,dq_3\,q_3\,\Theta\left(|q_1-q_2|\le q_3\le q_1+q_2\right) \\ &\times \frac{1+f(\omega_1)+f(\omega_2)+f(\omega_3)+f(\omega_1)f(\omega_2)+f(\omega_1)f(\omega_3)+f(\omega_2)f(\omega_3)}{\omega_1+\omega_2+\omega_3} \\ &\times \rho_1(\omega_1,q_1)\rho_2(\omega_2,q_2)\rho_3(\omega_3,q_3)\;. \end{aligned} \tag{A.22}$$

Using the antisymmetry of the spectral densities, I obtain

$$\begin{aligned} \mathcal{S} &= \frac{4}{(2\pi)^7}\int_0^{\infty}d\omega_1\,d\omega_2\,d\omega_3\,dq_1\,q_1\,dq_2\,q_2\,dq_3\,q_3\,\Theta\left(|q_1-q_2|\le q_3\le q_1+q_2\right) \\ &\times \Bigg[\frac{f(\omega_1)f(\omega_2)+f(\omega_1)f(\omega_3)+f(\omega_3)f(\omega_2)+f(\omega_1)+f(\omega_2)+f(\omega_3)+1}{\omega_1+\omega_2+\omega_3} \\ &\quad +\frac{f(\omega_1)f(\omega_3)-f(\omega_1)f(\omega_2)+f(\omega_2)f(\omega_3)+f(\omega_3)}{\omega_1+\omega_2-\omega_3} \\ &\quad +\frac{f(\omega_1)f(\omega_2)-f(\omega_1)f(\omega_3)+f(\omega_2)f(\omega_3)+f(\omega_2)}{\omega_1-\omega_2+\omega_3} \\ &\quad +\frac{f(\omega_1)f(\omega_2)+f(\omega_1)f(\omega_3)-f(\omega_2)f(\omega_3)+f(\omega_1)}{-\omega_1+\omega_2+\omega_3}\Bigg] \\ &\times \rho_1(\omega_1,q_1)\rho_2(\omega_2,q_2)\rho_3(\omega_3,q_3)\;. \end{aligned} \tag{A.23}$$

Finally, I discard the ultraviolet-divergent parts, and relabel the integration variables

$$\begin{aligned}\mathcal{S} &= \frac{4}{(2\pi)^7}\int_0^\infty d\omega_1\, d\omega_2\, d\omega_3\, dq_1\, q_1\, dq_2\, q_2\, dq_3\, q_3\, \Theta\left(|q_1-q_2| \le q_3 \le q_1+q_2\right) \\ &\times f(\omega_1)f(\omega_2)\left(\frac{1}{\omega_1+\omega_2+\omega_3}+\frac{1}{-\omega_1+\omega_2+\omega_3}+\frac{1}{\omega_1-\omega_2+\omega_3}+\frac{1}{-\omega_1-\omega_2+\omega_3}\right) \\ &\times [\rho_1(\omega_1,q_1)\rho_2(\omega_2,q_2)\rho_3(\omega_3,q_3)+\rho_1(\omega_1,q_1)\rho_2(\omega_3,q_2)\rho_3(\omega_2,q_3) \\ &\quad +\rho_1(\omega_2,q_1)\rho_2(\omega_3,q_2)\rho_3(\omega_1,q_3)]\ . \end{aligned} \tag{A.24}$$

A.2 In the improved Hartree approximation

In contrast to the improved Hartree-Fock approximation, the spectral density of the pion, ρ_π, in the improved Hartree approximation is just a delta-function, because the imaginary part of the pion self-energy if of order $\sim 1/N$ and thus neglected. Therefore the equations for the tadpole and the cut sunset diagrams, Eqs. (A.9) and (A.17) simplify, but one has to calculate additionally the real part of the cut sunset diagram. The full sunset diagram, discussed in A.1, is of order $\sim 1/N$ and is therefore neglected in the large-N limit.

The tadpole diagram

The Dyson-Schwinger and the condensate equations of the improved Hartree approximation contain *exclusively* the spectral density of the pion. Therefore one has to solve equations of the form

$$\mathcal{T} = \frac{4}{(2\pi)^3}\int_0^\infty d\omega\, dq\, q^2\, f(\omega)\, \rho_\pi(\omega,q)\ , \tag{A.25}$$

with different combinatorial factors in front. (Note that this is the version where the divergent term is already neglected, i.e., the equation in the trivial renormalisation scheme.) Using the fact that the spectral density of the pion is just a delta function, $\rho_\pi(\omega,k) = \pi/\omega_\pi(k)\{\delta[\omega-\omega_\pi(k)]-\delta[\omega+\omega_\pi(k)]\}$, one gets

$$\mathcal{T} = \frac{1}{2\pi^2}\int_0^\infty dq\, q^2[\omega_\pi(q)]^{-1} f[\omega_\pi(q)]. \tag{A.26}$$

The cut sunset diagram

In this section I derive the equations for the 4-momentum dependent imaginary and real part of the self-energy (arising from the sunset diagram). As discussed

in Sec. A.1 this diagram can be expressed as a function of the spectral density ρ_π in the imaginary time formalism

$$\begin{aligned}\Sigma(-i\omega_m,k) &= \left(\frac{4\lambda\sigma}{N}\right)^2 \frac{2N}{(2\pi)^4}\frac{1}{k}\int_{-\infty}^{\infty} d\omega_1\, d\omega_2 \frac{1+f(\omega_1)+f(\omega_2)}{i\omega_m+\omega_1+\omega_2} \\ &\times \int_0^\infty dq_1\, q_1\, dq_2\, q_2\, \Theta\left(|q_1-q_2|\le k\le q_1+q_2\right)\rho_\pi(\omega_1,q_1)\rho_\pi(\omega_2,q_2),\end{aligned} \tag{A.27}$$

where $f(\omega)=1/[\exp(\omega/T)-1]$ is the Bose-Einstein distribution function, and $\omega_m=2\pi mT$ are the Matsubara frequencies. To extract the imaginary part of the retarded self-energy, one uses the Dirac identity, $\mathrm{Im}1/(\mathrm{x}+\mathrm{i}\epsilon)=-\pi\delta(\mathrm{x})$, and analytic continuation, $-i\omega_m\to\omega+i\epsilon$,

$$\begin{aligned}\mathrm{Im}\,\Sigma(\omega,\mathrm{k}) &= \left(\frac{4\lambda\sigma}{N}\right)^2 \frac{N}{2(2\pi)^3}\frac{1}{k}\int_{-\infty}^{\infty} d\omega_1\, d\omega_2 [1+f(\omega_1)+f(\omega_2)]\,\delta(\omega-\omega_1-\omega_2) \\ &\times \int_0^\infty dq_1\, q_1\, dq_2\, q_2\, \Theta\left(|q_1-q_2|\le k\le q_1+q_2\right)\rho_\pi(\omega_1,q_1)\rho_\pi(\omega_2,q_2).\end{aligned} \tag{A.28}$$

As discussed in the improved Hartree approximation of the $O(N)$ model the spectral density of the pion is just a delta function (4.12),

$$\begin{aligned}\mathrm{Im}\,\Sigma(\omega,\mathrm{k}) &= \left(\frac{4\lambda\sigma}{N}\right)^2 \frac{N}{8\pi}\frac{1}{k}\int_{-\infty}^{\infty} d\omega_1\, d\omega_2 [1+f(\omega_1)+f(\omega_2)]\,\delta(\omega-\omega_1-\omega_2) \\ &\times \int_0^\infty dq_1\, q_1\, dq_2\, q_2\, \Theta\left(|q_1-q_2|\le k\le q_1+q_2\right)[\omega_\pi(q_1)\omega_\pi(q_2)]^{-1} \\ &\times \{\delta[\omega_1-\omega_\pi(q_1)]\,\delta[\omega_2-\omega_\pi(q_2)]+\delta[\omega_1+\omega_\pi(q_1)]\,\delta[\omega_2+\omega_\pi(q_2)] \\ &\quad -\delta[\omega_1-\omega_\pi(q_1)]\,\delta[\omega_2+\omega_\pi(q_2)]-\delta[\omega_1+\omega_\pi(q_1)]\,\delta[\omega_2-\omega_\pi(q_2)]\}\,,\end{aligned} \tag{A.29}$$

where $\omega_\pi(q)=\sqrt{q^2+M_\pi^2}$ is the quasiparticle energy of the pion. To simplify this expression one uses the $\delta(\omega-\omega_1-\omega_2)$ function to carry out the ω_2-integration,

$$\begin{aligned}\mathrm{Im}\,\Sigma(\omega,\mathrm{k}) &= \left(\frac{4\lambda\sigma}{N}\right)^2 \frac{N}{8\pi}\frac{1}{k}\int_{-\infty}^{\infty} d\omega_1 [1+f(\omega_1)+f(\omega-\omega_1)] \\ &\times \int_0^\infty dq_1\, q_1\, dq_2\, q_2\, \Theta\left(|q_1-q_2|\le k\le q_1+q_2\right)[\omega_\pi(q_1)\omega_\pi(q_2)]^{-1} \\ &\times \{\delta[\omega_1-\omega_\pi(q_1)]\,\delta[\omega-\omega_1-\omega_\pi(q_2)] \\ &\quad +\delta[\omega_1+\omega_\pi(q_1)]\,\delta[\omega-\omega_1+\omega_\pi(q_2)] \\ &\quad -\delta[\omega_1-\omega_\pi(q_1)]\,\delta[\omega-\omega_1+\omega_\pi(q_2)] \\ &\quad -\delta[\omega_1+\omega_\pi(q_1)]\,\delta[\omega-\omega_1-\omega_\pi(q_2)]\}\,,\end{aligned} \tag{A.30}$$

and the ω_1-integration with the help of the $\delta[\omega_1 \pm \omega_\pi(q_1)]$-functions

$$\begin{aligned}
\mathrm{Im}\,\Sigma(\omega,\mathrm{k}) &= \left(\frac{4\lambda\sigma}{N}\right)^2 \frac{N}{8\pi}\frac{1}{k}\int_0^\infty dq_1\, q_1\, dq_2\, q_2 \qquad (A.31)\\
&\times\ \Theta\left(|q_1-q_2| \le k \le q_1+q_2\right)\left[\omega_\pi(q_1)\omega_\pi(q_2)\right]^{-1}\\
&\times\ \big(\left\{1+f[\omega_\pi(q_1)]+f[\omega-\omega_\pi(q_1)]\right\}\delta[\omega-\omega_\pi(q_1)-\omega_\pi(q_2)]\\
&\quad +\left\{1+f[-\omega_\pi(q_1)]+f[\omega+\omega_\pi(q_1)]\right\}\delta[\omega+\omega_\pi(q_1)+\omega_\pi(q_2)]\\
&\quad -\left\{1+f[\omega_\pi(q_1)]+f[\omega-\omega_\pi(q_1)]\right\}\delta[\omega-\omega_\pi(q_1)+\omega_\pi(q_2)]\\
&\quad -\left\{1+f[-\omega_\pi(q_1)]+f[\omega+\omega_\pi(q_1)]\right\}\delta[\omega+\omega_\pi(q_1)-\omega_\pi(q_2)]\big)\,.
\end{aligned}$$

The $\delta[\omega+\omega_\pi(q_1)+\omega_\pi(q_2)]$ function has no support, because $\omega > 0$ and $\omega_\pi(q) > 0$. Note that evaluating the $\delta[\omega-\omega_\pi(q_1)+\omega_\pi(q_2)]$ and the $\delta[\omega+\omega_\pi(q_1)-\omega_\pi(q_2)]$ function, the latter two terms cancel each other. The remaining delta function can be transformed to a delta function in momentum-space,

$$\delta[\omega-\omega_\pi(q_1)-\omega_\pi(q_2)] = \left|\frac{\omega_\pi(q_0)}{q_0}\right|\left[\delta(q_1-q_0)+\delta(q_1+q_0)\right] \qquad (A.32)$$

where

$$q_0 \equiv \sqrt{[\omega-\omega_\pi(q_2)]^2 - M_\pi^2} \qquad (A.33)$$

is the root of the argument of the delta function. Note that in Eq. (A.31) $q_1 > 0$ and therefore there is no support of the $\delta(q_1+q_0)$ function. Carrying out the q_1-integration, using $\omega-\omega_\pi(q_0)=\omega_\pi(q_1)$, and relabelling $q \equiv q_2$, one gets

$$\begin{aligned}
\mathrm{Im}\,\Sigma(\omega,\mathrm{k}) &= \left(\frac{4\lambda\sigma}{N}\right)^2 \frac{N}{8\pi}\frac{1}{k}\int_0^\infty dq\; q\,[\omega_\pi(q)]^{-1}\Theta\left(|q_0-q| \le k \le q_0+q\right)\\
&\times\ \{1+f[\omega_\pi(q_0)]+f[\omega_\pi(q)]\}. \qquad (A.34)
\end{aligned}$$

To calculate the limit $k \to 0$, one starts best with Eq. (A.31), uses the following transformation

$$\begin{aligned}
1+f[\omega_\pi(q_1)]+f[\omega-\omega_\pi(q_1)] &= \left[1-\exp\left(-\frac{\omega}{T}\right)\right] \qquad (A.35)\\
&\times\ \left\{1+f[\omega_\pi(q_1)]\right\}\left\{1+f[\omega-\omega_\pi(q_1)]\right\},
\end{aligned}$$

the identity

$$\lim_{k\to 0}\frac{\Theta\left(|q_1-q_2| \le k \le q_1+q_2\right)}{k} = 2\,\delta(q_1-q_2) \qquad (A.36)$$

(to perform the q_1-integration), and relabels $q \equiv q_2$, to get

$$\begin{aligned} \mathrm{Im}\,\Sigma(\omega,0) &= \left(\frac{4\lambda\sigma}{N}\right)^2 \frac{N}{4\pi}\left[1-\exp\left(-\frac{\omega}{T}\right)\right]\int_0^\infty dq\, q^2\, \delta[\omega-2\omega_\pi(q)][\omega_\pi^2(q)]^{-1} \\ &\times \{1+f[\omega_\pi(q)]\}\{1+f[\omega-\omega_\pi(q)]\}. \end{aligned} \tag{A.37}$$

As explained in [Ris98] this expression can be calculated analytically, using the Spence integral,

$$\mathrm{Im}\,\Sigma(\omega,0) = \left(\frac{4\lambda\sigma}{\mathrm{N}}\right)^2 \mathrm{N}\frac{1}{8\pi}\sqrt{1-\frac{4\mathrm{M}_\pi^2}{\omega^2}}\coth\frac{\omega}{4\mathrm{T}}\,. \tag{A.38}$$

Note that in [Ris98] the calculation is performed for the special case $\omega = m_\sigma$, but this can be generalised without further problems.
To calculate the real part of Eq.(A.27), one has to integrate over the principal value of $1/(\omega_1+\omega_2-\omega)$, denoted by $\mathrm{P}\int\ldots$,

$$\begin{aligned} [\mathrm{Re}\,\Sigma(\omega,\mathrm{k})]_2 &= \left(\frac{4\lambda\sigma}{N}\right)^2 \frac{2N}{(2\pi)^4}\frac{1}{k}\mathrm{P}\int_{-\infty}^\infty d\omega_1\, d\omega_2 \frac{1+f(\omega_1)+f(\omega_2)}{\omega_1+\omega_2-\omega} \\ &\times \int_0^\infty dq_1\, q_1\, dq_2\, q_2\, \Theta\left(|q_1-q_2|\le k\le q_1+q_2\right)\rho_\pi(\omega_1,q_1)\rho_\pi(\omega_2,q_2). \end{aligned} \tag{A.39}$$

Again, one uses the fact that the spectral density of the pion is just a delta function to perform the ω_1- and the ω_2-integration, and employs trivial renormalisation, i.e., neglects the divergent parts. This leads to

$$\begin{aligned} [\mathrm{Re}\,\Sigma(\omega,\mathrm{k})]_2 &= \left(\frac{4\lambda\sigma}{N}\right)^2 \frac{N}{8\pi^2}\frac{1}{k}\mathrm{P}\int_0^\infty dq_1\, q_1\, dq_2\, q_2 \\ &\times \Theta\left(|q_1-q_2|\le k\le q_1+q_2\right)[\omega_\pi(q_1)\omega_\pi(q_2)]^{-1} \\ &\times \left\{\frac{f[\omega_\pi(q_1)]+f[\omega_\pi(q_2)]}{\omega_\pi(q_1)+\omega_\pi(q_2)-\omega}+\frac{f[\omega_\pi(q_1)]+f[\omega_\pi(q_2)]}{\omega_\pi(q_1)+\omega_\pi(q_2)+\omega}\right. \\ &\quad \left.+\frac{-f[\omega_\pi(q_1)]+f[\omega_\pi(q_2)]}{\omega_\pi(q_1)-\omega_\pi(q_2)-\omega}+\frac{-f[\omega_\pi(q_1)]+f[\omega_\pi(q_2)]}{\omega_\pi(q_1)-\omega_\pi(q_2)+\omega}\right\}. \end{aligned} \tag{A.40}$$

To evaluate the principal value numerically, in an appropriate way, one performs the following steps. First one introduces a new variable $x \equiv \omega_\pi(q_1)$ and transforms the q_1-integration to an x-integration, with $dq_1 = \omega_\pi(q_1)/q_1 dx$, and $q_1 = \sqrt{x^2-M_\pi^2} \equiv q^*$. Relabelling $q \equiv q_2$ leads to

$$[\mathrm{Re}\,\Sigma(\omega,\mathrm{k})]_2 = \left(\frac{4\lambda\sigma}{N}\right)^2 \frac{N}{8\pi^2}\frac{1}{k}\mathrm{P}\int_0^\infty dq\, q\,[\omega_\pi(q)]^{-1}dx\,\Theta\ \left(|q^*-q|\le k\le q^*+q\right)$$

$$\times \quad \left\{ \frac{f(x)+f[\omega_\pi(q)]}{x+\omega_\pi(q)-\omega} + \frac{f(x)+f[\omega_\pi(q)]}{x+\omega_\pi(q)+\omega} \right.$$
$$\left. + \frac{-f(x)+f[\omega_\pi(q)]}{x-\omega_\pi(q)-\omega} + \frac{-f(x)+f[\omega_\pi(q)]}{x-\omega_\pi(q)+\omega} \right\}. \qquad \text{(A.41)}$$

Second one transforms the x-integration to a sum over x_i, and uses the mean-value theorem to put the terms with the distribution functions in front of the integrals

$$\begin{aligned}
[\mathrm{Re}\,\Sigma(\omega,\mathrm{k})]_2 &= \left(\frac{4\lambda\sigma}{N}\right)^2 \frac{N}{8\pi^2}\frac{1}{k}\mathrm{P}\int_0^\infty dq\, q\,[\omega_\pi(q)]^{-1}\sum_i \Theta\ (|q^*-q| \le k \le q^*+q) \\
&\times \left(\{f(\hat{x})+f[\omega_\pi(q)]\}\int_{x_i}^{x_{i+1}} dx \frac{1}{x+\omega_\pi(q)-\omega} \right. \\
&\quad + \{f(\hat{x})+f[\omega_\pi(q)]\}\int_{x_i}^{x_{i+1}} dx \frac{1}{x+\omega_\pi(q)+\omega} \\
&\quad + \{-f(\hat{x})+f[\omega_\pi(q)]\}\int_{x_i}^{x_{i+1}} dx \frac{1}{x-\omega_\pi(q)-\omega} \\
&\quad \left. + \{-f(\hat{x})+f[\omega_\pi(q)]\}\int_{x_i}^{x_{i+1}} dx \frac{1}{x-\omega_\pi(q)+\omega} \right), \qquad \text{(A.42)}
\end{aligned}$$

where $x_i \le \hat{x} \le x_{i+1}$, and $q^* \equiv \sqrt{\hat{x}-M_\pi^2}$. Finally, the x-integrals can be performed analytically,

$$\begin{aligned}
[\mathrm{Re}\,\Sigma(\omega,\mathrm{k})]_2 &= \left(\frac{4\lambda\sigma}{N}\right)^2 \frac{N}{8\pi^2}\frac{1}{k}\int_0^\infty dq\, q\,[\omega_\pi(q)]^{-1}\sum_i \Theta\ (|q^*-q| \le k \le q^*+q) \\
&\times \left(\{f(\hat{x})+f[\omega_\pi(q)]\}\ln\left|\frac{[\omega_\pi(q)+x_{i+1}]^2-\omega^2}{[\omega_\pi(q)+x_i]^2-\omega^2}\right| \right. \\
&\quad \left. + \{-f(\hat{x})+f[\omega_\pi(q)]\}\ln\left|\frac{[\omega_\pi(q)-x_{i+1}]^2-\omega^2}{[\omega_\pi(q)-x_i]^2-\omega^2}\right| \right). \qquad \text{(A.43)}
\end{aligned}$$

In the limit $k \to 0$, using Eq. (A.36), the q-integration can be carried out,

$$\begin{aligned}
[\mathrm{Re}\,\Sigma(\omega,0)]_2 &= \left(\frac{4\lambda\sigma}{N}\right)^2 \frac{N}{4\pi^2}\sum_i q^*\,[\omega_\pi(q^*)]^{-1} \qquad \text{(A.44)} \\
&\times \left(\{f(\hat{x})+f[\omega_\pi(q^*)]\}\ln\left|\frac{[\omega_\pi(q^*)+x_{i+1}]^2-\omega^2}{[\omega_\pi(q^*)+x_i]^2-\omega^2}\right| \right. \\
&\quad \left. + \{-f(\hat{x})+f[\omega_\pi(q^*)]\}\ln\left|\frac{[\omega_\pi(q^*)-x_{i+1}]^2-\omega^2}{[\omega_\pi(q^*)-x_i]^2-\omega^2}\right| \right).
\end{aligned}$$

–Appendix B–

Deutsche Zusammenfassung

B.1 Allgemeines

Für masselose Quarks ist die Lagrangedichte der Quantenchromodynamik (QCD) invariant unter der globalen chiralen $U(N_f)_r \times U(N_f)_\ell$ Symmetrie, wobei N_f die Anzahl der Quark-"flavor"[1] ist. Die chirale Symmetrie ist isomorph zu der Vektor- und Axialvektor-Symmetrie $U(N_f)_V \times U(N_f)_A$, mit $V \equiv r + \ell, A \equiv r - \ell$. Im Vakuum bricht die $U(1)_A$ Anomalie [tH86] diese Symmetrie explizit zu einer $U(N_f)_V \times SU(N_f)_A$ Symmetrie. Darüber hinaus wird sie spontan durch ein chirales Quarkkondensat $\langle \bar{q}q \rangle \sim (300 \text{ MeV})^3$ zu einer $U(N_f)_V$ Symmetrie gebrochen [VW84], dies führt, gemäß Goldstones Theorem, zu $N_f^2 - 1$ masselosen pseudoskalaren Goldstone-Bosonen, z.B. Pionen, Kaonen, etc. In der Natur wird die chirale Symmetrie außerdem explizit durch nichtverschwindende Quarkmassen gebrochen, was zu den physikalischen Massen der Goldstone-Bosonen führt.
Bei Temperaturen der Größenordnung $\sim \langle \bar{q}q \rangle^{1/3}$ ist die thermische Anregung groß genug, um eine Restaurierung der chiralen Symmetrie zu erwarten. Bei solchen Energieskalen ist die Kopplungskonstante der QCD allerdings immer noch zu groß, um Störungstheorie anwenden zu können. Deswegen muss man sich andere, nichtstörungstheoretische Wege einfallen lassen, um die chirale Symmetrierestauration zu studieren. Ein sehr grundlegender Ansatz ist, QCD mit Hilfe der Methoden der Gittereichtheorie zu lösen [Kar02]. Gittereichrechnungen haben ergeben, daß die kritische Temperatur T_c, bei der die chirale Symmetrie restauriert wird, bei ca. 150 MeV ($\sim 10^{12}$ K) liegt [LP03]. Diese Gittereichrechnungen

[1] Deutsch: "Geschmack". Ich werde im Folgenden oft den geläufigeren englischen Fachbegriff verwenden und die deutsche Übersetzung nur als Fußnote angeben.

wurden allerdings bei verschwindendem chemischen Potential $\mu = 0$ durchgeführt und es treten einige technische Probleme auf, die ich im Folgenden kurz erwähnen werde.

Das erste Problem ist, daß sie numerisch sehr aufwendig werden für realistische, d.h. kleine Werte für die Massen der up- und down-Quarks. Obwohl in den letzten Jahren in diesem Bereich einige Verbesserungen erzielt wurden [FK04], benutzen doch die meisten Studien unphysikalisch hohe Werte für die Quarkmassen.

Ein anderes Problem ist die Einführung eines nichtverschwindendem chemischen Potentials, welches auf ein imaginäres Ergebniss führt (das sog. "fermion-sign"-Problem), das man durch geeignete Näherungsverfahren auf ein reeles Ergebniss zurüchführen muss. Dies macht Gittereichrechnungen sehr unglaubwürdig für große chemische Potentiale.

Ich werde in meiner Arbeit einen alternativen Weg beschreiten, um den QCD-Phasenübergang zu beschreiben, den Weg über sog. effektive Theorien. Diese Theorien haben dieselbe globale $U(N_f)_r \times U(N_f)_\ell$ Symmetrie wie die QCD, allerdings besitzen sie nicht dieselbe lokale $SU(3)_c$ (Farb) Symmetrie, weil die Quarks und Gluonen "ausintegriert" werden. Durch dieses "Ausintegrieren" entstehen neue effektive Freiheitsgrade, welche (in den hier benutzten Modellen) die skalaren und pseudoskalaren Mesonen repräsentieren. In der chiral restaurierten Phase entarten die chiralen Partner (jeweils skalare mit pseudoskalaren Mesonen) miteinander, z.B. die Pionen mit dem σ-Meson. Ein Modell, welches dies beschreiben kann, ist das lineare σ-Modell [Lev67, GML60]. Die Vorteile solcher Modelle gegenüber Gittereichrechnungen sind, daß sie (innerhalb einer Vielteilchen-Näherung) numerisch wesentlich einfacher zu behandeln sind und daß keine Probleme mit physikalischen (kleinen) Quarkmassen oder einem nichtverschwindendem chemischen Potential auftreten.

Bei nichtverschwindender Temperaturen $T \neq 0$ bricht normale Störungstheorie in der QCD-Kopplungskonstanten g in dem Sinne zusammen, daß man die Beiträge nicht mehr nach Ordnungen von g sortieren kann [DJ74]. Der Grund dafür ist, daß durch die Temperatur eine neue Energieskala eingeführt wird, die dazu führen kann, daß gT/p nicht mehr von der Ordnung g, ist sondern von der Ordnung 1 [BP90a, BP90b], wobei p der typische Impuls eines Prozesses ist. Dies führt dazu, daß man alle Terme der Ordnung gT/p mitnehmen, d.h. ganze Klassen von Feynmandiagrammen aufsummieren muss.

Eine sehr elegante Möglichkeit, dies zu tun, ist über die Erweiterung des Cornwall-Jackiw-Tomboulis (CJT)- Formalismus [CJT74] auf endliche Tempera-

turen und/oder chemische Potentiale. Der CJT-Formalismus ist äquivalent zum Φ-Funktional-Ansatz von Luttinger und Ward [LW60] und Baym [Bay62]. Er verallgemeinert das Konzept einer effektiven Wirkung $\Gamma[\bar{\phi}]$ für den Erwartungswert $\bar{\phi}$ der Einpunktfunktion in Anwesenheit externer Quellen, auf das einer effektiven Wirkung

$$\Gamma[\bar{\phi},\bar{G}] = S[\bar{\phi}] + \frac{1}{2}\,\mathrm{Tr}\ln\bar{G}^{-1} + \frac{1}{2}\mathrm{Tr}(G^{-1}\bar{G}-1) + \Gamma_2[\bar{\phi},\bar{G}] \tag{B.1}$$

für $\bar{\phi}$ und den Erwartungswert $\bar{G}$ der Zweipunktfunktion in Anwesenheit externer Quellen. Hier bezeichnet $S[\bar{\phi}]$ die "tree-level"[2]-Wirkung, G^{-1} die inverse "tree-level"-Zweipunktfunktion und $\Gamma_2[\bar{\phi},\bar{G}]$ die Summe über alle "two-particle irreducible"[3] (2PI) Vakuum-Diagramme, wobei die inneren Linien dieser Diagramme $\bar{G}$ entsprechen. (Für eine Erweiterung dieses Ansatzes auf Drei- und Mehrpunktfunktionen siehe [NC75, Kle82, Car04, Ber04].) Minimierung dieses Funktionals

$$\left.\frac{\delta\Gamma[\bar{\phi},\bar{G}]}{\delta\bar{\phi}}\right|_{\bar{\phi}=\varphi,\bar{G}=\mathcal{G}} = 0\ , \qquad \left.\frac{\delta\Gamma[\bar{\phi},\bar{G}]}{\delta\bar{G}}\right|_{\bar{\phi}=\varphi,\bar{G}=\mathcal{G}} = 0\ , \tag{B.2}$$

liefert selbstkonsistente Gleichungen für den Erwartungswert der Ein- und Zweipunktfunktionen $\bar{\phi}$ und $\bar{G}$ für verschwindende externe Quellen, welche als φ und $\mathcal{G}$ bezeichnet werden. Die Variation nach $\bar{G}$ ergibt gerade die Dyson-Schwinger Gleichung für den vollen Propagator[4],

$$\mathcal{G}^{-1} = G^{-1} + \Pi\ , \tag{B.3}$$

wobei

$$\Pi \equiv -2\,\left.\frac{\delta\Gamma_2[\bar{\phi},\bar{G}]}{\delta\bar{G}}\right|_{\bar{\phi}=\varphi,\bar{G}=\mathcal{G}} \tag{B.4}$$

die Selbstenergie ist. Würde man in Γ_2 *alle* möglichen 2PI-Diagramme mitnehmen, würde dies bedeuten, die QCD exakt zu lösen. Leider ist dies nicht möglich und man muss die Summe irgendwo abbrechen, z.B. ab einer bestimmten Anzahl von "Loops"[5]. Ein großer Vorteil des CJT-Formalismus ist es, daß *jede* Wahl von Γ_2 auf eine Vielteilchen-Näherung führt, welche die Symmetrien der "tree-level"-Wirkung erhält, unter der Voraussetzung, daß sich die

[2]Deutsch: "Baumgraphen-Niveau".

[3]Deutsch: "Nicht reduzierbare Zweiteilchen Diagramme". Das sind Diagramme, in denen man *zwei beliebige* innere Linien durchschneiden kann, ohne daß sie in Subdiagramme zerfallen.

[4]Der volle Propagator ist gerade durch $\mathcal{G}$ gegeben.

[5]Deutsch: "Schleifen".

Erwartungswerte $\bar{\phi}$ und $\bar{G}$ wie Tensoren ersten bzw. zweiten Ranges unter dieser Symmetrie transformieren [Bay62]. In diesem Fall sind die Lösungen der Gleichungen (B.2) thermodynamisch konsistent und erhalten die Nöther-Ströme.

Eine sehr häufig benutzte Vielteilchen-Näherung ist die sog. Hartree-Fock-Näherung, in der Γ_2 alle Diagramme mit einer "double-bubble"[6] Topologie enthält, vgl. Abb. 1.4 a–c. Lässt man die Austauschterme weg, erhält man die Hartree-Näherung, die im Fall des linearen σ Modells mit $O(N)$ Symmetrie auch "large-N"-Näherung genannt wird [Pet99, LR00]. Betrachtet man die Gleichung (B.4), sieht man, daß sich die Diagramme, die in der Selbstenergie Π enthalten sind, durch das "Durchschneiden"[7] einer inneren Linie der Diagramme aus Γ_2 ergeben. Dadurch erhält man in der Hartree- oder Hartree-Fock-Näherung gerade Diagramme mit einer "tadpole"[8] Topologie, vgl. Abb. 3.1 b,c und 3.2 a,c. Diese Näherungen wurden in den letzten Jahren sehr ausführlich auf effektive Theorien der QCD angewendet, wie z.B. auf das lineare σ-Modell mit $U(N_f)_r \times U(N_f)_\ell$ oder mit $O(N)$ Symmetrie [BG77, BK96, RM98, AC97, Pet99, LR00, LRSB00, RRR03]. Nichtsdestotrotz sind sie sehr vereinfachende Näherungen, da die Diagramme mit "tadpole" Topologie keinen Imaginärteil haben und somit auf keine nichtverschwindende Zerfallsbreite der Teilchen führen, d.h. in diesen Näherungen werden alle Teilchen nur als stabile Quasiteilchen behandelt. Darüber hinaus sind diese Diagramme und somit die Dyson-Schwinger-Gleichungen Energie- und impulsunabhängig, d.h. sie sind einfache Fixpunktgleichungen für die effektiven Massen der Teilchen im Medium.

Es treten allerdings Probleme in der Hartree-Fock-Näherung auf, die damit zu tun haben, daß man nicht alle 2PI-Diagramme in Γ_2 aufsummieren kann. Im Falle des linearen σ-Modells mit $O(N)$ Symmetrie ergibt sich nicht die richtige Ordnung des chiralen Phasenübergangs und das Goldstone-Theorem wird verletzt, d.h. die Goldstone-Bosonen bleiben bei nichtverschwindenden Temperaturen unterhalb des Phasenübergangs $0 < T < T_c$ nicht masselos. Es gibt einige Ansätze, um diese Probleme zu beheben. Der einfachste Weg ist es, Beiträge der Ordnung $1/N$ auf der Ebene der Dyson-Schwinger- und der Kondensatgleichungen, zu vernachlässigen, was gerade auf die Hartree- (oder "large-N"-) Näherung

[6] Deutsch: "Doppelblasen".

[7] Die funktionale Ableitung $\delta\bar{G}/\delta\bar{G}$ ergibt gerade eine Deltafunktion, welche zum Ausführen einer Integration verwendet werden kann. In der graphischen Sprache von Feynman-Diagrammen bedeutet dies gerade, daß eine Linie durchgeschnitten wird.

[8] Deutsch: "Kaulquappe".

führt [Pet99, LR00]. In dieser Näherung bleibt das Goldstone-Boson masselos (für $T < T_c$) und man erhält einen Phasenübergang zweiter Ordnung, wie er erwartet wird [PW84a]. Eine andere Lösung, um das Goldstone-Theorem zu erfüllen, ergibt sich durch die Einführung sog. "externen" Propagatoren [ABW98, vHK02a, vHK02c, vHK02b, AAB$^+$02]. Als letztes möchte ich noch die Möglichkeit erwähnen, in Γ_2 nicht alle 2PI-Diagramm sondern alle "two-particle point-irreducible"[9] (2PPI)-Diagramme aufzusummieren, welches ebenfalls auf die richtige Ordnung des Phasenübergangs führt [VC92, Ver01, BM03].

B.2 Kapitel 2

Im zweiten Kapitel stelle ich eine Arbeit vor, die ich mit Adrian Dumitru und Jörg Ruppert [DRR04] über die Quarkmassenabhängigkeit der Temperatur des Phasenübergangs der QCD gemacht habe.
Im ersten Teil dieses Kapitels wird das lineare σ-Modell mit $O(4)$ Symmetrie in der Hartree-Fock-Näherung benutzt, um den Phasenübergang der QCD mit der Restaurierung der chiralen Symmetrie zu verknüpfen. Die Parameter dieses Modells werden durch die Vakuum-Massen des Pions und des σ-Mesons, m_π und m_σ, und die Vakuum-Zerfallsbreite des Pions f_π bestimmt, vgl. Glg. 1.23. Mit Hilfe von Gittereichrechnungen [CH03, K$^+$04b] können diese Vakuumwerte als Funktion der Quarkmasse berechnet werden. Der Ordnungsparameter für den chiralen Phasenübergang ist das chirale Kondensat (gegeben als der Erwartungswert der Einpunktfunktion in Abwesenheit externer Felder φ, Glg. B.2). Löst man nun die Gleichungen B.2, sieht man, daß das Kondensat für große Temperaturen asymptotisch gegen null strebt, Abb. 2.3 (rechts). Dies ist gerade das Verhalten eines Ordnungsparameters bei einem "crossover"[10] -Übergang[11]. Die kritische Temperatur T_c bei einem "crossover"-Übergang wird als diejenige Temperatur definiert, bei der die chirale Suszeptibilität $\partial\varphi/\partial T$ ihr Maximum annimmt. Die Ergebnisse für T_c im linearen σ Modell (Abb. 2.3, links), zeigen einen *wesentlich* steileren Anstieg mit der Pionenmasse, als er durch Gittereichrechnungen (die Datenpunkte in der Abbildung) vorhergesagt wird [KLP01].

[9] Der Unterschied zu 2PI-Diagrammen ist, daß man nicht zwei beliebige Linien der Diagramme durchschneiden können muss, sondern zwei Linien, die an demselben Vertex hängen.

[10] Deutsch: "Kreuzung".

[11] Bei einem echten Phasenübergang n ter Ordnung ist der Ordnungsparameter in der einen Phase identische null und in der anderen ungleich null.

Im zweiten Teil dieses Kapitels wird der Phasenübergang durch das "Polyakov-loop"-Modell an die Restaurierung der $Z(N_c)$ Symmetrie geknüpft. Im Gegensatz zum linearen σ-Modell baut dieses nicht auf der chiralen Symmetrie (welches eine exakte Symmetrie der QCD für masselose Quarks ist), sondern auf der diskreten $Z(3)$ Symmetrie der reinen Eichtheorie auf. Im Gegensatz zum ersten Teil dieses Kapitels werden nun die Übergangstemperaturen T_c (aus den Gittereichrechnungen) vorgegeben und man untersucht, wie "stark" die $Z(3)$ Symmetrie gebrochen werden muss, um diese Temperaturen zu reproduzieren. In Abbildung 2.4 (links) sind die Ergebnisse für den Erwartungswert des "Polyakov-loops"[12] in Abhängigkeit der Modellparameter b_1 und b_2[13] aufgetragen. Der Modellparameter b_1 gibt an, wie stark die $Z(3)$ Symmetrie gebrochen ist. Wie zu erkennen ist, ergibt sich für $b_1 < 0.026$ ein Phasenübergang erster Ordnung und für größere Werte von b_1 ein "crossover"-Übergang. Auf der rechten Seite der Abbildung 2.4 ist die Abhängigkeit des Parameters b_1 von der Pionmasse m_π aufgetragen. Es werden nur sehr kleine Werte für b_1 benötigt (bzw. man muss die $Z(3)$ Symmetrie nur sehr schwach brechen), um die Daten zu reproduzieren. Der Grund dafür ist, daß das Potential im "Polyakov-loop"-Modell sehr flach ist, vgl. z.B. die Abb. in [DP01, DP02b, SDL02], d.h. es reicht ein kleines "Kippen" des Potentials aus, um sein Minimum stark zu verschieben. Im Grenzfall unendlich vieler Farbfreiheitsgrade $N_c \to \infty$ ist dieses Potential sogar komplett flach [GW80, KSS82, DHL$^+$04]. Mit diesen Ergebnissen ergibt sich der kritische Punkt des QCD-Phasendiagrams in der Masse-Temperatur-Ebene, in dem der "crossover"-Übergang in einen Phasenübergang erster Ordnung übergeht (vgl. Abb. 5.1) als $m_\pi \approx 1.8$ GeV ($\hat{=} m_q \approx 0.9$ GeV) und $T \approx 240$ MeV.
In den beiden Abschnitten dieses Kapitels wurden zwei sehr verschiedene Ansätze für die zugrundeliegende Symmetrie benutzt. Im ersten Fall nimmt man an, daß die Quarks masselos sind, wodurch die QCD-Lagrangedichte chiral symmetrisch wird, und im zweiten Teil, daß sie unendlich schwer sind, wodurch die QCD-Lagrangedichte eine diskrete $Z(3)$ Symmetrie aufweist. Es gibt zwar Ergebnisse aus Gittereichrechnungen, die nahe legen, daß diese beiden Ansätze dieselbe kritische Temperatur T_c ergeben [Kar02], aber prinzipiell ist der Zusammenhang zwischen diesen beiden Ansätzen eine immer noch offene Frage in der Physik, vgl. z.B. [MST04, SKT04, KL99].

[12] Analog zum Erwartungswert der Einpunktfunktion ist der Erwartungswert des "Polyakov-loops" der Ordnungsparameter für den Phasenübergang in diesem Modell.

[13] Welcher selbst wiederum eine Funktion der Temperatur ist.

B.3 Kapitel 3

Im dritten Kapitel präsentiere ich eine Arbeit, die ich mit Dirk H. Rischke und Jörg Ruppert [RRR05] über die Verbesserung der normalen Hartree-Fock-Näherung dadurch, daß man den Mesonen selbstkonsistent eine nichtverschwindende Zerfallsbreite gibt, gemacht habe. Wie oben erklärt, sind in den Selbstenergien der normalen Hartree-Fock-Näherung nur Diagramme mit "tadpole"-Topologie enthalten, welche keinen Imaginärteil haben und somit nur auf stabile Quasiteilchen mit verschwindender Zerfallsbreite führen. Der einfachste Weg, eine nichtverschwindende Zerfallsbreite einzuführen, ist es, Diagramme mit "sunset"[14]-Topologie in Γ_2 bzw. dem effektiven Potential des Modells aufzunehmen (vgl. Abb. 1.4. d und e). Diese führen auf Diagramme in den Selbstenergien, die einen Real- *und* einen Imaginärteil haben (vgl. Abb. 3.1 d, e, und 3.2 d). Abgesehen von dem Imaginärteil ist der große Unterschied dieser Diagramme im Vergleich zu den "tadpole"-Diagrammen, daß sie von der externen Energie und dem externen Impuls, ω und k, abhängen. Dies führt dazu, daß die Dyson-Schwinger-Gleichungen für die vollen Propagatoren zu Integralgleichungen werden, die man auf einen Energie-Impuls-Gitter lösen muss. In diesem Kapitel liegt mein Hauptaugenmerk auf dem Einfluss der nichtverschwindenden Zerfallsbreite, deshalb lasse ich als ersten Ansatz die Realteile der Selbstenergien, die von den "sunset"-Diagrammen kommen, weg.
Ich wende in diesem Kapitel die verbesserte Hartree-Fock-Näherung auf das lineare σ-Modell mit $O(4)$ Symmetrie an. Das qualitative Verhalten des chiralen Kondensates σ (vgl. Abb. 3.3, links) ist in beiden Näherungen dasselbe, das Kondensat fällt deutlich mit steigender Temperatur ab, verschwindet aber nicht komplett, d.h. man hat einen "crossover"-Übergang vorliegen. Der Grund dafür ist, daß ich hier nur den Fall mit explizit gebrochener chiraler Symmetrie untersuche, womit man die oben erwähnten Probleme der Verletzung des Goldstone-Theorem und der falschen Ordnung des chiralen Phasenübergangs umgeht. Wie im zweiten Kapitel erwähnt, definiert man die kritische Temperatur eines "crossover"-Übergangs T_χ als diejenige Temperatur, bei der die chirale Suszeptibilität $\partial\sigma/\partial T$ ihr Maximum annimmt. Quantitativ führt die Einführung der nichtverschwindenden Zerfallsbreite zu einer Erniedrigung dieser Übergangstemperatur um ca. 20% im Vergleich zur normalen Hartree-Fock-Näherung. Das Resultat $T_\chi \approx 175$ MeV, ist (innerhalb der Fehlergenauigkeit)

[14]Deutsch: "Sonnenuntergang".

genau der Wert, der mit Hilfe von Gittereichrechnungen im chiralen Limes ermittelt wurde.

Auf der rechten Seite der Abbildung 3.3 sieht man die effektiven Massen des σ-Mesons und des Pions, M_σ und M_π, als Funktion der Temperatur, wiederum in beiden Näherungen. Da die Zerfallsbreite des Pions relativ klein ist (vgl. Abb. 3.4), führt ihre Hinzunahme auch nicht zu großen Änderungen in der effektiven Masse des Pions. Auf der anderen Seite führt die Einführung der Zerfallsbreite des σ-Mesons zu einer deutlichen Änderung in dem Temperaturbereich unterhalb T_χ, wo seine Zerfallsbreite sehr groß ist. In diesem Temperaturbereich fällt die Masse des σ-Mesons in der verbesserten Hartree-Fock-Näherung wesentlich steiler mit der Temperatur ab. Für größere Temperatur $T > T_\chi$ wird auch die Zerfallsbreite des σ-Meson sehr klein und es gibt keine großen Unterschiede zwischen den beiden Näherungen. Die Massen des σ-Mesons und des Pions entarten bei hohen Temperaturen, wie man es bei chiralen Partnern erwartet.

In der Abbildung 3.4 sieht man die Zerfallsbreiten[15] Γ der beiden Mesonen als Funktionen der Temperatur. Für kleine Temperaturen ist die Zerfallsbreite des σ-Mesons sehr groß (in der Größenordnung seiner Masse) wegen des recht wahrscheinlichen Zerfalls in zwei Pionen. Die Zerfallsbreite im Vakuum, d.h. bei $T = 0$, liegt mit $\Gamma_\sigma \simeq 460$ MeV recht nahe an dem experimentell gemessenen Wert von $\Gamma_\sigma \sim (600 - 1000)$ MeV [EHO$^+$04], ohne einen extra Parameter justieren zu müssen. Sie steigt bis zu einem Maximum von ca. 500 MeV an und fällt dann steil mit der Temperatur ab. Die Zerfallsbreite des Pions verschwindet bei $T = 0$, steigt dann bis zu einem Maximum von ca. 180 MeV ($\approx 0.5 M_\pi$) an, um dann, wie die Zerfallsbreite des σ-Mesons, steil mit der Temperatur abzufallen. Obwohl beide Zerfallsbreiten für $T > T_\chi$ sehr klein werden, entarten sie jedoch nicht. Die Zerfallsbreite des σ-Mesons bleibt immer ca. einen Faktor 8 größer als die des Pions. Dies kann man auf den Unterschied in den Symmetriefaktoren der "tadpole"-Diagramme in den Selbstenergien zurückführen. Er verschwindet bei einem echten Phasenübergang n ter Ordnung wegen $\Gamma \sim \mathrm{Im}\Pi \sim \sigma^2 = 0$ für $\sigma = 0$.

Die selbstkonsistent berechneten Ergebnisse für die Spektraldichten des σ-Mesons und des Pions, ρ_σ und ρ_π, sind in Abbildung 3.5 und 3.6 als Funktion der externen Energie ω und des externen Impulses k, und in Abbildung 3.7 nur als

[15] Die Zerfallsbreite Γ ist definiert als $\Gamma \equiv \mathrm{Im}\Pi(\omega, \mathbf{k})/\omega$, wobei ω die Quasiteilchenenergie des Mesons ist [Wel83, LB00].

Funktion von ω bei festem k, für vier Temperaturen $T = 80$, 160, 240 und 320 MeV dargestellt. Die Spektraldichte des Pions zeigt bei allen Temperaturen ein scharfes Maximum bei der Quasiteilchenenergie $\omega_\pi(k) = \sqrt{k^2 + M_\pi^2(\sigma)}$. Für Temperaturen unterhalb von 200 MeV ist die effektive Masse des Pions ungefähr gleich seinem Vakuumwert $M_\pi \simeq m_\pi = 139.5$ MeV (vgl. Abb. 3.3), dementsprechend ist das Maximum bei einer Energie von $\omega_\pi(325\,\mathrm{MeV}) \simeq 350$ MeV. Oberhalb von $T \sim 200$ MeV steigt die effektive Masse des Pions deutlich an und die Position des Maximums wird zu höheren Energien verschoben. Die Verbreiterung des Maximums bei $T = 160$ MeV ist auf die Streuung des Pions am σ-Meson im Medium zurückzuführen. Hingegen weist die Spektraldichte des σ-Mesons für Temperaturen kleiner als ~ 170 MeV kein scharfes Maximum bei der Quasiteilchenenergie $\omega_\sigma(k) = \sqrt{k^2 + M_\sigma^2(\sigma)}$ auf. Der Grund dafür ist, daß die Energie des σ-Mesons groß genug ist für den Zerfall in zwei Pionen. Hingegen wird für Temperaturen größer als ~ 170 MeV dieser Zerfallskanal mehr und mehr geschlossen, da die Massen der beiden chiralen Partner mehr und mehr entarten, und auch die Spektraldichte des σ-Mesons weist nun ein scharfes Maximum auf.

B.4 Kapitel 4

Im vierten Kapitel berücksichtige ich nun auch noch den impulsabhängigen Realteil der Selbstenergie, der von den "sunset"-Diagrammen kommt [Röd05]. Allerdings tue ich dies nicht in der Hartee-Fock- sondern in der Hartree-Näherung des linearen σ-Modells mit $O(N)$ Symmetrie. Dies führt dazu, daß der Imaginärteil der Selbstenergie und damit die Zerfallsbreite des Pions verschwindet. Für das Pion ist dies aber immer noch eine gute Näherung, da man aus den Ergebnissen des dritten Kapitels gelernt hat, daß die Auswirkung der Zerfallsbreite des Pions klein ist. Dahingegen bleibt ein Teil des σ-Meson-Zerfallskanals $\sigma \to 2\pi$ erhalten. Ein anderer Aspekt, den ich untersuche, ist die Auswirkung der Wahl der Vakuummasse des σ-Mesons, $m_\sigma = (400 - 1200)$ MeV [EHO$^+$04], die zur Bestimmung der Parameter des Modells benötigt wird. Ich vergleiche die Fälle $m_\sigma = 400$, 600 und 800 MeV mit explizit gebrochener chiraler Symmetrie und im chiralen Limes, vgl. Tab. 4.1.

Der impulsunabhängige Teil der Masse und das chirale Kondensat, Abb. 4.1, zeigen das zu erwartende Verhalten eines "crossover"-Übergangs im Fall explizit gebrochener chiraler Symmetrie und einen Phasenübergang zweiter Ordnung im

chiralen Limes [PW84a]. Der impulsabhängige Teil des Realteils der Selbstenergie, Abb. 4.2 und 4.3, ist relativ klein, verglichen mit den (quadratischen) effektiven Massen in Abb. 4.1 .

Die Zerfallsbreite des σ-Mesons (Abb. 4.4), zeigt eine sehr große Abhängigkeit von der Vakuummasse des σ-Mesons, was daran liegt, daß $\Gamma \sim \mathrm{Im}\Pi \sim \lambda^2 \sim \mathrm{m}_\sigma^4$. Auch die Vergrößerung der Zerfallsbreite im Fall des chiralen Limes ($m_\pi = 0$) im Vergleich zum Fall der expliziten Symmetriebrechung kann auf die Bestimmung des Parameters λ zurückgeführt werden: $\Gamma \sim \mathrm{Im}\Pi \sim \lambda^2 \sim (\mathrm{m}_\sigma^2 - \mathrm{m}_\pi^2)^2 \leq \mathrm{m}_\sigma^4$. Der Unterschied im Vergleich zu der Zerfallsbreite aus dem dritten Kapitel, Abb. 4.5, ist im Wesentlichen auf unterschiedliche Symmetriefaktoren der Diagramme in den Selbstenergien zurückzuführen.

Ein auffälliger Unterschied zwischen den Ergebnissen der Spektraldichte im Fall expliziter chiraler Symmetriebrechung und des chiralen Limes, Abb. 4.6 und 4.7, ist, daß es in ersterem Fall einen Energiebereich gibt, in dem die Spektraldichte verschwindet. Dieser kommt durch den "threshold"[16]-Effekt des $\sigma \to 2\pi$ Zerfalls zustande, der bei einer Energie von $\omega = 2M_\pi$ liegt, d.h. im chiralen Limes bei $\omega = 0$. Wie schon bei der Diskussion der Zerfallsbreite erwähnt, nimmt die Breite mit zunehmender Vakuummasse des σ-Mesons zu. Vergleicht man diese Resultate mit den Ergebnissen aus Kapitel 3, Abb. 4.8, sieht man, daß der "threshold"-Effekt durch die Einführung der Pion-Zerfallsbreite verwischt wird. Hingegen führt die impulsabhängige Komponente der Selbstenergie, die von den "sunset"-Diagrammen kommt, zu keiner qualitativen Änderung. Um ihren quantitativen Einfluss abzuschätzen, habe ich für die beiden Fälle, die in Abb. 4.8 dargestellt sind, die mittlere Änderung der Spektraldichte mit und ohne diesen Anteil berechnet, dieser Wert ist mit $5.61 \pm 2.90\%$ für $T = 160$ MeV und $0.44 \pm 0.01\%$ für $T = 320$ MeV nicht sehr groß.

[16]Deutsch: "Schwelle".

Bibliography

[A+99] Constantia Alexandrou et al. The deconfinement phase transition in one-flavor QCD. *Phys. Rev.*, D60:034504, 1999.

[AAB+02] Gert Aarts, Daria Ahrensmeier, Rudolf Baier, Jurgen Berges, and Julien Serreau. Far-from-equilibrium dynamics with broken symmetries from the 2PI-1/N expansion. *Phys. Rev.*, D66:045008, 2002.

[ABR99] Mark G. Alford, Jurgen Berges, and Krishna Rajagopal. Unlocking color and flavor in superconducting strange quark matter. *Nucl. Phys.*, B558:219–242, 1999.

[ABW98] Z. Aouissat, O. Bohr, and J. Wambach. The octet of goldstone modes in the SU(3) linear sigma model in the QRPA. *Mod. Phys. Lett.*, A13:1827–1836, 1998.

[AC97] Giovanni Amelino-Camelia. Thermal effective potential of the O(N) linear sigma model. *Phys. Lett.*, B407:268–274, 1997.

[AK03] N. G. Antoniou and A. S. Kapoyannis. Bootstraping the QCD critical point. *Phys. Lett.*, B563:165–172, 2003.

[Alf01] Mark G. Alford. Color superconducting quark matter. *Ann. Rev. Nucl. Part. Sci.*, 51:131–160, 2001.

[ARW98] Mark G. Alford, Krishna Rajagopal, and Frank Wilczek. QCD at finite baryon density: Nucleon droplets and color superconductivity. *Phys. Lett.*, B422:247–256, 1998.

[AY89] M. Asakawa and K. Yazaki. Chiral restoration at finite density and temperature. *Nucl. Phys.*, A504:668–684, 1989.

[B+88] P. Bacilieri et al. On the order of the deconfining phase transition in pure gauge QCD. *Phys. Rev. Lett.*, 61:1545, 1988.

[B+90] Frank R. Brown et al. On the existence of a phase transition for QCD with three light quarks. *Phys. Rev. Lett.*, 65:2491–2494, 1990.

[B+97] Claude W. Bernard et al. The equation of state for two flavor QCD at N(T) = 6. *Phys. Rev.*, D55:6861–6869, 1997.

[Bay62] Gordon Baym. Selfconsistent approximation in many body systems. *Phys. Rev.*, 127:1391–1401, 1962.

[BCD+88] F. R. Brown, N. H. Christ, Y. F. Deng, M. S. Gao, and T. J. Woch. Nature of the deconfining phase transition in SU(3) lattice gauge theory. *Phys. Rev. Lett.*, 61:2058, 1988.

[BCPG94] A. Barducci, R. Casalbuoni, Giulio Pettini, and Raoul Gatto. Chiral phases of QCD at finite density and temperature. *Phys. Rev.*, D49:426–436, 1994.

[Bec05] C. Beckmann. Selfconsistent calculations of hadrons at finite temperature. *Acta Phys. Hung.*, A22:215–221, 2005.

[Ber04] Jurgen Berges. N-particle irreducible effective action techniques for gauge theories. *Phys. Rev.*, D70:105010, 2004.

[BG77] G. Baym and G. Grinstein. Phase transition in the sigma model at finite temperature. *Phys. Rev.*, D15:2897–2912, 1977.

[BJW99] J. Berges, D. U. Jungnickel, and C. Wetterich. Two flavor chiral phase transition from nonperturbative flow equations. *Phys. Rev.*, D59:034010, 1999.

[BK96] Alexander Bochkarev and Joseph I. Kapusta. Chiral symmetry at finite temperature: linear vs nonlinear σ-models. *Phys. Rev.*, D54:4066–4079, 1996.

[BL84] D. Bailin and A. Love. Superfluidity and superconductivity in relativistic fermion systems. *Phys. Rept.*, 107:325, 1984.

[BM03] Jurgen Baacke and Stefan Michalski. The O(N) linear sigma model at finite temperature beyond the hartree approximation. *Phys. Rev.*, D67:085006, 2003.

[BP90a] Eric Braaten and Robert D. Pisarski. Resummation and gauge invariance of the gluon damping rate in hot QCD. *Phys. Rev. Lett.*, 64:1338, 1990.

[BP90b] Eric Braaten and Robert D. Pisarski. Soft amplitudes in hot gauge theories: a general analysis. *Nucl. Phys.*, B337:569, 1990.

[BU83] Tom Banks and A. Ukawa. Deconfining and chiral phase transitions in quantum chromodynamics at finite temperature. *Nucl. Phys.*, B225:145, 1983.

[Car04] M. E. Carrington. The 4PI effective action for phi**4 theory. *Eur. Phys. J.*, C35:383–392, 2004.

[CH03] Ting-Wai Chiu and Tung-Han Hsieh. Light quark masses, chiral condensate and quark-gluon condensate in quenched lattice QCD with exact chiral symmetry. *Nucl. Phys.*, B673:217–237, 2003.

[CJT74] John M. Cornwall, R. Jackiw, and E. Tomboulis. Effective action for composite operators. *Phys. Rev.*, D10:2428–2445, 1974.

[CL84] T. Cheng and L. Li. *Gauge theory of elementary particle physics.* Clarendon press, oxford, 1984.

[COVV05] D. Cabrera, E. Oset, and M. J. Vicente Vacas. Evaluation of the pi pi scattering amplitude in the sigma-channel at finite density. *Phys. Rev.*, C72:025207, 2005.

[CP75] John C. Collins and M. J. Perry. Superdense matter: neutrons or asymptotically free quarks? *Phys. Rev. Lett.*, 34:1353, 1975.

[Das97] Ashok Das. *Finite temperature field theory.* World Scientific, 1997.

[dFP02] Philippe de Forcrand and Owe Philipsen. The QCD phase diagram for small densities from imaginary chemical potential. *Nucl. Phys.*, B642:290–306, 2002.

[DHL+04] Adrian Dumitru, Yoshitaka Hatta, Jonathan Lenaghan, Kostas Orginos, and Robert D. Pisarski. Deconfining phase transition as a matrix model of renormalized polyakov loops. *Phys. Rev.*, D70:034511, 2004.

[DJ74] L. Dolan and R. Jackiw. Symmetry behavior at finite temperature. *Phys. Rev.*, D9:3320–3341, 1974.

[DO03] Dmitri Diakonov and Michaela Oswald. Covariant derivative expansion of yang-mills effective action at high temperatures. *Phys. Rev.*, D68:025012, 2003.

[DP01] Adrian Dumitru and Robert D. Pisarski. Event-by-event fluctuations from decay of a condensate for Z(3) wilson lines. *Phys. Lett.*, B504:282–290, 2001.

[DP02a] Adrian Dumitru and Robert D. Pisarski. Degrees of freedom and the deconfining phase transition. *Phys. Lett.*, B525:95–100, 2002.

[DP02b] Adrian Dumitru and Robert D. Pisarski. Explosive collisions at rhic? *Nucl. Phys.*, A698:444–447, 2002.

[DP02c] Adrian Dumitru and Robert D. Pisarski. Test of the polyakov loop model. *Nucl. Phys. Proc. Suppl.*, 106:483–485, 2002.

[DP02d] Adrian Dumitru and Robert D. Pisarski. Two-point functions for SU(3) polyakov loops near T_c. *Phys. Rev.*, D66:096003, 2002.

[DRR04] Adrian Dumitru, Dirk Röder, and Jörg Ruppert. The quark-mass dependence of T_c in QCD: Working up from m = 0 or down from m = ∞? *Phys. Rev.*, D70:074001, 2004.

[E+04] Shinji Ejiri et al. Study of QCD thermodynamics at finite density by taylor expansion. *Prog. Theor. Phys. Suppl.*, 153:118–126, 2004.

[EFR+89] J. Engels, J. Fingberg, K. Redlich, H. Satz, and M. Weber. The onset of deconfinement in SU(2) lattice gauge theory. *Z. Phys.*, C42:341, 1989.

[EHO+04] S. Eidelman, K.G. Hayes, K.A. Olive, M. Aguilar-Benitez, C. Amsler, D. Asner, K.S. Babu, R.M. Barnett, J. Beringer, P.R. Burchat, C.D. Carone, C. Caso, G. Conforto, O. Dahl, G. D'Ambrosio, M. Doser, J.L. Feng, T. Gherghetta, L. Gibbons, M. Goodman, C. Grab, D.E. Groom, A. Gurtu, K. Hagiwara, J.J. Hernández-Rey, K. Hikasa, K. Honscheid, H. Jawahery, C. Kolda, Kwon Y., M.L. Mangano, A.V. Manohar, J. March-Russell, A. Masoni, R. Miquel, K. Mönig, H. Murayama, K. Nakamura, S. Navas, L. Pape, C. Patrignani, A. Piepke, G. Raffelt, M. Roos, M. Tanabashi, J. Terning, N.A. Törnqvist, T.G. Trippe, P. Vogel, C.G. Wohl, R.L. Workman, W.-M. Yao, P.A. Zyla, B. Armstrong, P.S. Gee, G. Harper, K.S. Lugovsky, S.B. Lugovsky, V.S. Lugovsky, A. Rom, M. Artuso, E. Barberio, M. Battaglia, H. Bichsel, O. Biebel, P. Bloch, R.N. Cahn, D. Casper, A. Cattai, R.S. Chivukula, G. Cowan, T. Damour, K. Desler, M.A. Dobbs, M. Drees, A. Edwards, D.A. Edwards, V.D. Elvira, J. Erler, V.V. Ezhela, W. Fetscher, B.D. Fields, B. Foster, D. Froidevaux, M. Fukugita, T.K. Gaisser, L. Garren, H.-J. Gerber, G. Gerbier, F.J. Gilman, H.E. Haber, C. Hagmann, J. Hewett, I. Hinchliffe, C.J. Hogan, G. Höhler, P. Igo-Kemenes, J.D. Jackson, K.F. Johnson, D. Karlen, B. Kayser, D. Kirkby, S.R. Klein, K. Kleinknecht, I.G. Knowles, P. Kreitz, Yu.V. Kuyanov, O. Lahav, P. Langacker, A. Liddle, L. Littenberg, D.M. Manley, A.D. Martin, M. Narain, P. Nason, Y. Nir, J.A. Peacock, H.R. Quinn, S. Raby, B.N. Ratcliff, E.A. Razuvaev, B. Renk, G. Rolandi, M.T. Ronan, L.J. Rosenberg, C.T. Sachrajda, Y. Sakai, A.I. Sanda, S. Sarkar, M. Schmitt, O. Schneider, D. Scott, W.G. Seligman, M.H. Shaevitz, T. Sjöstrand, G.F. Smoot, S. Spanier, H. Spieler, N.J.C. Spooner, M. Srednicki, A. Stahl, T. Stanev, M. Suzuki, N.P. Tkachenko, G.H. Trilling, G. Valencia, K. van Bibber, M.G. Vincter, D. Ward, B.R. Webber, M. Whalley, L. Wolfenstein, J. Womersley, C.L. Woody, O.V. Zenin, and R.-Y. Zhu. Review of Particle Physics. *Physics Letters B*, 592:1+, 2004.

[EKR95] J. Engels, F. Karsch, and K. Redlich. Scaling properties of the energy density in SU(2) lattice gauge theory. *Nucl. Phys.*, B435:295–310, 1995.

[EMSZ96] J. Engels, S. Mashkevich, T. Scheideler, and G. Zinovev. Critical

behaviour of SU(2) lattice gauge theory a complete analysis with the χ^2-method. *Phys. Lett.*, B365:219–224, 1996.

[ES97] J. Engels and T. Scheideler. The pseudospecific heat in SU(2) gauge theory: Finite size dependence and finite temperature effects. *Phys. Lett.*, B394:147–151, 1997.

[ES99] J. Engels and T. Scheideler. The calculation of critical amplitudes in SU(2) lattice gauge theory. *Nucl. Phys.*, B539:557–576, 1999.

[FK02] Z. Fodor and S. D. Katz. Lattice determination of the critical point of QCD at finite T and μ. *JHEP*, 03:014, 2002.

[FK04] Z. Fodor and S. D. Katz. Critical point of QCD at finite T and μ, lattice results for physical quark masses. *JHEP*, 04:050, 2004.

[Fuk04] Kenji Fukushima. Chiral effective model with the polyakov loop. *Phys. Lett.*, B591:277–284, 2004.

[GGG05] Mark I. Gorenstein, Marek Gazdzicki, and Walter Greiner. Critical line of the deconfinement phase transition. 2005.

[GGP94] Sean Gavin, Andreas Gocksch, and Robert D. Pisarski. QCD and the chiral critical point. *Phys. Rev.*, D49:3079–3082, 1994.

[GK84] F. Green and F. Karsch. Mean field analysis of SU(N) deconfining transitions in the presence of dynamical quarks. *Nucl. Phys.*, B238:297, 1984.

[GL89] P. Gerber and H. Leutwyler. Hadrons below the chiral phase transition. *Nucl. Phys.*, B321:387, 1989.

[GML60] Murray Gell-Mann and M Levy. The axial vector current in beta decay. *Nuovo Cim.*, 16:705, 1960.

[Gol83] H. Goldberg. Chiral symmetry restoration at finite temperature in the SU(3) x SU(3) sigma model. *Phys. Lett.*, B131:133, 1983.

[GPY81] David J. Gross, Robert D. Pisarski, and Laurence G. Yaffe. QCD and instantons at finite temperature. *Rev. Mod. Phys.*, 53:43, 1981.

[GSS01] W. Greiner, S. Schramm, and S. Stein. *Quantum Chromodynamics*. Springer Verlag, Berlin, 2001.

[GW73] D. J. Gross and Frank Wilczek. Asymptotically free gauge theories. 1. *Phys. Rev.*, D8:3633–3652, 1973.

[GW80] D. J. Gross and Edward Witten. Possible third order phase transition in the large N lattice gauge theory. *Phys. Rev.*, D21:446–453, 1980.

[HI03] Yoshitaka Hatta and Takashi Ikeda. Universality, the QCD critical / tricritical point and the quark number susceptibility. *Phys. Rev.*, D67:014028, 2003.

[HKS95] H.V.Klapdor-Kleingrothous and A. Staudt. *Teilchenphysik ohne Beschleuniger*. Teubner Studienbücher, Physik, 1995.

[HM84] F. Halzen and A.D. Martin. *Quarks and leptons: An introduction course in modern particle physics*. John Wiley & Sons, Inc., 1984.

[IZ85] Claude Itzykson and Jean-Bernard Zuber. *Quantum Field Theory*. McGraw-Hill International Editions, Physics Series, 1985.

[K$^+$04a] F. Karsch et al. Where is the chiral critical point in 3-flavor QCD? *Nucl. Phys. Proc. Suppl.*, 129:614–616, 2004.

[K$^+$04b] Teiji Kunihiro et al. Scalar mesons in lattice QCD. *Phys. Rev.*, D70:034504, 2004.

[Kap93] Joseph I. Kapusta. *Finite temperature field theory*. Cambridge University Press, 1993.

[Kar00] Frithjof Karsch. Lattice QCD at finite temperature and density. *Nucl. Phys. Proc. Suppl.*, 83:14–23, 2000.

[Kar02] Frithjof Karsch. Lattice QCD at high temperature and density. *Lect. Notes Phys.*, 583:209–249, 2002.

[KKLL00] Olaf Kaczmarek, Frithjof Karsch, Edwin Laermann, and Martin Lutgemeier. Heavy quark potentials in quenched QCD at high temperature. *Phys. Rev.*, D62:034021, 2000.

[KKPZ02] O. Kaczmarek, F. Karsch, P. Petreczky, and F. Zantow. Heavy quark anti-quark free energy and the renormalized polyakov loop. *Phys. Lett.*, B543:41–47, 2002.

[KL99] Frithjof Karsch and Martin Lutgemeier. Deconfinement and chiral symmetry restoration in an SU(3) gauge theory with adjoint fermions. *Nucl. Phys.*, B550:449–464, 1999.

[Kle82] H. Kleinert. Higher effective actions for bose systems. *Fortsch. Phys.*, 30:187–232, 1982.

[KLP01] F. Karsch, E. Laermann, and A. Peikert. Quark mass and flavor dependence of the QCD phase transition. *Nucl. Phys.*, B605:579–599, 2001.

[KLS01] F. Karsch, E. Laermann, and C. Schmidt. The chiral critical point in 3-flavor QCD. *Phys. Lett.*, B520:41–49, 2001.

[KRT03] F. Karsch, K. Redlich, and A. Tawfik. Thermodynamics at non-zero baryon number density: A comparison of lattice and hadron resonance gas model calculations. *Phys. Lett.*, B571:67–74, 2003.

[KSS82] John B. Kogut, Michael Snow, and Michael Stone. Mean field and monte carlo studies of SU(N) chiral models in three-dimensions. *Nucl. Phys.*, B200:211, 1982.

[Kug97] Taichiro Kugo. *Eichtheorie*. Springer-Verlag Berlin Heidelberg, 1997.

[Lae98] E. Laermann. Thermodynamics using wilson and staggered quarks. *Nucl. Phys. Proc. Suppl.*, 63:114–125, 1998.

[Lan97] P. V. Landshoff. Introduction to thermal field theory. 1997.

[LB00] Michel Le Bellac. *Thermal Field theory*. Cambridge University Press, 2000.

[Lev67] M. Levy. *Nuovo Cim.*, 52:23, 1967.

[LM05a] L. Li and Y. Meurice. About a possible 3rd order phase transition at T = 0 in 4D gluodynamics. 2005.

[LM05b] L. Li and Y. Meurice. Is there a third-order phase transition in quenched QCD? 2005.

[LP03] Edwin Laermann and Owe Philipsen. Status of lattice QCD at finite temperature. *Ann. Rev. Nucl. Part. Sci.*, 53:163, 2003.

[LR00] Jonathan T. Lenaghan and Dirk H. Rischke. The O(N) model at finite temperature: Renormalization of the gap equations in Hartree and large-N approximation. *J. Phys.*, G26:431–450, 2000.

[LRSB00] Jonathan T. Lenaghan, Dirk H. Rischke, and Jürgen Schaffner-Bielich. Chiral symmetry restoration at nonzero temperature in the $SU(3)_r \times SU(3)_\ell$ linear sigma model. *Phys. Rev.*, D62:085008, 2000.

[LSS81] C. B. Lang, P. Salomonson, and B. S. Skagerstam. Large N lattice gauge theory without third order phase transition. *Nucl. Phys.*, B190:337, 1981.

[LvW87] N. P. Landsman and C. G. van Weert. Real and imaginary time field theory at finite temperature and density. *Phys. Rept.*, 145:141, 1987.

[LW60] J. M. Luttinger and J. C. Ward. Ground state energy of a many fermion system. 2. *Phys. Rev.*, 118:1417–1427, 1960.

[MMO02] Peter N. Meisinger, Travis R. Miller, and Michael C. Ogilvie. Phenomenological equations of state for the quark-gluon plasma. *Phys. Rev.*, D65:034009, 2002.

[MMOP94] D. Metzger, H. Meyer-Ortmanns, and H. J. Pirner. Chiral symmetry restoration at finite temperature in the linear sigma model. *Phys. Lett.*, B321:66–74, 1994.

[MO95] Peter N. Meisinger and Michael C. Ogilvie. An effective action for finite temperature lattice gauge theories with dynamical fermions. *Phys. Rev.*, D52:3024–3029, 1995.

[MOPP92] H. Meyer-Ortmanns, H. J. Pirner, and A. Patkos. Mass sensitivity of chiral symmetry restoration at finite temperature. *Phys. Lett.*, B295:255–262, 1992.

[MST04] Agnes Mocsy, Francesco Sannino, and Kimmo Tuominen. Confinement versus chiral symmetry. *Phys. Rev. Lett.*, 92:182302, 2004.

[NC75] R. E. Norton and J. M. Cornwall. On the formalism of relativistic many body theory. *Ann. Phys.*, 91:106, 1975.

[OM00] Michael C. Ogilvie and Peter N. Meisinger. Landau-ginzburg theory of quark confinement. *Nucl. Phys. Proc. Suppl.*, 83:378–380, 2000.

[Pet99] Nicholas Petropoulos. Linear sigma model and chiral symmetry at finite temperature. *J. Phys.*, G25:2225–2241, 1999.

[Pis00] Robert D. Pisarski. Quark-gluon plasma as a condensate of SU(3) wilson lines. *Phys. Rev.*, D62:111501, 2000.

[Pis02] Robert D. Pisarski. Notes on the deconfining phase transition. 2002.

[Pol73] H. David Politzer. Reliable perturbative results for strong interactions? *Phys. Rev. Lett.*, 30:1346–1349, 1973.

[Pol78] Alexander M. Polyakov. Thermal properties of gauge fields and quark liberation. *Phys. Lett.*, B72:477–480, 1978.

[PP04] P. Petreczky and K. Petrov. Free energy of a static quark anti-quark pair and the renormalized polyakov loop in three flavor QCD. *Phys. Rev.*, D70:054503, 2004.

[PS95] Michal E. Peskin and Daniel V. Schroeder. *An introduction to quantum field theory.* Perseus book, 1995.

[PW84a] Robert D. Pisarski and Frank Wilczek. Remarks on the chiral phase transition in chromodynamics. *Phys. Rev.*, D29:338–341, 1984.

[PW84b] Robert D. Pisarski and Frank Wilczek. Remarks on the chiral phase transition in chromodynamics. *Phys. Rev.*, D29:338–341, 1984.

[Ris98] Dirk H. Rischke. Forming disoriented chiral condensates through fluctuations. *Phys. Rev.*, C58:2331–2357, 1998.

[Ris04] Dirk H. Rischke. The quark-gluon plasma in equilibrium. *Prog. Part. Nucl. Phys.*, 52:197–296, 2004.

[Riv88] R.J. Rivers. *Path integral methods in quantum field theory.* Cambridge University Press, cambridge monographs on mathematical physics edition, 1988.

[RM98] Heui-Seol Roh and T. Matsui. Chiral phase transition at finite temperature in the linear sigma model. *Eur. Phys. J.*, A1:205–220, 1998.

[Röd05] Dirk Röder. Selfconsistent calculations of σ-meson properties at finite temperature. 2005.

[RR05] Jörg Ruppert and Thorsten Renk. Non-perturbative finite T broadening of the rho meson and dilepton emission in heavy ion collisions. *Phys. Rev.*, C71:064903, 2005.

[RRR03] Dirk Röder, Jörg Ruppert, and Dirk H. Rischke. Chiral symmetry restoration in linear sigma models with different numbers of quark flavors. *Phys. Rev.*, D68:016003, 2003.

[RRR05] Dirk Röder, Jörg Ruppert, and Dirk H. Rischke. Selfconsistent calculations of spectral densities in the O(N) model: Improving the Hartree-Fock approximation by including nonzero decay widths. 2005.

[RSSV98] R. Rapp, Thomas Schafer, Edward V. Shuryak, and M. Velkovsky. Diquark bose condensates in high density matter and instantons. *Phys. Rev. Lett.*, 81:53–56, 1998.

[RW93] Krishna Rajagopal and Frank Wilczek. Static and dynamic critical phenomena at a second order QCD phase transition. *Nucl. Phys.*, B399:395–425, 1993.

[RW00] Krishna Rajagopal and Frank Wilczek. The condensed matter physics of QCD. 2000.

[SDJ01] O. Scavenius, A. Dumitru, and A. D. Jackson. Explosive decomposition in ultrarelativistic heavy ion collision. *Phys. Rev. Lett.*, 87:182302, 2001.

[SDL02] O. Scavenius, A. Dumitru, and J. T. Lenaghan. The K/π ratio from condensed polyakov loops. *Phys. Rev.*, C66:034903, 2002.

[Sho04] Igor A. Shovkovy. Two lectures on color superconductivity. 2004.

[SKT04] D. K. Sinclair, J. B. Kogut, and D. Toublan. Finite density lattice gauge theories with positive fermion determinants. *Prog. Theor. Phys. Suppl.*, 153:40–50, 2004.

[SMMR01] O. Scavenius, A. Mocsy, I. N. Mishustin, and D. H. Rischke. Chiral phase transition within effective models with constituent quarks. *Phys. Rev.*, C64:045202, 2001.

[Ste] Strüber Stefan. (in preparation).

[Ste04] M. Stephanov. The phase diagram of QCD and the critical point. *Acta Phys. Polon.*, B35:2939–2962, 2004.

[SY82] Benjamin Svetitsky and Laurence G. Yaffe. Critical behavior at finite temperature confinement transitions. *Nucl. Phys.*, B210:423, 1982.

[tH76a] Gerard 't Hooft. Computation of the quantum effects due to a four-dimensional pseudoparticle. *Phys. Rev.*, D14:3432–3450, 1976.

[tH76b] Gerard 't Hooft. Symmetry breaking through bell-jackiw anomalies. *Phys. Rev. Lett.*, 37:8–11, 1976.

[tH78] Gerard 't Hooft. On the phase transition towards permanent quark confinement. *Nucl. Phys.*, B138:1, 1978.

[tH86] Gerard 't Hooft. How instantons solve the U(1) problem. *Phys. Rept.*, 142:357–387, 1986.

[tHV72] Gerard 't Hooft and M. J. G. Veltman. Regularization and renormalization of gauge fields. *Nucl. Phys.*, B44:189–213, 1972.

[Uka90] Akira Ukawa. QCD phase transitions at finite temperatures. *Nucl. Phys. Proc. Suppl.*, 17:118–136, 1990.

[Uka97] Akira Ukawa. Finite-temperature QCD on the lattice. *Nucl. Phys. Proc. Suppl.*, 53:106–119, 1997.

[VC92] H. Verschelde and M. Coppens. A variational approach to quantum field theory. *Phys. Lett.*, B287:133–137, 1992.

[Ver01] Henri Verschelde. Summation and renormalization of bubble graphs to all orders. *Phys. Lett.*, B497:165–171, 2001.

[vHK02a] Hendrik van Hees and Joern Knoll. Renormalization in self-consistent approximations schemes at finite temperature. I: Theory. *Phys. Rev.*, D65:025010, 2002.

[vHK02b] Hendrik van Hees and Jorn Knoll. Renormalization in self-consistent approximation schemes at finite temperature. III: Global symmetries. *Phys. Rev.*, D66:025028, 2002.

[vHK02c] Hendrik van Hees and Jorn Knoll. Renormalization of self-consistent approximation schemes. II: Applications to the sunset diagram. *Phys. Rev.*, D65:105005, 2002.

[VVO02] M. J. Vicente Vacas and E. Oset. sigma meson mass and width at finite density. 2002.

[vW] Ch.G. van Weert. Statistical field theory. Lecture notes, 2001.

[VW84] C. Vafa and Edward Witten. Restrictions on symmetry breaking in vector - like gauge theories. *Nucl. Phys.*, B234:173, 1984.

[Wei95a] Steven Weinberg. *The quantum theory of fields, Volume I: Foundations*. Cambridge universtiy press, 1995.

[Wei95b] Steven Weinberg. *The quantum theory of fields, Volume II: Modern applications*. Cambridge universtiy press, 1995.

[Wel83] H. Arthur Weldon. Simple rules for discontinuities in finite temperature field theory. *Phys. Rev.*, D28:2007, 1983.

[Wir02] J. Wirstam. One-loop QCD corrections to the thermal wilson line model. *Phys. Rev.*, D65:014020, 2002.

[YS82] L. G. Yaffe and B. Svetitsky. First order phase transition in the SU(3) gauge theory at finite temperature. *Phys. Rev.*, D26:963, 1982.

[Zan03] F. Zantow. On the renormalization of the polyakov loop. 2003.

Danksagung

Im Folgendem möchte ich mich bei allen Leuten bedanken, die mir in meiner Zeit als Diplomand und später auch als Doktorand an der Johann Wolfgang Goethe Universität in Frankfurt am Main beigestanden haben.

Als erstes möchte ich meiner Frau Julia und meinen beiden Söhnen Justus und Philipp für ihre Liebe und mein Zuhause danken, in dem ich mich von der Physik erholen durfte.

Meiner Mutter Kirsten und meinem Vater Toni danke ich für ihre vorbehaltlose Unterstützung, sowohl geistlicher als auch finanzieller Natur.

Meinem Doktorvater Dirk Rischke, der bereits meine Diplomarbeit betreut hat, möchte ich für die gute Zusammenarbeit und meine Stelle als wissenschaftlicher Mitarbeiter bei ihm bedanken.

Für eine immer gute Arbeitsatmosphäre und viele angeregte Diskussionen möchte ich meinem Schöngeist Christian Beckmann und meinem ehemaligen Zimmergenossen Detlef Zschiesche danken.

Mein Dank gilt ganz besonders meinem guten Freund Jörg Ruppert, mit dem ich schon seit meiner Zeit als Diplomand eng zusammengearbeitet habe.

Adrian Dumitru danke ich für die Zusammenarbeit in unserer gemeinsamen Veröffentlichung und für die vielen lehrreichen Unterhaltungen.

Für die gute und aufopferungsvolle Betreuung des Netzwerkes danke ich den Administratoren des Netzwerkes des Institutes für Theoretische Physik und des Center for Scientific Computing der Johann Wolfgang Goethe-Universität: Manuel Reiter, Kerstin Paech, Alexander Achenbach, Gebhard Zeeb, Stefan Schramm und Boris Wagner.

Allen Professoren und sonstigen Mitgliedern des Institutes für Theoretische Physik möchte ich für die ganz besondere Arbeitsatmosphäre danken, die dieses

Institut zu dem macht, was es ist.

Ein Institut kann nicht ohne Verwaltung funktionieren, deshalb danke ich den Sekretärinnen: Daniela Radulescu, Veronika Palade, Astrid Steidl und Laura Quist.

Neben den Mitgliedern der Institutes für Theoretische Physik danke ich allen Kommilitonen, die mit mir studiert haben. Ganz besonders möchte ich hier Christian Glässner aus dem Institut für Angewandte Physik hervorheben, der mich seit dem ersten Semester begleitet hat.

Nicht zuletzt möchte ich meinen Akademischen Lehrern an der Johann Wolfgang Goethe-Universität danken, die ich auf der kommenden Seite aufgezählt habe. Sie haben maßgeblich zu meiner wissenschaftlichen Entwicklung beigetragen.

Akademische Lehrer

Prof. Dr. D. H. Rischke
Prof. Dr. J. A. Maruhn
JProf. Dr. A. Dumitru
Apl. Prof. Dr. S. Schramm
HD. PD Dr. J. Schaffner-Bielich
Prof. Dr. H. Stöcker
Prof. Dr. Dr. h. c. mult. W. Greiner
Prof. Dr. R. Kulze
Prof. Dr. P. Stolmann
Prof. Dr. J. Weidmann
Prof. Dr. H. Schmidt-Bcking
Prof. Dr. Dr. h.c. R. Stock
Prof. Dr. A. Schempp
Prof. Dr. M. Huth
Prof. Dr. H. Roskos
Prof. Dr. J. Baumeister
Prof. Dr. P. E. Kloeden
Prof. Dr. A. Schaarschmidt
Prof. Dr. R. Becker
Prof. Dr. A. Wakolbinger
Prof. Dr. H. Dinges
Prof. Dr. C.-P. Schnorr
Prof. Dr. W. Aßmus
Prof. Dr. B. Fink

Curriculum Vitae

Persönliche Daten:

Name:	Dirk Röder
Wohnort:	Hofheim am Taunus
Geburtstag/-ort:	26.04.1976, Frankfurt am Main
Familienstand:	verheiratet, zwei Kinder

Bildungsweg:

1983 – 1986	Max von Gagern-Schule (Grundschule) in Kelkheim
1986 – 1993	Eichendorf-Schule (Gesamtschule) in Kelkheim
1993 – 1997	Brühlwiesen-Schule (Gymnasium) in Hofheim
Juli 1997	Abitur (Gesamtnote: 2.0)
Sept. 1997 – Sept. 1998	Zivildienst
Okt. 1998 – März 2003	J.W.Goethe-Universität (Studium der Physik) in Frankfurt am Main
Juni 2000	Vordiplom (Gesamtnote: Sehr Gut)
März 2003	Diplom (Gesamtnote: Sehr Gut) Diplomarbeitsthema: "Chirale Symmetrierestauration in linearen Sigma-Modellen mit $U(N_f)_\ell \times U(N_f)_r$-Symmetrie"
seit April 2003	Doktorand am Institut für Theoretischen Physik der J.W.Goethe-Universität, Frankfurt am Main